ERDC/GSL TR-16-15

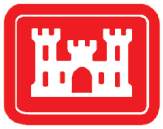

US Army Corps
of Engineers®
Engineer Research and
Development Center

ERDC
INNOVATIVE SOLUTIONS
for a safer, better world

Full-Scale Instrumented Evaluations of Multiple Airfield Matting Systems on Soft Soil to Characterize Permanent Deformation

Lyan Garcia

June 2016

Geotechnical and Structures Laboratory

The U.S. Army Engineer Research and Development Center (ERDC) solves the nation's toughest engineering and environmental challenges. ERDC develops innovative solutions in civil and military engineering, geospatial sciences, water resources, and environmental sciences for the Army, the Department of Defense, civilian agencies, and our nation's public good. Find out more at www.erdc.usace.army.mil.

To search for other technical reports published by ERDC, visit the ERDC online library at http://acwc.sdp.sirsi.net/client/default.

ERDC/GSL TR-16-15
June 2016

Full-Scale Instrumented Evaluations of Multiple Airfield Matting Systems on Soft Soil to Characterize Permanent Deformations

Lyan Garcia

Geotechnical and Structures Laboratory
U.S. Army Engineer Research and Development Center
3909 Halls Ferry Road
Vicksburg, MS 39180-6199

Final report

Prepared for Headquarters, Air Force Civil Engineer Center
Tyndall Air Force Base, FL 32403-5319

Under Project Number P2457442

Abstract

Airfield matting systems are used for the expedient construction of temporary airfields and rapid expansion of existing airfields to provide maneuvering support for military aircraft. They protect the subgrade by distributing the load exerted by aircraft over a larger area. Six airfield matting systems of varying materials and designs were evaluated through the construction of full-scale test sections to determine their effectiveness at reducing the accumulation of subgrade deformation and decreasing the pressure experienced by the subgrade. The matting systems were tested on a California Bearing Ratio (CBR) of 6 and subjected to simulated F-15E aircraft traffic while monitoring mat breakage, deformation, and subgrade earth pressure. The systems were compared in terms of the rate of subgrade permanent deformation. Based on test results, a simplified expression was developed to predict subgrade deformation on a CBR of 6 as a function of F-15E aircraft passes and airfield mat properties.

Contents

Figures and Tables

Figures

Tables

Preface

This study was conducted for the U.S. Air Force Civil Engineer Center (AFCEC). Technical oversight was provided by Jeb S. Tingle.

The work was performed by the Airfields and Pavements Branch (APB) of the Engineering Systems and Materials Division (ESMD), U.S. Army Engineer Research and Development Center, Geotechnical and Structures Laboratory (ERDC-GSL). At the time of publication, Timothy W. Rushing was Chief, APB; Dr. Gordon W. McMahon was Chief, ESMD; and Nicholas Boone was the Technical Director for Force Projection and Maneuver Support. The Deputy Director of ERDC-GSL was Dr. William P. Grogan, and the Director was Bartley P. Durst.

COL Bryan S. Green was the Commander of ERDC, and Dr. Jeffery P. Holland was the Director.

Unit Conversion Factors

Multiply	By	To Obtain
feet (ft)	0.3048	meters
inches (in.)	0.0254	meters
inch-pounds (force)	0.1129848	newton meters
pounds (force) (lb)	4.448222	newtons
pounds (force) per square foot (lb/ft$^{2)}$	47.88026	pascals
pounds (force) per square inch (lb/in.^{2})	6.894757	kilopascals
pounds (mass) per cubic foot (lb/ft^3)	16.01846	kilograms per cubic meter
pounds (mass) per cubic inch (lb/in.^{3})	2.757990 E+04	kilograms per cubic meter
pounds (mass) per square foot (lb/ft^2)	4.882428	kilograms per square meter
square feet (ft^2)	0.09290304	square meters
square inches (in.^{2})	6.4516 E-04	square meters

1 Introduction

1.1 Background

Expedient construction of temporary airfields and rapid expansion of existing airfields have a long history in the U.S. military. It is useful for providing maneuvering support of aircraft for immediate emergency use and for increasing maximum-on-ground capacity. Conventional construction techniques, such as asphalt and portland cement concrete paving, require considerable resources and time periods that usually inhibit rapid deployment for airfields. The ability to rapidly construct or expand airfield facilities enables the military to deploy supplies and materials quickly and stage aircraft at forward operating bases. This can be accomplished through expedient surfacings that are prefabricated and can be transported quickly into construction areas. Matting systems can be classified as expedient surfacings because they allow for rapid construction of airfields (and roadways) in areas where conventional methods are impractical.

Matting systems have a wide range of commercial applications in addition to their military uses. They have gained popularity as new designs, fabrication processes, and materials have been introduced. Typical uses include protection for large outdoor events, tent floors, platforms for the oil and gas industry, construction platforms in areas with sensitive subgrade disturbance requirements, temporary walkways, temporary roadways, and emergency disaster relief.

For expeditionary airfield applications, available products are limited. Numerous efforts have been conducted since the 1940s by the U.S. Army Engineer Waterways Experiment Station (WES), later the U.S. Army Engineer Research and Development Center (ERDC), to find suitable solutions. Early airfield matting system investigations in the U.S. were conducted as the need arose for rapidly constructed airfields designed for short periods of intensive use. Two characteristics were placed as priority: speed of installation and weight not to exceed a two-man carry. Their primary purpose and essential features have remained fundamentally the same. However, mat materials, geometry, design, and assembly have changed. Since then, designs have evolved from heavy duty steel planks towards lightweight material panels that include standard and

experimental aluminum alloys, magnesium, fiberglass, plastic, and polyethylene, and designs with composite material cross sections. Research efforts have continuously been focused on finding matting solutions that are logistically optimal, but strong enough to handle governing military aircraft.

Currently, the primary method used by the U.S. military for expedient airfield construction is preparing the natural foundation of an area and surfacing it with the AM2 mat system. AM2 is an aluminum mat system developed in the 1960s that has had success offering a short term airfield surfacing solution. However, AM2 can be logistically cumbersome due to its weight and large panel dimensions. M19, a light-weight aluminum honeycomb core mat, was also developed in the 1960s, but production ceased in the 1970s, as performance problems led to vast procurements of the better performing AM2. More recently, renewed emphasis has been placed on investigating alternative materials and mat systems. A program was initiated by the U.S. Air Force and was implemented to find lightweight options to AM2. A key component of the investigation was full-scale testing conducted at ERDC over a period of several years.

1.2 Objective and scope

This report presents full-scale instrumented evaluations of six airfield matting systems of varying materials and designs. The mat systems include AM2, M19, and four other matting designs. The tests were conducted from 2005 through 2011 as part of a program with an objective of finding lightweight alternatives to AM2. The test sections, experimental program, and results are described in more detail in a series of reports authored by Rushing and Tingle (2007), Rushing et al. (2011), and Rushing et al. (2012). Each evaluation consisted of constructing a soil subgrade to a California Bearing Ratio (CBR) of 6, surfacing it with airfield matting, and applying simulated F-15E aircraft traffic on the mat surface while monitoring damage and deformation. Earth pressure cells were installed at different depths and locations in the subgrade to monitor stress as a function of aircraft traffic.

The objective was to evaluate and compare the different mat types tested in terms of subgrade permanent deformation for constant support conditions and aircraft load. Information regarding individual mat system characteristics, construction of the full-scale test sections, simulated aircraft traffic operations, data collection, and subsequent analysis of data

to evaluate permanent deformation behavior are provided. The data compiled were used for developing permanent deformation prediction relationships as a function of F-15E aircraft passes and mat properties. Recommendations for use of the performance prediction relationships and future work are also discussed.

2 Literature Review

2.1 Overview of literature review

Temporary, portable, expeditionary pavement materials have been investigated by the military for decades for applications focused on the rapid construction of roadways, airfields, and flooring for military facilities, among others. Matting systems have been an expedient surfacing solution for these applications by offering a reliable alternative to assembling the thousands of tons of base material, asphalt, or concrete required in more permanent, conventional designs. This chapter examines matting development and testing, mostly conducted at ERDC. A review of recent approaches developed for characterizing mat behavior under given conditions is also presented.

2.2 Development and testing of matting systems

There is an extensive history of military matting interest for a variety of applications. Historical matting designs that were initially investigated included light-duty mat types, such as flexible wire mesh, laminated wood, laminated fencing, and more robust materials such as steel and aluminum planks. For military airfield applications, the heavy duty steel and aluminum mat designs proved to be the best options. However, light-duty mats were continually sought to reduce the need for larger aircraft to carry heavy duty mats (Tolbert 1945).

Substantial contributions to the development and testing of expedient surfaces were made during World War II as a need arose for rapid construction of usable surfaces over all types of terrain in the Pacific Theatre of Operations. Designs adopted in Europe and common materials became the forerunners for future designs.

Tolbert (1945) and Greulich (1943) published articles discussing airfield matting development for maintaining Allied air power that focused on the most notable accomplishment of that decade, Pierced Steel Plank (PSP). At the time, England and France had developed what was commonly called the “Chevron” grid, which consisted of longitudinal T-sections interconnected with a bar forming a herring-bone-pattern type of panels. However, assembly proved to be time consuming, and severe damage of

airplane tires during take-offs and landings created safety hazards. Therefore, a different design was needed that was capable of being rapidly connected in the field and had sufficient strength to handle 50,000-lb aircraft. After a series of engineering and service tests of experimental designs and modifications, the result was the development of PSP. Due to its satisfactory performance, it was adopted as the standard type of landing mat, and approximately 800 million square feet of the mat were produced during World War II (Robinson 1992).

With the onset of the Cold War and the addition of sophisticated fighter aircraft to military inventories, research was conducted on experimental materials for expedient surfaces. The goal was to provide stronger mats that could withstand longer operation times and have a potential for reuse. Important developments included M8 steel, M9 aluminum, and a series of "T-mats" that were made from magnesium, aluminum, plastic, or a combination of the same (WES 1951; Garrett and Horslev 1957; Turner 1961). M8 steel was a modified version of PSP, and M9 was very similar to M8 steel in all respects except in thickness, weight, and characteristics of the two metals. M8 steel and M9 aluminum were tested at WES to determine if a single layer of each could sustain the normal operations of military aircraft with the following characteristics: (a) a dual-wheel load of 80,000 lb and a tire pressure of 180 psi and (b) a single-wheel load of 50,000 lb and a tire pressure of 190 psi. Damage to both from 50,000-lb single-wheel load was substantial (WES 1951). Subsequent tests involved newer mat configurations such as T7 magnesium and T12 plastic. Laboratory testing of T7 showed that it had greater beam strength and stiffness than M8, and field evaluations proved its performance was beyond project requirements. However, assembly for creating an operating surface and replacement of damaged panels was difficult (Garrett and Horslev 1957). T12 was engineered and tested at WES and was made with a glass-fabric-reinforced phenolic resin honeycomb-structured core, bonded top and bottom to glass-fabric-reinforced phenolic resin facings. Despite its state-of-the art design, it failed under a single-wheel load of 50,000 lb (Turner 1961).

Mat research continued into the 1960s with the escalation of the Vietnam conflict. The answer for the waterproofing and dustproofing issues in the foreign environment was the introduction of AM2 extruded aluminum matting and M19 aluminum honeycomb matting (also called MX19) for use in bases in South Vietnam (Burns and Barker 1967; Carr and Ellison

1973). AM2 was initially produced by different extruders and fabricators and underwent a series of comparative field performance tests until a final configuration was accepted. Small lots from different manufacturers were subjected to the loads and tire pressures of the most damaging fighter aircraft (i.e., single-wheel load of 27,000 lb and tires inflated to an internal pressure of 400 psi) on a CBR of 4. The different designs were modified throughout the years, mostly because of the influence of weld quality to general mat performance (Burns and Barker 1967; Burns and Wolf 1969).

The current production of AM2 is Mod 5 and is manufactured by Alfab, Inc. Since its development, AM2 has been the primary expeditionary airfield surfacing used by the U.S. However, its weight is a limiting factor in deployment where aircraft payload limits are exceeded without approaching volume limits. Varying from traditional rectangular or strip mat designs, the M19 mat's dimensions were an almost-square panel. Its measurements and weight aided in providing relatively convenient proportions for packaging, transportation, and installation. Production of the mat was discontinued due to the better performance and larger procurements of AM2, but sufficient quantities of the mat were produced. It is still encountered in the theater or is stored in war reserve stockpiles.

Matting systems have evolved with the introduction of new materials and fabrications processes. Modern matting system materials include fiberglass, light aluminum alloys, polymers, and composites. They are manufactured with varying assemblies that include continuous rolls for ease of deployment, folded mats, and individual panels with unique locking mechanisms for securing panels in place. Comprehensive reviews of a few examples are provided by Rushing and Garcia (2013), Rushing (2010), and Gartrell (2007). Figures 1 and 2 show examples of matting systems discussed by Rushing and Garcia (2013) and Rushing (2010). Table 1 shows a list of commercially available mat systems, materials, and typical uses, according to the information available on each manufacturer's website.

Rushing and Howard (2011) evaluated a variety of commercial matting systems to determine their effectiveness in carrying heavy military vehicle traffic over loose sands (beach access) and mudflats. Mat system designs included fiberglass-reinforced mats, plastic and aluminum hexagonal mats, and high-density polyethylene mats (HDPE) with installation methods ranging from continuous rolls of material to individual panel placement. Representative sections were constructed with either sand or clayey silt,

Figure 1. DuraDeck mat (Rushing and Garcia 2013).

Figure 2. Spa-Trac (Rushing 2010).

Table 1. Summary of commercially available mat systems and typical uses.

Mat Name	Source	Manufacturer	Material	Typical Uses						
				Special events (stadiums, arenas, etc.)	Temporary walkways	Staging equipment/ utility vehicles	Temporary roadway for heavy vehicles	Work/construction platform	Drilling platform	Disaster relief
EventDeck	Event Deck (2010)	Signature Systems Group	High-impact polypropylene co-polymer	X	X					
ULTRAdeck				X	X	X				
HEXADECK			High density polyethylene	X	X	X	X			X
DuraDeck				X	X	X	X	X	X	X
MEGADECK	Signature Systems Group, LLC. (2012)			X	X	X	X	X	X	X
PortaFloor Max	Portafloor (2014a)	PortaFloor	Recycled polypropylene		X	X	X	X	X	
PortaFloor PRO	Portafloor (2014b)		High-impact polypropylene co-polymer	X	X					
DURA-BASE	Dura-Base Technical Information (2014)	Newpark Mats and Integrated Services	High density polyethylene	X	X	X	X	X	X	X
TerraPro HD	TerraPro (2014)	TerraPro Group, Inc.		X	X	X	X	X	X	X
MUD-TRAKS	SVE Portable Roadway Systems (2014)	SVE Portable Roadway Systems	Composite, reinforced fiberglass	X	X	X	X	X	X	
Composite construction mats	Industrial Matting-Composite Mats (2014)	Industrial Matting	Recycled structural composite			X	X	X	X	
I-Trac	Macroplastics (2014a)	MACROPLASTICS	High-impact polypropylene	X	X	X	X	X	X	
Supa-Trac	Macroplastics (2014b)			X	X	X				

surfaced with the individual matting systems, and continuously trafficked with a six-wheel truck carrying a 7-ton payload. Total earth pressure cells (EPCs) were installed in the sand subgrade 12 in. below the surface of each tested mat to provide insight on the relationship between mat breakage, surface deformation, and subgrade pressure. Deformation rates were predicted using two best fit equations (Equations 1 and 2) through the measured deformation points of mat systems, where $D_{R\text{-}S}$ = depth of rut on sand subgrade, in., $D_{R\text{-}W}$ = depth of rut on silty clay subgrade, in., P = the number of passes, and C_1 and C_2 are the regression constants.

$$D_{R-S} = C_1[ln(P)] + C_2 \quad (1)$$

$$D_{R-W} = C_1[P] + C_2 \quad (2)$$

Recommendations were presented for the use of each mat system based on rutting and mat breakage. Vertical pressure measurements at one depth did not provide any compelling evidence of correlation for predicting permanent deformations of the subgrade absent other information. The pressure data were largely intended to show how the varying combinations of moduli and dimensional properties of the mat systems could affect confinement and stress states of the supporting material. The authors emphasized the value of instrumentation data for future modeling efforts that could help understand matting behavior.

For airfield applications, products readily available through the commercial industry are limited since some aircraft loads and tire pressures are much higher than conventional vehicle traffic, and there is considerable risk associated with personnel and operation of expensive aircraft. Examples of recent work dedicated to development and testing of commercially available mat systems for use in airfield applications are provided by Anderton and Gartrell (2005), Gartrell (2007), and Gartrell et al. (2009). Full-scale evaluations were conducted on matting systems intended to serve contingency airfield requirements to sustain C-17 and C-130 transport aircraft loads and to mitigate dust at military helicopter landing zones. The work was conducted under the Joint Rapid Airfield Construction (JRAC) Program with its main goal to provide tools and systems for increasing the U.S. military's contingency airfield upgrade and construction capabilities. The Army's capabilities included helipad construction using AM2 and M19 matting. Test sections with subgrades that were constructed to various CBRs and surfaced with different commercially available matting systems

were initially tested under C-130 loads. Those that performed well under C-130 loads were then tested under C-17 aircraft loads on the same subgrade conditions. Instrumentation was installed in one of the soil-support conditions where the three best performing mat systems were subjected to C-17 aircraft loads. Mat system materials included HDPE and fiberglass, with typical commercial applications that included those listed in Table 1. Some of the systems were recommended for helipad construction, and others showed potential for C-130 and C-17 operations if recommended modifications to the configurations or connections were made.

More recently, the U.S. Air Force initiated a program, called the AMX program, which focused on developing and testing airfield matting prototypes that could potentially replace AM2 for airfield expansion. The work conducted pertains to the information obtained for developing this report. The intent of the program is for mats to be lighter and thinner than AM2, but be able to sustain the load carrying capabilities of AM2 under both F-15E and C-17 aircraft traffic. To determine the requirements for the lightweight mats, AM2 was tested over various subgrade strengths (i.e., CBRs of 6, 10, 15, 25, and 100) to determine the sensitivity of the mat's performance to changes in subgrade strength under present day controlling aircraft (Rushing and Tingle 2007; Rushing et al. 2008; Rushing and Mason 2008; Garcia et al. 2014a; Garcia et al. 2014b). New systems are required to meet or exceed the performance of AM2.

As part of the program, M19 was also tested on a CBR of 6 to determine the suitability of aluminum honeycomb technology for modern aircraft (Rushing and Tingle 2007). During the study, several prototypes were tested in full-scale. Lightweight composite material prototypes, such as carbon fiber (Foster and Anderson 2003), and new welding techniques recently introduced into the inventory of potential mat designs were evaluated. Additionally, systems manufactured and used by the allied nations of the U.S. were tested, since recent operations in foreign environments have introduced the U.S. Military to expedient surfaces that have not been independently evaluated under modern aircraft by the U.S. military. Many nations use the Faun Trackway aluminum systems (Rushing et al. 2012; Rushing et al. 2014), including the Military Load Class (MLC) 70 matting system, for aircraft operations. The system had previously been tested by Burgmann and Ingebretson (1969) under tank traffic and by Rollings (1975) as a bomb damage repair option for F-4 fighter aircraft when it was formerly called the MLC-60 matting system.

However, the information obtained from these sources failed to address the current operational needs, i.e., F-15E and C-17 traffic.

2.3 Airfield mat modeling and behavior prediction approaches

To evaluate matting systems such as those discussed thus far, the most common approach has been to build a full-scale test section with a controlled subgrade overlaid by a matting surface that is trafficked to failure using simulated loads. Although this has provided a realistic performance measure, full-scale testing of matting systems is costly. Therefore, a few more recent efforts have used full-scale data to develop techniques for predicting airfield matting behavior through different approaches. The following paragraphs summarize recent characterization research.

Gonzalez and Rushing (2010) used a stress-based approach to develop a mechanistic model for the purpose of predicting passes-to-failure of a mat system based on subgrade strength in terms of CBR. They used a simple bending test setup described by Berney et al. (2006) and a finite element implementation of the Mindlin plate solution (Mindlin 1951) for determining the unit section modulus ($E_c^{NJ(2)}$) of different mat systems. $E_c^{NJ(2)}$ is the overall material resistance to deflection not considering joint properties. An overall composite modulus including the joint ($E_c^{J(2)}$) was also determined and included in the analysis.

The test method of Berney et al. (2006) involved placing a panel on a simply supported beam setup with four deflection gauges placed underneath the mat panel while being loaded with blocks of known weights (Figure 3). A steel C-section served as a load distributor. Deflection data were recorded continuously by a computer program for the duration of the test to capture the responses of the mat panels during all loading and unloading cycles. Mats were tested in single and multiple panel configurations to evaluate the influence of the panel joint system.

After deflection data were collected, Gonzalez and Rushing (2010) back calculated the flexural rigidity of each mat using the finite element implementation of the Mindlin plate solution. Data that included the mat panel dimensions, plate areas in contact with the supports (beams), load distribution area, maximum applied load, Poisson's ratio, and modulus ($E_c^{NJ(2)}$ or $E_c^{J(2)}$) were input into the model. $E_c^{NJ(2)}$ or $E_c^{J(2)}$ and the Poisson's ratios were varied until the model deflection in the center of the panel was

equal to the one measured as shown in Figure 3. A corresponding flexural rigidity was then chosen from the results of the model. Using the measured properties of the mat systems, the maximum deviatory stress in the subgrade below the mats was determined using the ERDC layered elastic analysis computer program, WINJULEA. The maximum deviatoric stress was then related to known mat performance (i.e., passes to failure) to develop the performance criteria for the design methodology. Full-scale instrumented test section data for the AM2 and M19 matting systems and mats tested by Anderton and Gartrell (2005) were included in the Gonzalez and Rushing (2010) data set.

Figure 3. Simply supported beam test setup used for determining $E_c^{NJ(2)}$.

Doyle et al. (2014) performed three-dimensional finite element analysis (FEA) modeling on instrumented test sections described by Gartrell (2007) and Anderton and Gartrell (2005). Material property inputs for the mat systems evaluated included the composite modulus absent of the influence of joints (E_c^{NJ}) and an overall composite modulus including joints (E_c^{J}) as determined by the test setup and an FEA back-calculation procedure described by Berney et al. (2006).

Berney et al. (2006) used load-deflection data from the setup shown in Figure 3 to determine the unit section modulus of different mats using an FEA program called STUBBS. Mats were modeled as simply supported plane strain beams that were assumed to be 1-in. thick. A Poisson's ratio

was initially set for the analysis, and a trial-and-error procedure was used by changing the Young's modulus (E_c^{NJ} and E_c^J). The unit section modulus was calculated by running the program and matching the center deflection of the model to the center deflection obtained in the test for the first applied load.

ABAQUS 6.10-2 was used by Doyle et al. (2014) for developing and analyzing the FEA models intended for characterizing mat performance. Since E_c^{NJ} and E_c^J were used to represent matting systems, consideration of structural degradation of the mats and increase in deformation were not considered by the analysis. EPC data recorded during the first few passes of the full-scale tests were used for model calibration and other guidance. Simulations were performed for each combination of mat system, load application location, and soil modulus input. Although FEA modeling provided reasonable predictions of soil response in some cases, it was considerably less effective for thin composite matting systems with the inputs available. FEA modeling was recommended as a preliminary tool to be used prior to full-scale testing.

Rushing and Howard (2015) developed an empirical method for characterizing rutting resistance of the AM2 mat system. Data collected from full-scale testing of AM2 over CBRs of 6, 10, 15, 25, and 100 were used to develop correlations between subgrade soil deformation rate, number of applied F-15E passes, and underlying soil's CBR. Flexural properties of AM2 were determined by a 3-point bending test using a universal testing machine where load and vertical displacement were measured. Linear regressions were initially fitted to the measured subgrade deformation (δ_s) data collected for each test as a function of simulated F-15E aircraft passes (i.e., $y = m^*\log_{10}(x)$), where $y = \delta_s$, in., m = regression constant, and x = number of passes). The equations were then used to relate δ_s to subgrade CBR. The result was a power function that allows the approximation of δ_s for a given subgrade strength and number of passes. The simplified expression below (Equation 3) was developed, where δ_s = the subgrade deformation, in., P = the number of passes, and CBR is the strength of the subgrade underneath the structural mat system.

$$\delta_s = log_{10}P * 1.64 * CBR^{-0.61} \quad (3)$$

A set of design curves (Figure 4) were developed as an alternative to Equation 3, so a user can quickly determine an approximate answer.

Figure 4. AM2 subgrade deformation predictions for a given number of passes and CBR (Rushing and Howard 2015).

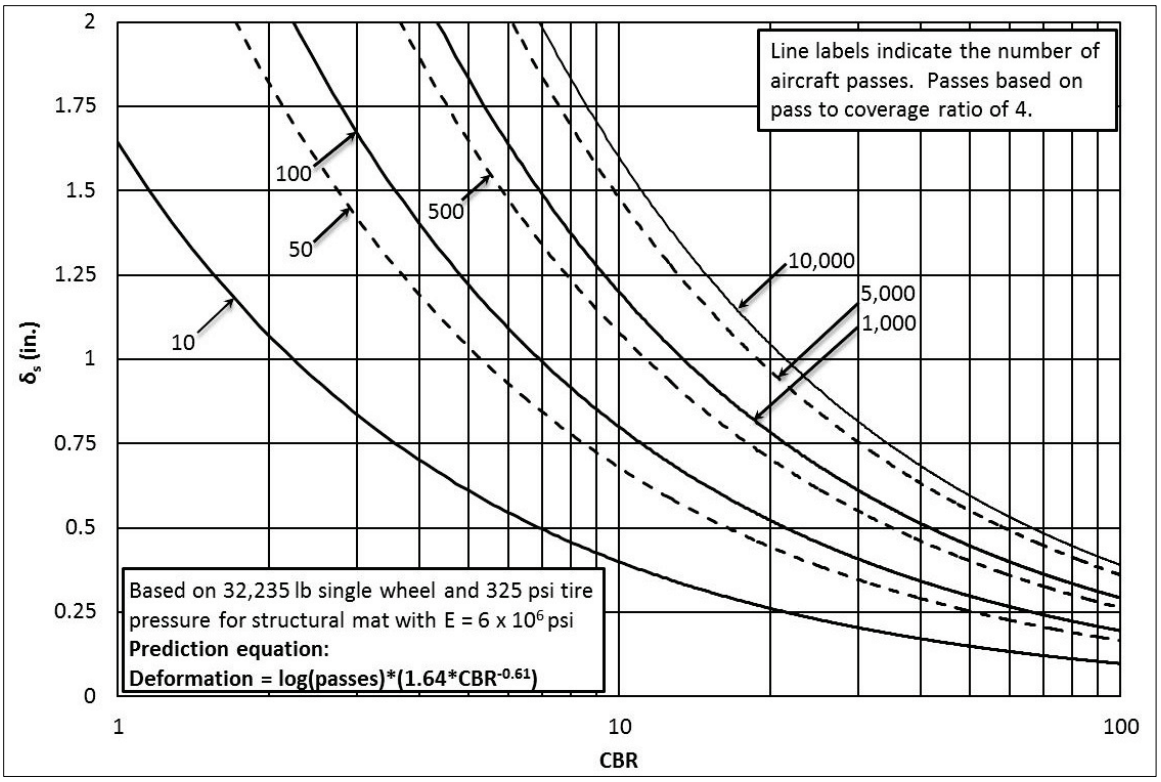

2.4 Summary of literature review

This chapter reviewed mat development and testing and the most recent progress in characterizing mat performance. Gonzalez and Rushing (2010) and Doyle et al. (2014) presented comprehensive approaches, but the techniques lacked a direct correlation to failure components, i.e., mat breakage and permanent deformation. Of the methods discussed, those by Rushing and Howard (2011; 2015) are the most directly applicable to the work discussed herein. Rushing and Howard (2011) developed an empirical technique for predicting surface deformation and furthered their analysis by using instrumentation measurements, but the study focused on matting for roadways. Rushing and Howard (2015) used full-scale data from simulated F-15E traffic tests, but limited their study to AM2 and did not incorporate measured earth pressure for relating mat modulus to confinement provided by the system. Components of both of these approaches were adopted for the work and analysis presented herein.

3 Materials and Test Sections

The six mat systems considered were described in three ERDC technical reports written between 2007 and 2012.

3.1 Materials

Pertinent properties of all matting systems tested are shown in Table 2. The composite modulus ($E_c^{NJ(2)}$) is the overall material resistance to deflection and is currently one of the most reasonable measures available of each mat's elastic properties. $E_c^{NJ(2)}$ was determined using the back-calculation procedure described by Gonzalez and Rushing (2010) and the test setup described by Berney et al. (2006).

Table 2. Properties of mats tested.

Mat	L (in.)	W (in.)	t (in.)	D (psf)	$E_c^{NJ(2)}$ (ksi)	Source of $E_c^{NJ(2)}$
AM2	144.0	24.0	1.50	6.10	3,970	Gonzalez and Rushing (2010)
M19	50.2	49.5	1.50	4.30	500	Gonzalez and Rushing (2010)
Carbon Fiber Composite	84.0	50.0	1.25	4.26	2,455	Rushing et al. (2011)
Aluminum Honeycomb Composite	104.0	42.0	1.25	4.02	2,420	Rushing et al. (2011)
MLC-70 Trackway	180.0	9.0	1.25	6.55	550	Rushing et al. (2012)
Aluminum Truss	104.0	21.0	1.2	5.70	---	---

L = length of one panel; *W* = width of one panel; *t* = thickness; *D* = unit weight; $E_c^{NJ(2)}$= composite modulus

Gonzalez and Rushing (2010) included AM2 and M19 in their analysis and published values of $E_c^{NJ(2)}$ for both systems. Rushing and Howard (2015) published flexural properties for AM2, but they were not used for the analyses for consistency with information available for the other mats. For the Carbon Fiber Composite and the Aluminum Honeycomb Composite mat systems, Rushing et al. (2011) conducted the tests described by Berney et al. (2006) and analytical procedure described by Gonzalez and Rushing (2010) individually and reported their values in the publications shown in Table 2. The same was conducted for the MLC-70 Trackway system by

Rushing et al. (2012). The Aluminum Truss mat was a second generation prototype, therefore, $E_c^{NJ(2)}$ was not measured as part of the test program.

3.1.1 AM2 matting

The AM2 Mod 5 airfield mat is the primary expeditionary airfield surfacing used by the U.S. military. Each panel is fabricated from a single 6061-T6 aluminum alloy extrusion with welded end connectors. The mat is also made in half-panels to allow placement of a staggered brickwork configuration. Panels are joined along the two long edges by a hinge-type male/female connection. The adjacent short ends are joined by an overlap/underlap connection secured by an aluminum locking bar. Each panel is coated with a non-skid material to increase the surface friction. A photograph of a stack of AM2 panels placed on an assembled AM2 mat surface is shown in Figure 5.

Figure 5. AM2 mat stack.

3.1.2 M19 matting

M19 aluminum matting has panels nearly square that consist of a honeycomb core made of 0.125-in. hexagonal cells of aluminum foil. The core is bonded top and bottom to rolled-aluminum sheets by an epoxy adhesive. The edge connectors are welded to the top and bottom sheets and bonded with a potting compound to the core. Panels are joined along two edges by a hinge-type male/female connection. The other two edges consist of overlap/underlap end connectors that are secured by an aluminum locking

bar, much like AM2. The panels are coated with a non-skid material to increase surface friction. M19 mat used for testing was purchased from war reserve material stockpiles, so the history of the purchased mat was unknown. However, the mat was visually inspected and seemed to be in good structural condition. There were no cracked welds, nor was there any deformation. A photograph of an M19 aluminum mat panel is shown in Figure 6.

Figure 6. M19 mat panel.

3.1.3 Carbon Fiber Composite matting

The Carbon Fiber Composite mat system panels are composed of carbon fiber top and bottom skins and a foam-filled carbon fiber core. The core is constructed with vertical carbon fiber stiffeners spanning perpendicular to each other. Panels are connected on each edge by aluminum extrusions that are designed to accept an H-shaped nylon locking bar. The top and bottom skins of the individual panels are bonded by an epoxy adhesive to the aluminum extrusions. The nylon locking bars are designed to fit individually along longitudinal joints and stagger along continuous transverse joints so the system could be constructed in a brickwork configuration. The panels are coated with a non-skid material to increase the surface friction. A photograph of a stack of Carbon Fiber Composite mat panels is shown Figure 7.

Figure 7. Carbon Fiber Composite mat panels.

3.1.4 Aluminum Honeycomb Composite matting

The Aluminum Honeycomb Composite mat system panels have an aluminum honeycomb core made of 0.125-in. hexagonal cells of aluminum foil. The mat was made to resemble M19 in its honeycomb structure. The core is bonded to top and bottom skins by an epoxy adhesive. The top and bottom skins are composed of a carbon fiber sheet sandwiched between two aluminum sheets. The mat is framed with welded aluminum connector rails. The connection along the long dimension of the mat is a hinge-type male/female system similar to that of AM2. The short ends are connected by H-shaped nylon locking bars similar to the Carbon Fiber Composite mat system. A photograph of an Aluminum Honeycomb Composite mat panels' stack is shown in Figure 8.

3.1.5 MLC-70 Trackway matting

The MLC-70 Trackway matting system was developed in the 1960s to create temporary roadways for heavy military vehicles used by the United Kingdom Ministry of Defense. Each panel is made from a single aluminum extrusion. When the panels are assembled in an array, they can be rolled up for storage and transportation. The connection system along the long dimension is a male/female t-slot. To join the panels, the male edge is slid into the female edge of the adjoining panel. Shoot bolts are inserted into slots in the male edge of the panel to prevent lateral movement of the panels along each row. No connection system is included along short edges. A photograph of bundles of MLC-70 Trackway mat panels is shown in Figure 9.

Figure 8. Aluminum Honeycomb Composite mat panels.

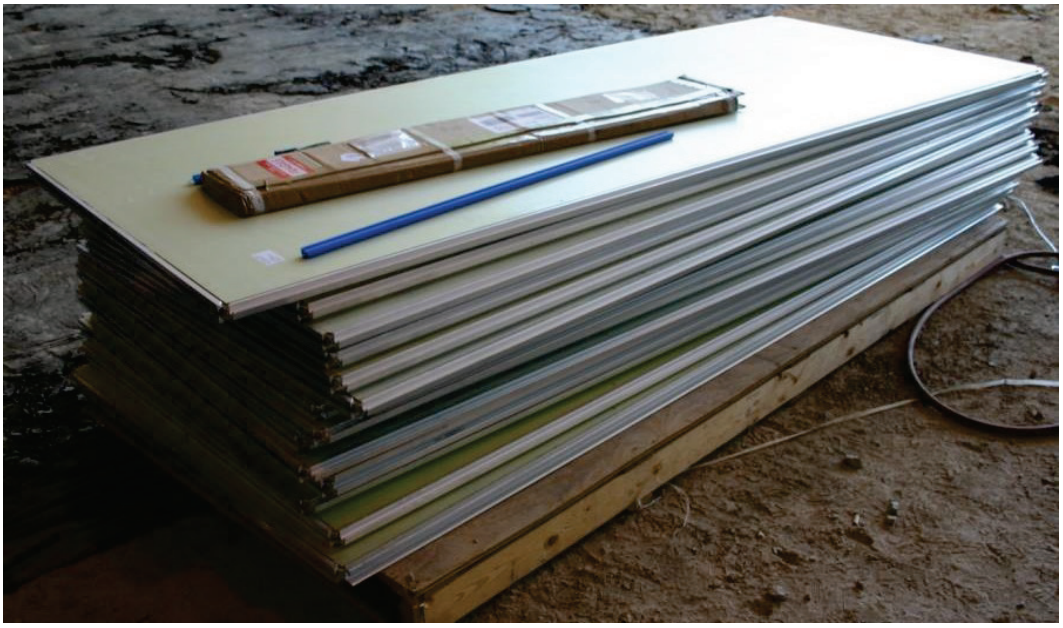

Figure 9. MLC-70 Trackway panels bundled for transport.

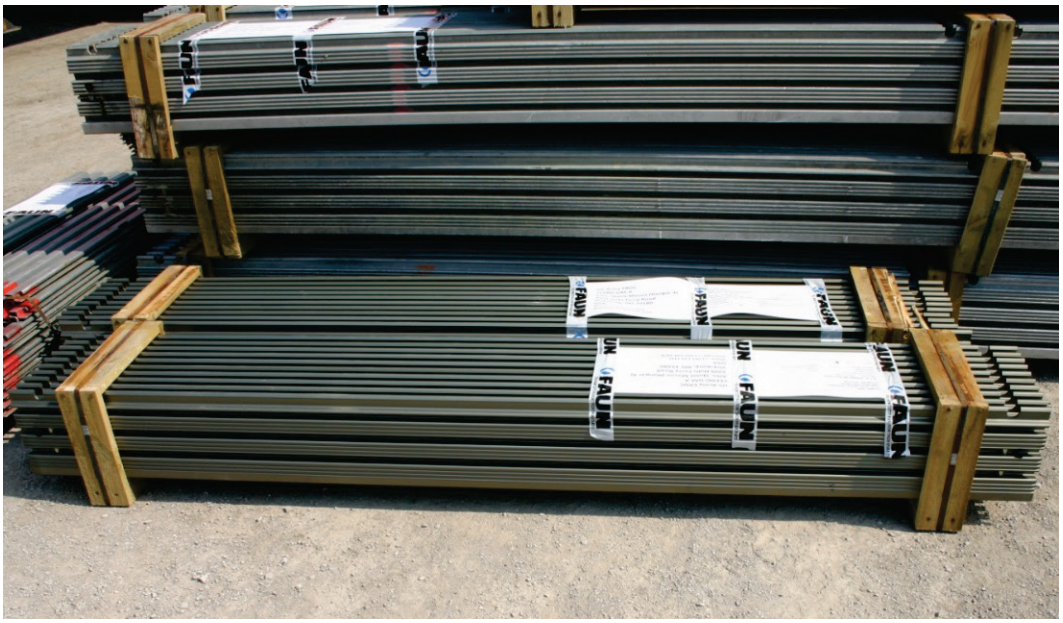

3.1.6 Aluminum Truss matting

The Aluminum Truss system is a second generation prototype. Mat panels are made from two aluminum extrusions with isosceles triangle cross sections that are friction stir welded together. The connectors along the short ends of each panel are hand welded to the extrusions to create a single panel. Panels are connected on the short end by a double-arrow-shaped locking key inserted into connector slots in the welded end

connectors. The connection along the long dimension is a hinge-type male/female system similar to that of AM2. A photograph of an Aluminum Truss mat panel is shown in Figure 10.

Figure 10. Aluminum Truss mat panel.

3.1.7 Subgrade soil

Each full-scale test section incorporated a high-plasticity clay, which classifies as a CH according to the Unified Soil Classification System, subgrade constructed to a CBR of 6 ± 1. The CH was procured from a local source in Vicksburg, MS and is commonly referred to as Vicksburg Buckshot clay. Moisture content-density and moisture content-CBR relationships were established through laboratory testing (ASTM D1557 and ASTM D1883). These data were used to determine the target moisture content and dry density (Table 3) required to obtain the target CBR of 6 ± 1. Compaction and moisture content-CBR curves for a representative batch of material are shown in Figures 11 and 12, respectively. Table 3 shows classification data for the soil determined according to ASTM D422, ASTM D4318, and ASTM D2487. Although slight variations may have occurred between batches procured for each test, the relationships shown in Figures 11 and 12 and the values shown in Table 3 are typical, representative properties of the soil.

Table 3. Properties of soil conditions tested.

Description	Vicksburg Buckshot Clay
Color	Gray
USCS Group Classification	CH
LL	77
PL	27
PI	50
Max DD, kg/m³ (pcf) [a]	1,670 (104)
OMC, %	19.4
Fines (%)	90
% Clay	46
G_s	2.74
MC for CBR of 6, %	34 ± 2
DD for CBR of 6, kg/m³ (pcf)	1,377 (86)

Note: DD = dry density; OMC = optimum moisture content; CBR = California Bearing Ratio; G_s = specific gravity.

[a]ASTM D1557.

Figure 11. Compaction curve for CH subgrade material.

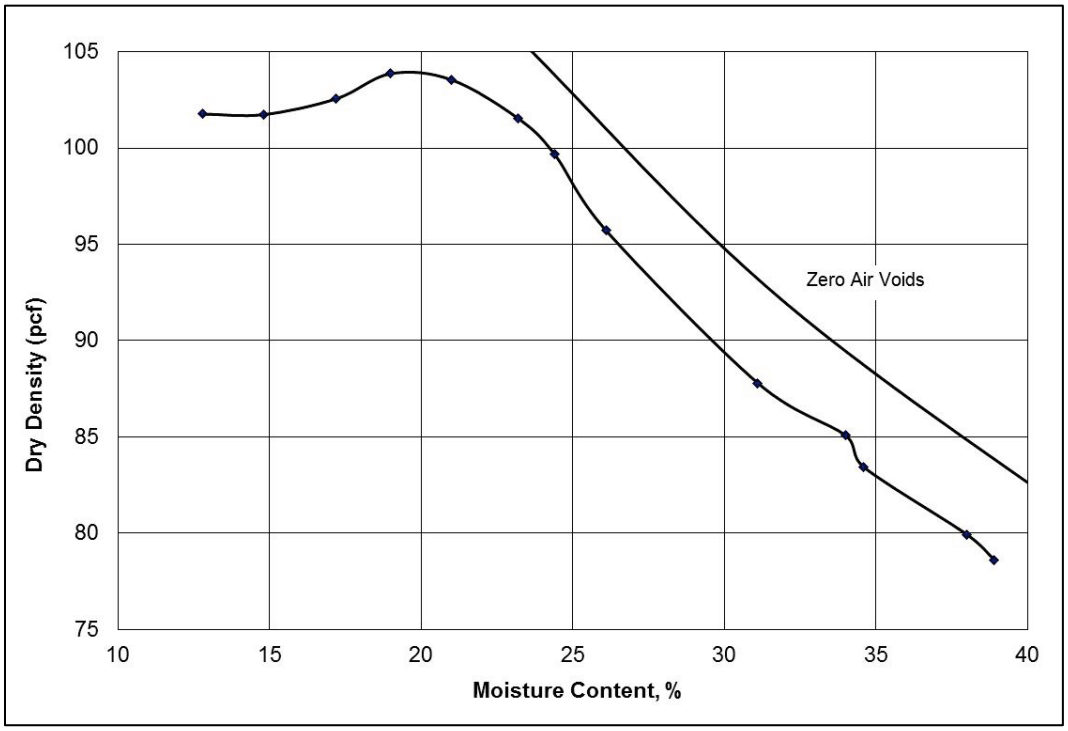

Figure 12. CBR vs. moisture content for CH subgrade material.

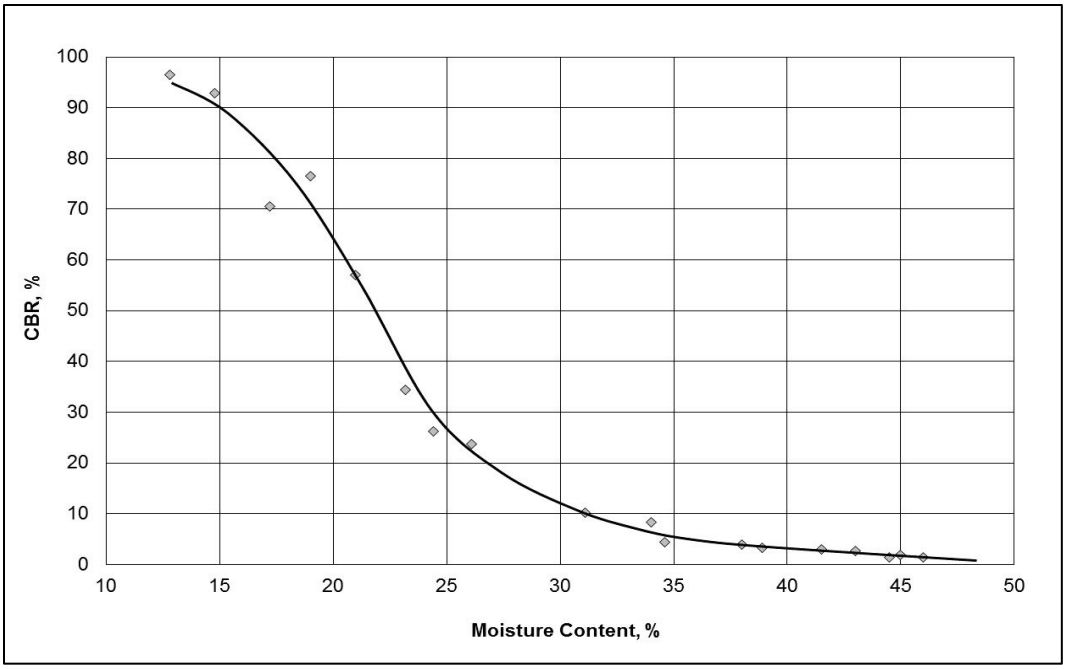

3.2 Descriptions of test sections

Evaluations were conducted on full-scale test sections constructed and trafficked under shelter in the Hangar 4 pavement test facility at ERDC in Vicksburg, MS. The following paragraphs describe the individual test sections, including mat panel layouts and designated traffic lane(s). Each mat surface was placed on a CH subgrade constructed to a CBR of 6 over a low-plasticity silt (ML) foundation having a CBR less than 20. Panels in each test section, except for MLC-70 Trackway panels, were identified with a number to track damage during trafficking. Table 4 summarizes test section geometry for each mat experiment. Each mat surface was subjected to simulated F-15E traffic in a normally distributed wander pattern, as described in Chapter 4.

Table 4. Test section geometry for each mat experiment.

Mat	Subgrade Depth (ft)	Dimensions[a]	
		L (ft)	W (ft)
AM2	5	40	22
M19	5	40	22
Carbon Fiber Composite	3	34	21
Aluminum Honeycomb Composite	3	28	26
MLC-70 Trackway	3	40	24
Aluminum Truss	2	14	22

[a]Dimensions of F-15E item if section had two test items.

3.2.1 AM2 test section

The AM2 test section consisted of a 60-ft-wide by 40-ft-long section of matting that was subsequently divided into two test areas (defined as "test items") that were subjected to different traffic conditions. A 22-ft-wide item had a lane at its center that was designated for simulated F-15E traffic. A 38-ft-wide item had a lane at its center that was designated for simulated C-17 traffic. Each test item was named according to the simulated aircraft loads it was subjected to (e.g., F-15E item). Data collected from the C-17 item were not used for the purpose of this report. The test section CH subgrade was 5 ft deep. Panels were assembled in a brickwork pattern, as shown in Figure 13.

3.2.2 M19 test section

The M19 test section had a 5-ft-deep subgrade that was surfaced with a 60-ft-wide by 40-ft-long section of M19 matting assembled in a brickwork pattern. The section was then divided into two test items, an F-15E item and a C-17 item. The F-15E item was 22 ft wide and had a lane designated for simulated F-15E traffic at its center. The C-17 item was 38 ft wide and was subjected to simulated C-17 traffic at its center. Only the data collected from the F-15E item were used for analysis. A layout of the test section is shown in Figure 14.

3.2.3 Carbon Fiber Composite test section

The Carbon Fiber Composite mat panels were assembled on a 3-ft-deep subgrade. The mat surface was 21 ft wide by 34 ft long and was assembled in a brickwork pattern. The center of the test section had a lane designated for simulated F-15E traffic. A layout of mat panel placement is shown in Figure 15.

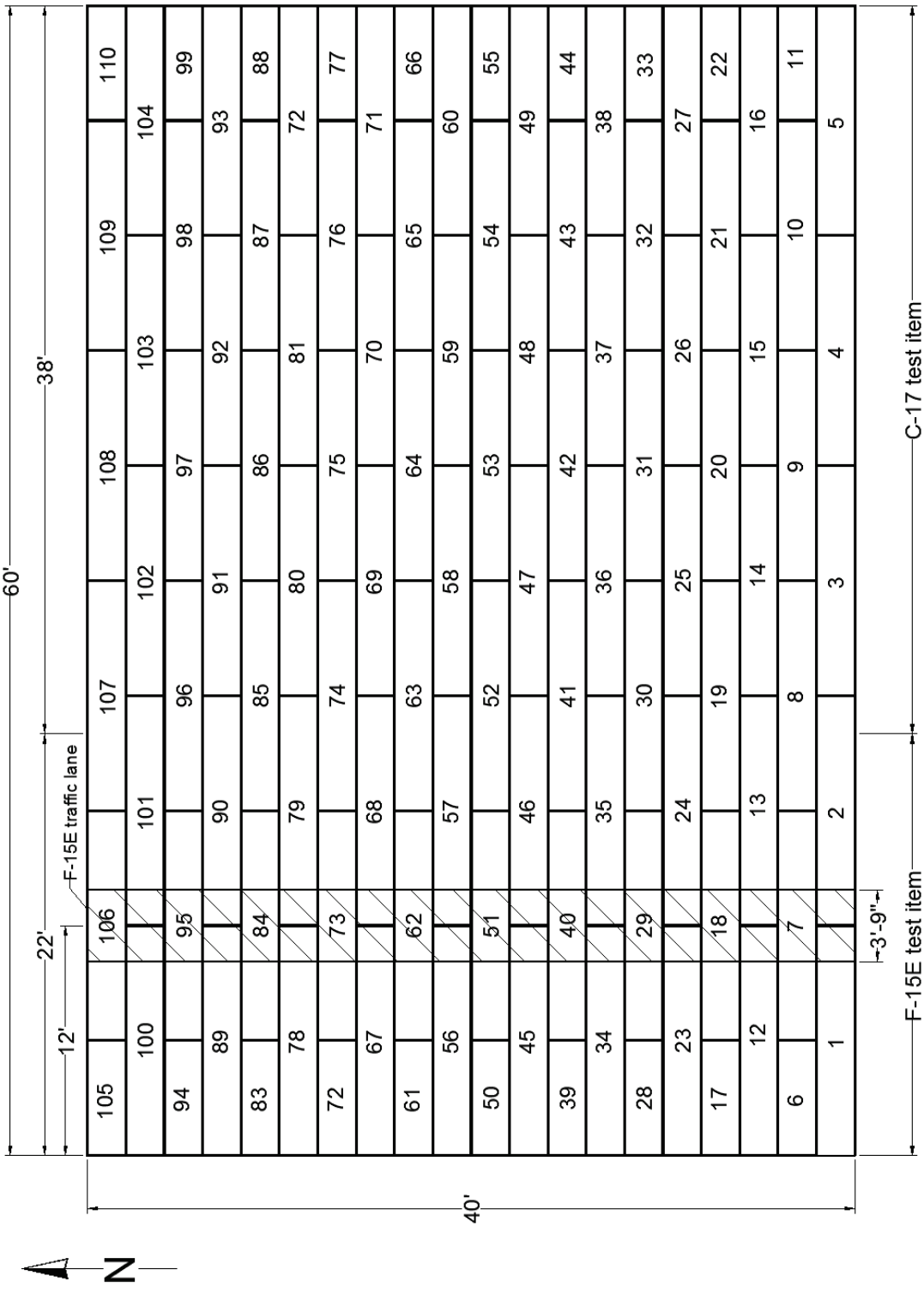

Figure 13. Plan view of AM2 mat panel layout.

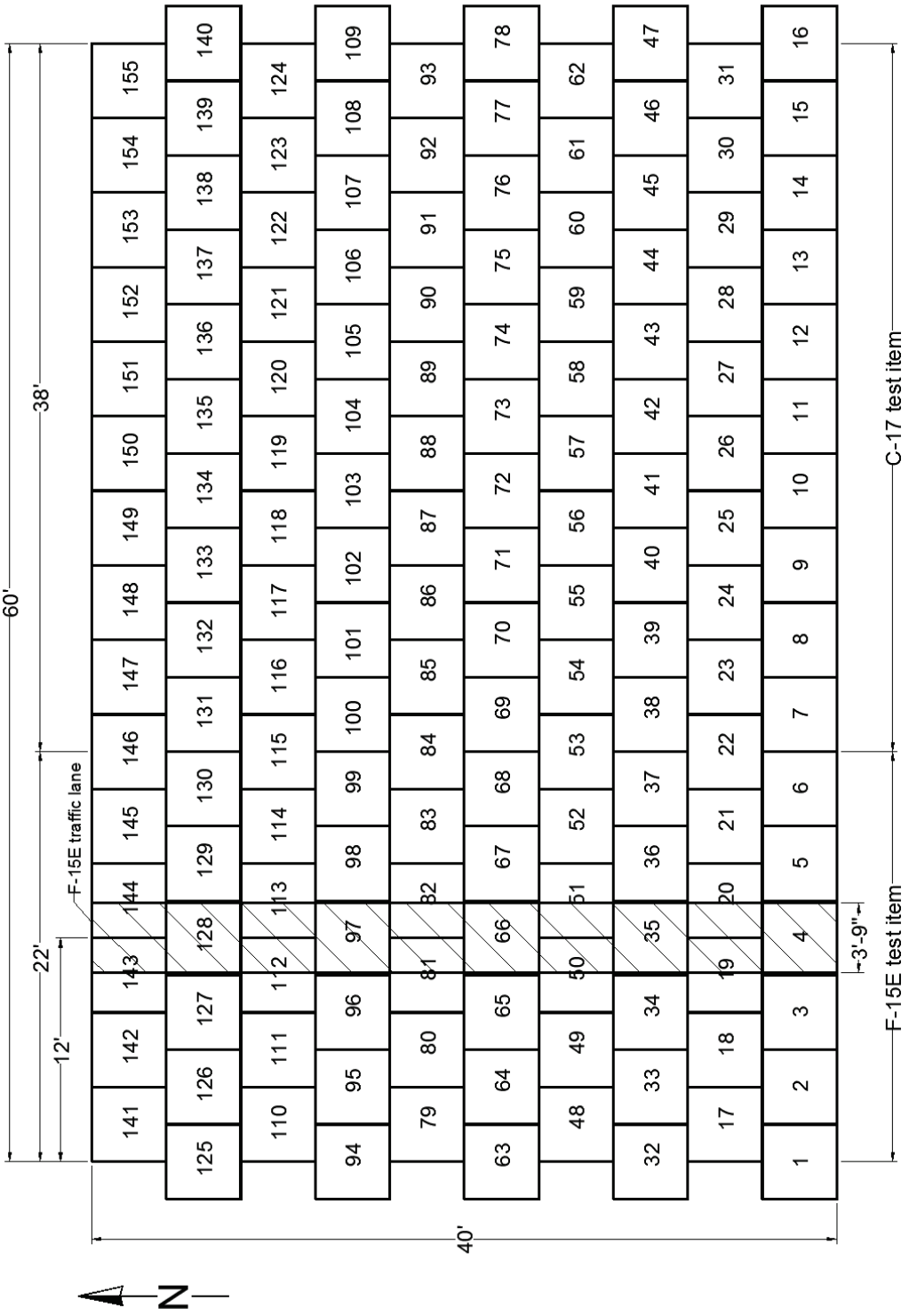

Figure 14. Plan view of M19 mat panel layout.

Figure 15. Plan view of Carbon Fiber Composite mat panel layout.

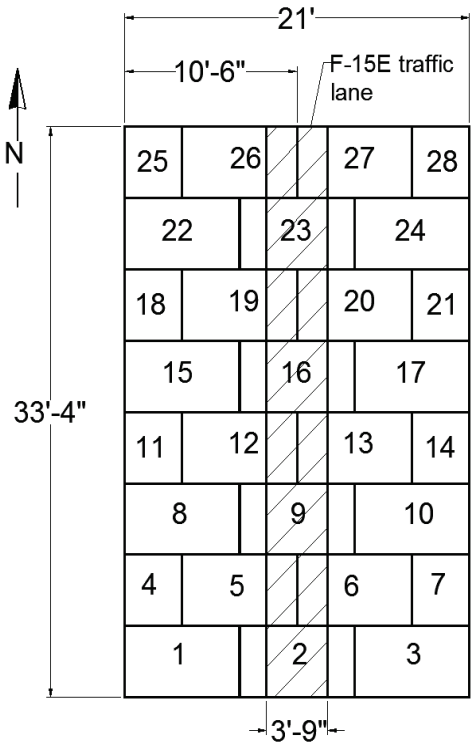

3.2.4 Aluminum Honeycomb Composite test section

The Aluminum Honeycomb Composite mat panels were assembled next to the Carbon Fiber Composite assembled mat surface on the same test subgrade. The assembled panels formed a 26-ft-wide by 28-ft-long mat surface that had a lane at its center for simulated F-15E traffic. A layout of the assembled section, also in a brickwork pattern, is shown in Figure 16.

3.2.5 MLC-70 Trackway test section

The subgrade for the MLC-70 Trackway test section was 3 ft thick. The test section consisted of a 60-ft-wide by 40-ft-long section of matting that was subsequently divided into a 24-ft-wide and a 36-ft-wide test item. The center of the 24-ft-wide item had a traffic area designated for simulated F-15E traffic. The center of the 36-ft-wide item had a traffic area designated for simulated C-17 traffic. Data relative to the C-17 item were not used. A layout of the test section is shown in Figure 17.

Figure 16. Plan view of Aluminum Honeycomb Composite mat panel layout.

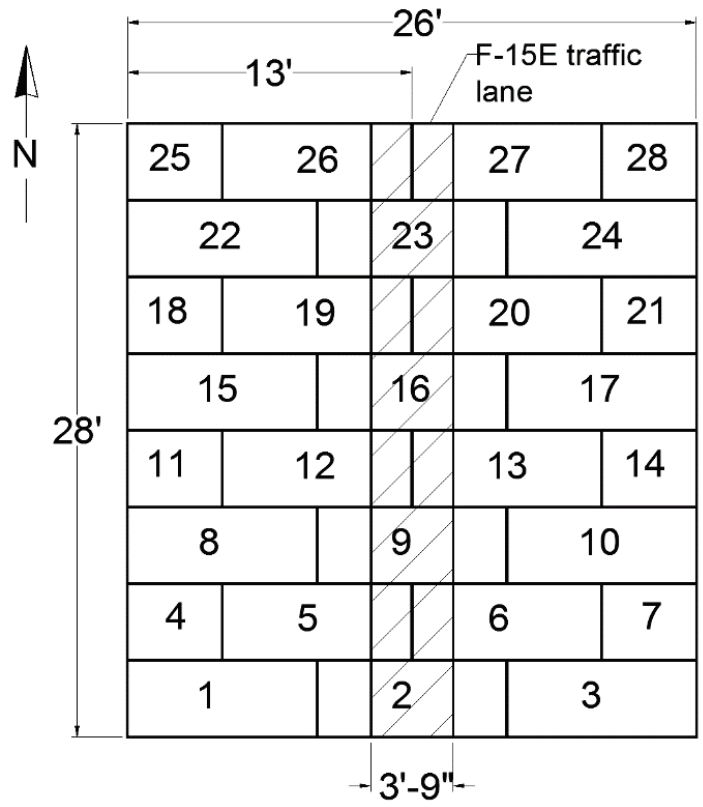

3.2.6 Aluminum Truss test section

To determine if the Aluminum Truss system would benefit from a reduced number of in-line end joints directly in the traffic pattern, two panel configurations were designed. The first assembly was a traditional brickwork pattern made of full and half panels. The second pattern was made of a combination of three different size panels. Only the data obtained for the brickwork pattern (Figure 18) were used for comparison to the other systems presented in this report. The assembled brickwork pattern mat surface was 22 ft wide by 14 ft long and was placed on a subgrade with a thickness of 2 ft. The center of the section had a lane for simulated F-15E traffic.

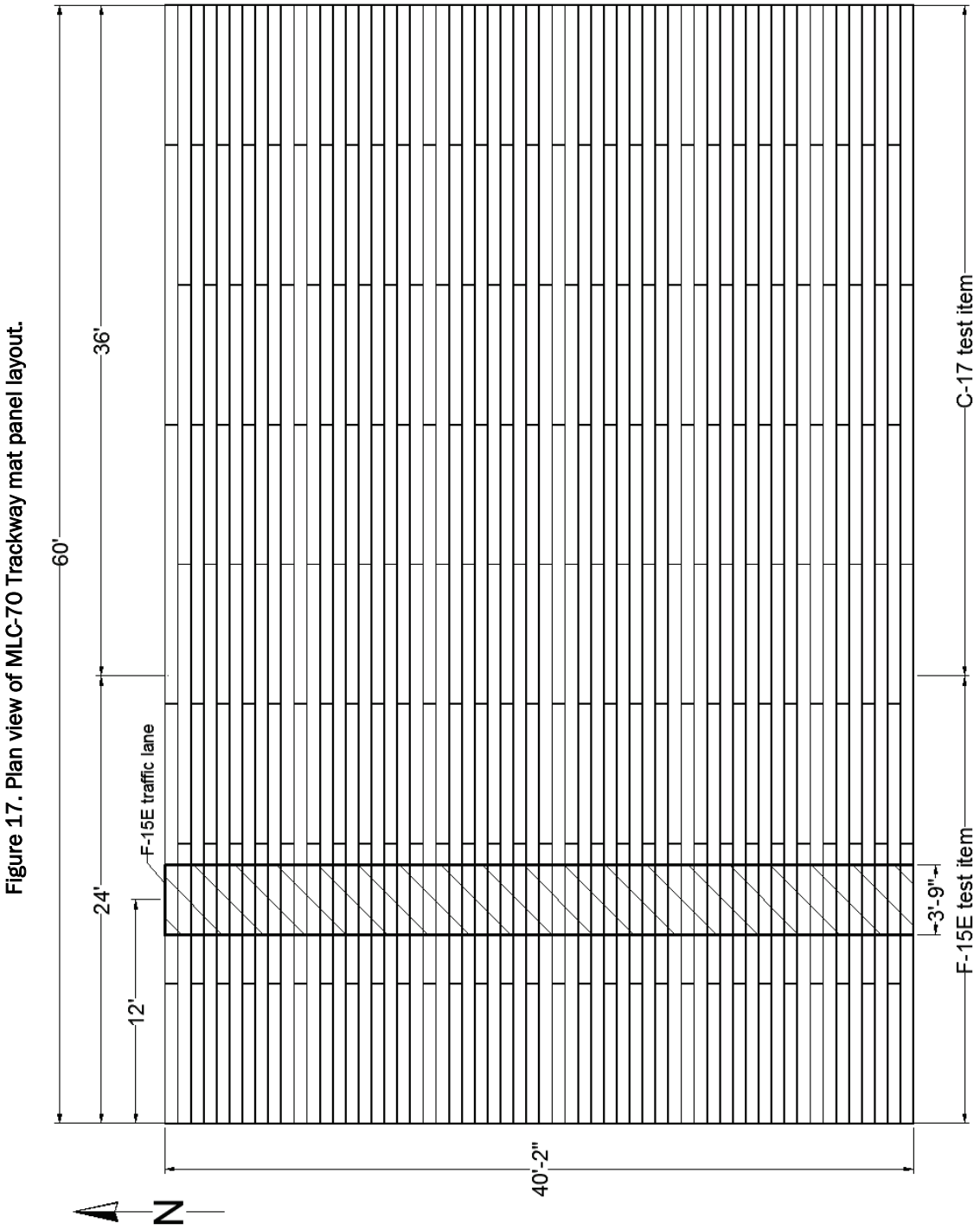

Figure 17. Plan view of MLC-70 Trackway mat panel layout.

Figure 18. Plan view of Aluminum Truss mat panel layout.

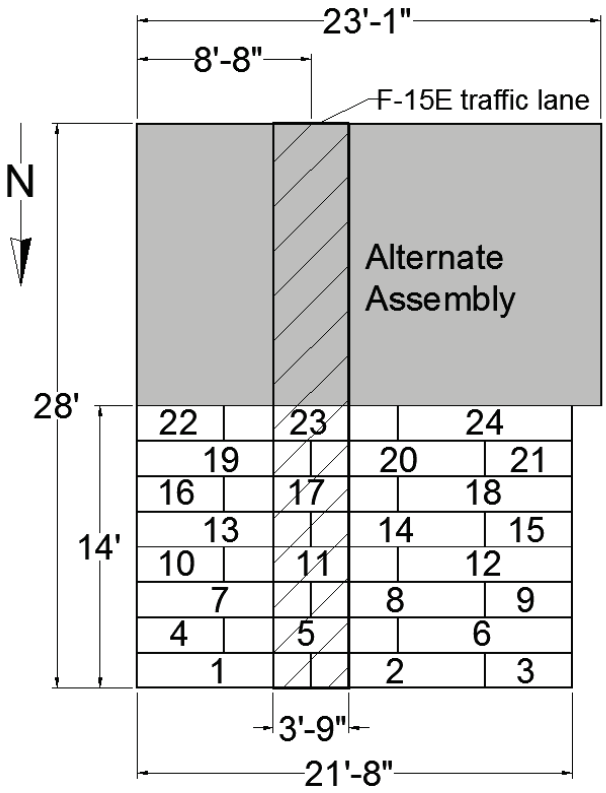

3.3 Construction of test sections

The following describes test section construction, including subgrade, instrumentation installation, and mat installation. Subgrade construction generally involved the same material processing procedures, compaction methods, and field quality control tests for each evaluation. To minimize costs, the subgrades for three test sections (M19, MLC-70 Trackway, and Aluminum Truss) were prepared from the remains of test beds used for other evaluations that were constructed using the same material and methods described herein.

3.3.1 Subgrade construction

The subgrade for each test was constructed below the finished grade of a covered facility. A test pit was excavated according to the dimensions required for the test. The soil at the bottom of the excavated pit (i.e., below the subgrade) was an ML having a CBR less than 20. A general profile of the foundation of each test is shown in Figure 19. The subgrade thickness for each test is provided in Table 4.

Figure 19. General profile of test sections.

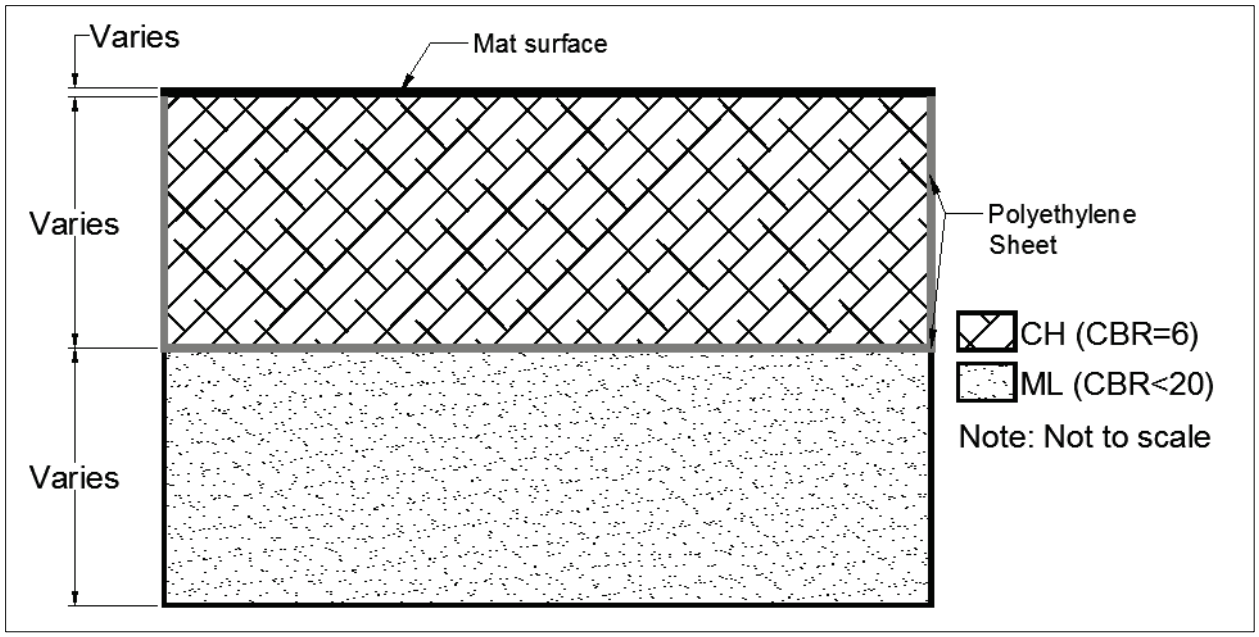

The existing ML material was leveled with a bulldozer and compacted with pneumatic roller and vibratory steel-wheel compactors to ensure that the remainder of the test section was constructed over a stable foundation. The bottom and sides of the test pit were lined with impervious 6-mil-thick polyethylene sheeting to minimize moisture migration from the CH soil serving as the test section subgrade.

The CH was processed at a nearby preparatory site by spreading the material to a uniform 12-in. thickness, pulverizing the material with a rotary mixer, adjusting the moisture content, pulverizing the material again, and stockpiling the material. This was an iterative process necessary to achieve a uniform distribution of moisture throughout the material. Once the CH had been processed to the target moisture content, it was placed in the test section, spread by a bulldozer in 8-in. lifts, and compacted with a pneumatic roller to a thickness of 6 in. Each compacted lift was subjected to the test methods listed in Table 5 to verify that target values had been met. Generally, these test methods were conducted at two to three locations along the centerline of the test section, and measurements were averaged to report one value for each lift. For sections having two test items (as defined in Section 3.3.2), the tests were conducted beneath the centerline of both test items, and one value was reported for each test item.

Table 5. Field tests on each constructed lift.

Test Name	Test Designation
Standard Test Method for In-Place Density and Water Content of Soil and Soil-Aggregate by Nuclear Methods (Shallow Depth)	ASTM D 6938
Standard Test Method for Laboratory Determination of Water Content of Soil and Rock by Mass	ASTM D 2216
Standard Test Method for Determining the California Bearing Ratio of Soils	CRD-C 654-95

If the average pretest CBR of a lift was not between 5 and 7, the lift was removed and reprocessed. Each lift was surveyed to obtain an average thickness. After data collection and prior to placement of the following lift, the surface was scarified to an average depth of 1 in. with a rotary mixer to facilitate interface bonding.

For the M19 test section, the same subgrade test bed used for the AM2 test section was used after completing the AM2 mat evaluation. The upper 12 in. of the subgrade material were removed, and newly processed CH soil was placed in two lifts and compacted to restore the 6 CBR strength. Each newly compacted lift was subjected to the methods listed in Table 5. The same approach was taken for the MLC-70 Trackway test section. The subgrade was originally constructed for the Carbon Fiber Composite and Aluminum Honeycomb Composite test sections, and the top 12 in. were removed and replaced with newly processed material. For the Aluminum Truss test section, the subgrade was originally constructed to a CBR of 6 for a roadway test section described by Bell and Mason (2012) and was reused for testing the Aluminum Truss system. In situ CBR tests were conducted on the surface and showed that the material retained a CBR value within acceptable limits, i.e., between 5 and 7. Photographs of the general construction process are shown in Figures 20 through 25. Subgrade properties prior to installing matting on each test section are in Table 6. Once trafficking was completed, posttest forensics were conducted to determine the depth of subgrade that might have undergone gradual drying and possible densification under traffic. Some decreases in moisture and increases in CBR were expected. Subgrade properties after completing each test are in Table 7.

Figure 20. Test pit lined with polyethylene sheeting.

Figure 21. Pulverizing CH with rotary mixer.

Figure 22. Adding water to CH to adjust moisture content.

Figure 23. Compacting CH.

Figure 24. In situ CBR test.

Figure 25. In situ CBR test dial gages.

Table 6. In-place properties of constructed subgrades prior to installing mats.

Test Depth Below Subgrade Surface	Nuclear Gage Test			CBR Test	
	Wet Density, pcf	Dry Density, pcf	Moisture,%	Moisture, %	CBR
AM2					
Surface	118.4	90.5	30.8	35.1	6.0
6 in.	119.7	91.9	30.3	33.3	5.9
12 in.	119.3	92.0	29.7	33.4	6.2
18 in.	118.3	90.6	30.6	33.2	6.1
24 in.	119.4	91.3	30.8	33.5	6.0
30 in.	116.0	88.4	31.4	32.3	5.7
Average	*118.5*	*90.8*	*30.6*	*33.5*	*6.0*
M19					
Surface	118.8	92.2	28.9	32.9	6.5
6 in.	116.4	88.9	30.9	32.7	5.4
Average [a]	*118.0*	*90.6*	*30.4*	*33.0*	*6.0*
Carbon Fiber Composite					
Surface	118.4	91.4	29.6	33.4	5.8
6 in.	119.4	92.1	29.6	33.6	6.1
12 in.	119.7	93.8	29.7	31.1	6.1
18 in.	120.5	93.9	28.3	31.0	6.2
24 in.	119.4	91.3	30.7	32.4	5.5
Average	*119.5*	*92.5*	*29.6*	*32.3*	*5.9*
Aluminum Honeycomb Composite					
Surface	118.5	91.9	28.9	33.3	5.7
6 in.	117.9	91.2	29.4	32.0	6.1
12 in.	119.6	92.3	29.5	31.7	5.9
18 in.	119.8	92.9	29.0	31.8	6.1
24 in.	118.9	91.6	29.7	32.8	5.7
Average	*118.9*	*92.0*	*29.3*	*32.3*	*5.9*
MLC-70 Trackway					
Surface	120.3	93.1	29.2	30.5	5.9
6 in.	118.9	90.8	30.9	31.5	6.2
12 in.	120.3	92.9	29.5	30.5	6.8
Average [b]	*119.8*	*92.3*	*29.8*	*31.1*	*6.2*
Aluminum Truss					
Surface	121.2	93.3	29.9	31.6	6.5
6 in. [c]	111.2	86.4	28.7	31.8	5.9
12 in. [c]	118.6	92.1	28.8	31.4	6.1
18 in. [c]	116.4	88.9	30.9	31.6	5.7
Average	*116.8*	*90.2*	*29.6*	*31.6*	*6.1*

[a] Avg. of new lifts and existing lifts from AM2 test section (12 in.-30 in.).
[b] Avg. of new lifts and existing lifts from Carbon Fiber Composite/Aluminum Honeycomb Composite test section (18 in.-24 in.).
[c] Data from Bell and Mason (2012).

Table 7. In-place properties of subgrades after completing mat evaluations.

Test Depth Below Subgrade Surface	Nuclear Gage Test			CBR Test	
	Wet Density, pcf	Dry Density, pcf	Moisture, %	Moisture, %	CBR
AM2					
Surface	119.8	92.0	30.3	34.7	8.1
6 in.	---	---	---	---	9.1
12 in.	114.7	83.6	37.1	33.2	10.0
M19					
Surface	118.9	90.4	31.7	33.3	7.3
6 in. Below Surface	---	---	---	33.3	6.6
Carbon Fiber Composite					
Surface	120.3	92.7	29.7	32.2	8.7
6 in.	120.0	92.0	30.4	31.2	8.5
12 in.	117.1	88.5	32.4	31.8	7.0
Aluminum Honeycomb Composite					
Surface	118.8	92.0	29.2	31.6	10.2
6 in.	117.3	89.9	30.5	31.7	8.1
12 in.	118.6	90.5	31.1	31.5	8.5
MLC-70 Trackway					
Surface	120.5	94.8	27.2	31.7	7.0
6 in.	118.5	89.6	32.3	31.3	9.7
Aluminum Truss					
Surface	---	---	---	31.0	7.0

3.3.2 EPC Installation

Subgrades were instrumented with 9-in.-diam Geokon® total earth pressure cells (EPCs) to monitor the stress distribution provided by the mat systems (except for the Aluminum Truss mat test section). EPCs were not installed beneath the Aluminum Truss system, since original project objectives did not require the data and because of time and budget constraints. EPCs were placed at different depths during subgrade construction, as shown in Figure 26, and surveyed for elevation to ensure placement at the proper depths. Table 8 summarizes EPC locations for each test section.

Figure 26. EPC placement during subgrade construction.

Table 8. EPC locations for each test section.

Depth[a] (in.)	Offset[b] (in.)	AM2	M19	Carbon Fiber Composite	Aluminum Honeycomb Composite	MLC-70 Trackway	Aluminum Truss
6.0	0	-	-	Y	Y	Y	-
12.0	0	Y	Y	Y	Y	Y	-
24.0	0	-	-	Y	Y	Y	-
30.0	0	Y	Y	-	-	-	-
54.0	0	Y	Y	-	-	-	-
30.0	72.0	Y	Y	-	-	-	-
54.0	72.0	Y	Y	-	-	-	-

[a] Depth from subgrade surface.

[b] Offset from centerline.

Note: "Y" indicates that an EPC was installed; "-" indicates that no EPC was installed.

3.3.3 Mat installation

The mat systems were installed according to manufacturers' guidelines and recommendations by an experienced installation crew. The layouts were established by using stakes, strings, and measuring tapes to mark the centerline and data collection locations. Once mats were installed, lead blocks were placed on the section edges to represent the resistance to movement provided by a large expanse of matting. Steel or lead blocks were

used in the center of larger matting sections with more than one test lane. Lines were painted on the surface to mark data collection locations and to designate traffic areas for aiding in simulated traffic operations during testing. To facilitate the entrance and exit of the test vehicle, AM2 panels at ERDC's facility were installed along the ends of the traffic lane(s). An example of a fully constructed test section is shown in Figure 27. Brief descriptions of individual mat system panel placement are provided in the following paragraphs.

Figure 27. Test section surfaced with AM2.

3.3.3.1 AM2 and M19 mat installation

The AM2 and M19 mat sections were assembled in a similar fashion. The first mat panel was placed flat on the ground with the male/female hinge connection perpendicular to the direction of traffic. The second panel was positioned by allowing its overlapping end connector to drop into position over the underlapping end connector of the first panel. An aluminum locking bar was inserted into the slot made between the end connectors. This process was continued until the first row was installed. For the second row, the female hinge connector was attached to the male hinge connector of panels from the first row, and the panel was pivoted into place. This process was repeated until the entire mat section was assembled in a brickwork configuration. Figures 28 through 30 show photographs of the AM2 and M19 mat installations.

Figure 28. Installation of AM2 panel.

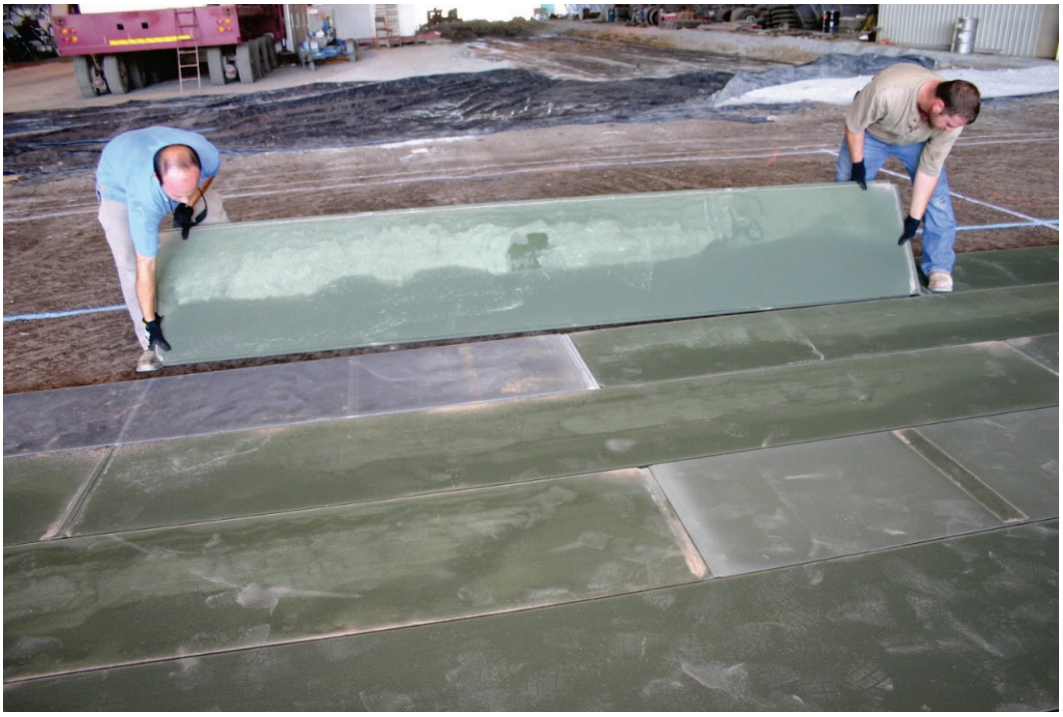

Figure 29. Insertion of AM2 locking bar.

Figure 30. M19 mat panel installation.

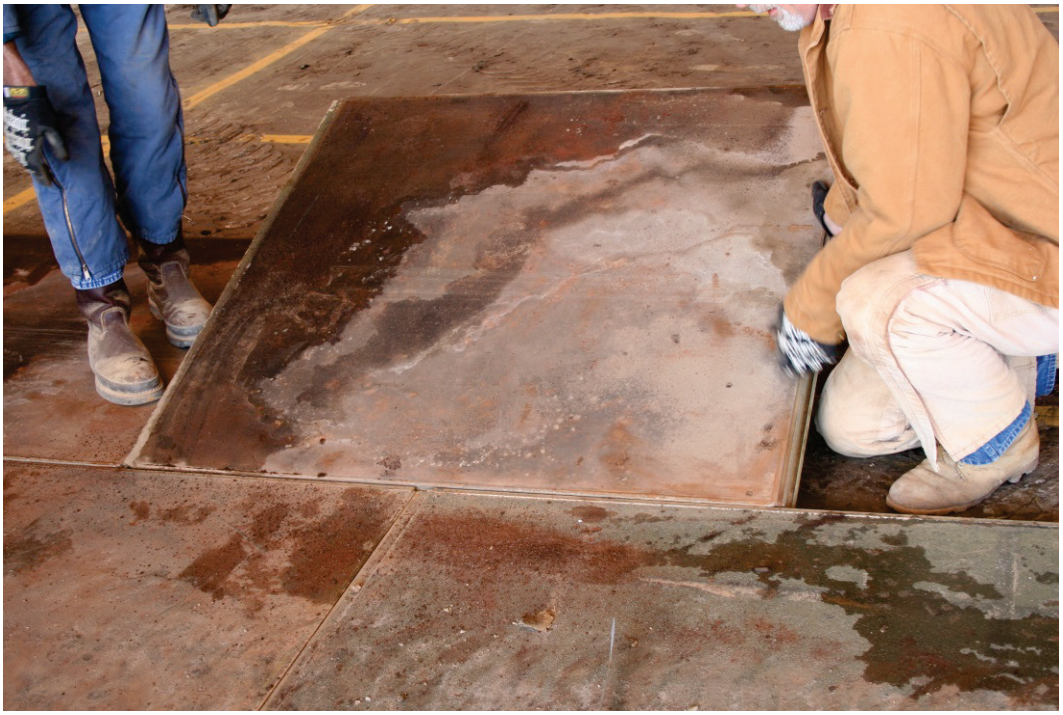

3.3.3.2 *Carbon Fiber Composite mat installation*

The first panel was installed with its longer edge perpendicular to the direction of traffic. The second panel was placed next to the first at their shorter edges, allowing the aluminum edge rails of both panels to form an H-shaped slot for insertion of the nylon locking bar (Figure 31). Once the first row was completed, the first panel in the second row was placed against those in the first row. A nylon locking bar was threaded through the H-shaped slot formed by the first row and the second row. This pattern was continued, maintaining the half-panel stagger at the end of successive rows until each row was completed.

3.3.3.3 *Aluminum Honeycomb Composite mat installation*

Each panel in the first row was placed so that the male hinge connector was perpendicular to the direction of traffic. The aluminum edge rails between these panels formed H-shaped slots that allowed for the insertion of a nylon locking bar. To assemble the second row, panels in the second row were pivoted into place by hooking their female hinge connector to the male hinge connector of panels in the first row (Figure 32). A nylon locking bar was then inserted between each panel in the second row. This pattern was followed until a staggered pattern was assembled.

Figure 31. Insertion of locking key between Carbon Fiber Composite panels.

Figure 32. Installation of Aluminum Honeycomb Composite panel.

3.3.3.4 MLC-70 Trackway mat installation

The first panel was placed on the subgrade surface with the female hinge perpendicular to the direction of traffic. Subsequent rows were attached by inserting the male edge of a panel into the female edge of a panel already on the subgrade surface and then sliding the panels together along their entire length while flat on the ground surface (Figure 33). No connection system was required on the short ends of the panels, so they could be assembled from both sides of the test area concurrently. Once panels were in position, shoot bolts were inserted into supplied notches in the male connector edges.

3.3.3.5 Aluminum Truss mat installation

Two panels were placed along the baseline of the test area with their short ends aligned parallel to the traffic centerline. An end connector key was inserted into the H-shaped slot created between the two panels. Panels for subsequent rows were then attached by hooking the female hinge connector onto the male hinge side of an installed panel and rotating the new panel into place (Figure 34). A locking key was then inserted between panels in the same row.

Figure 33. Installation of MLC-70 Trackway panel.

Figure 34. Installation of Aluminum Truss panel.

4 Experimental Program

The following sections describe the load cart, traffic application, data collection procedures, and failure criteria. The experimental program described herein was generally implemented uniformly throughout each test, with some exceptions that are detailed in the data collection procedures sections.

4.1 Load cart and traffic application

A load cart designed to simulate a fully-loaded F-15E aircraft was used for trafficking each mat surfaced test section. The load cart was equipped with a single 36-in. by 11-in. 30-ply tire inflated to an internal pressure of 325 psi to represent the test tire. An F-15E aircraft loaded to its maximum capacity weighs 81 kips, with the main gear carrying 87 percent of that load (i.e., 70.5 kips). Therefore, the load cart was designed such that the test wheel was supporting half of the main gear load (i.e., 35.2 kips). The F-15E load cart was equipped with one outrigger wheel to prevent over-turning and was powered by the front half of a U.S. Army 2.5-ton transport truck. The front axle supported a load of approximately 8 kips with a tire pressure of 60 psi. The load at the outrigger wheel was about 3 kips and had a tire pressure of 50 psi. A photograph of the load cart is shown in Figure 35.

Traffic on each mat surface was applied in a normally distributed wander pattern that simulated the traffic distribution, or wander width, of the main landing gear wheel of the F-15E aircraft when taxiing to and from an active runway. The traffic area was 3.75 ft wide and was divided into five lanes, where the width of each lane corresponded to the measured contact width (9 in.) of the F-15E tire when fully loaded. Figure 36 shows a representation of the traffic pattern. Traffic was applied by driving the load cart forward and then backward over the length of the mat test section and then shifting the path of the load cart laterally approximately one tire width on each forward path. Tracking guides were attached to assist the driver in shifting the load cart the proper amount for each forward path. For F-15E simulated traffic, one pattern of normally distributed traffic is equal to 16 passes. A pass is defined as the crossing of a single point by the test vehicle, either forward or backwards.

Figure 35. F-15E load cart.

Figure 36. Normally distributed traffic pattern applied to each mat surface.

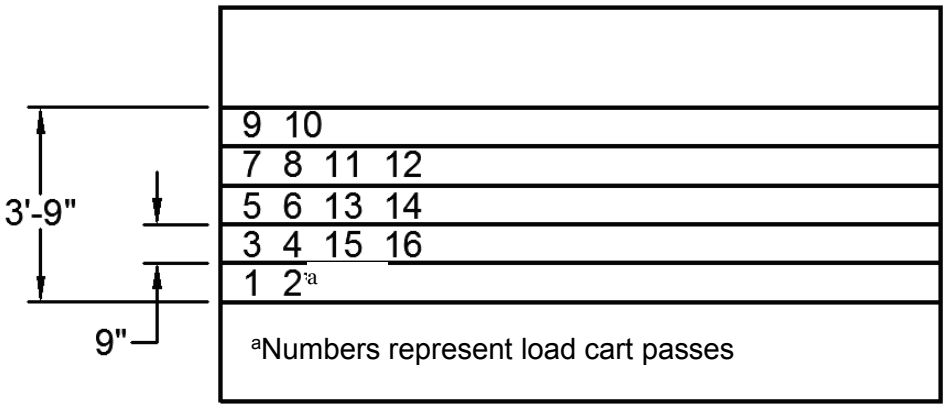

4.2 Data collection procedures

The following subsections describe data collection activities that are important for deriving conclusions from these evaluations.

4.2.1 Mat breakage

Before mat installation, panels were inspected to verify that there were no damage or defects that could affect performance during the test. When a scheduled data collection point was reached, the mat surface was visually

inspected for damage or fatigue and to verify if any mat breakage posed a risk to the load cart tire. In some cases, if a panel was considered failed and caused instability of the load cart, the panel was replaced with a new one in order to continue the test. After completing the test, mat panels were inspected individually while they were removed from the subgrade surface to document post traffic damage.

4.2.2 Deformation measurements

Deformation was monitored at transverse lines (cross sections) located near the quarter-points (or third-points) along the length of each test section. These locations were chosen to characterize the average performance of the mat while avoiding potential effects associated with the boundary conditions at the edges of the test section. Survey data were collected at 1-ft intervals along each cross section using a rod and level or robotic total station and prism. Rut depth was measured at each cross section with a straightedge and ruler. Survey data were also collected along the centerline of traffic at 1-ft intervals to determine if the mat system worked well in preventing roughness from occurring along the profile. The latter two measurements were not used for analysis and are thus not reported in Chapter 5. An example of data collection locations is shown in Figure 37.

Survey data were collected on both the subgrade and mat surfaces. On the subgrade surface, data were collected prior to installing mat panels and after completing the traffic test and removing panels from the subgrade surface. Data on the mat surface were collected at scheduled pass levels. Typically, traffic was paused for measurements at 0, 16, 32, 48, 112, 240, and 496 passes, and at about every 500 additional passes after pass 496 (i.e., 1,008, 1,520, etc.).

Both plastic deformation of the mat surface (δ_m) and subgrade (δ_s) were measured at the scheduled pass levels. δ_m was easily determined from the survey data collected along each cross section. An example showing how δ_m was calculated is shown in Chapter 5. δ_s was more difficult to monitor throughout traffic, since observation holes were not drilled through the mats to collect physical measurements underneath the mat panels. Two methods were implemented in an effort to measure δ_s at different pass levels.

Figure 37. Deformation data collection locations on Carbon Fiber Composite mat test section (shown as an example).

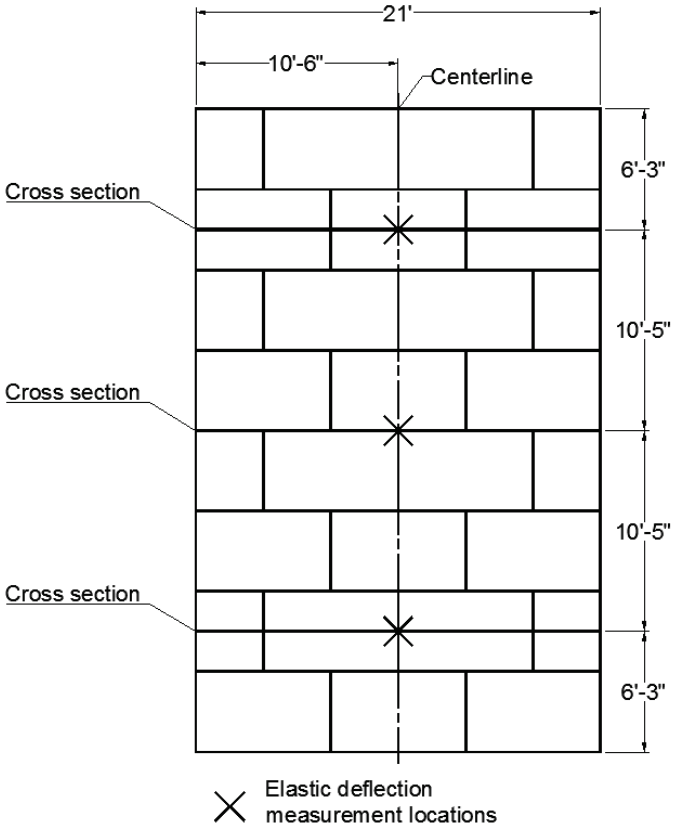

One method attempted was taking rod and level readings at certain locations on the unloaded mat surface and then parking the load cart test tire at the same locations and taking rod and level measurements immediately adjacent to the tire (Figure 38). An example of these locations on the Carbon Fiber Composite mat test section is shown in Figure 37. The difference between the unloaded and loaded measurements was the "elastic deflection" of the mat and subgrade as the test wheel moved over the mat surface. The sum of the average δ_m on the mat surface and the average elastic deflection was used to approximate δ_s and is given the term $\delta_{s\text{-}1}$. An example of these calculations is shown in Chapter 5. However, the amount of deformation of each individual element (i.e., mat and subgrade) could not be determined with this procedure, since the magnitude of subgrade elasticity was unknown. Therefore, another mechanism was used in addition to this method.

Figure 38. Rod and level measurement next to load cart tire corresponding to δ_{s-1} measurement.

An attempt was made to monitor δ_s by adding a 6-kip load next to each cross section location with a forklift carrying 4 kips of lead blocks. The forklift was parked adjacent to each cross section, with the front axle located at the centerline (Figure 39). The purpose was to deform the mat panels just enough to contact the subgrade surface without causing elastic deformation of the subgrade. Survey data were then collected at 1-ft intervals along each cross section. This method was designated the "loaded deflection" procedure, according to Rushing and Howard (2015), and the data collected at each cross section were averaged and used to approximate the term δ_{s-2}. An example of δ_{s-2} determination is shown in Chapter 5.

δ_s measurement methods varied for each test; however, sufficient data were collected so a direct comparison could be made between each mat type. For the AM2, M19, Carbon Fiber Composite, Aluminum Honeycomb Composite, and the MLC-70 Trackway tests, measurements required to determine δ_{s-1} were available. For the Carbon Fiber Composite, Aluminum Honeycomb Composite, MLC-70 Trackway, and the Aluminum Truss tests, loaded deflection measurements were obtained to determine δ_{s-2}.

Figure 39. Loaded deflection procedure used to determine $\delta_{s\text{-}2}$.

4.2.3 EPC data acquisition

The AM2, M19, Carbon Fiber Composite, Aluminum Honeycomb Composite, and MLC-70 test sections had the subgrade instrumented with EPCs. EPCs were not installed beneath Aluminum Truss system, since original project objectives did not require the data. Even though EPC locations varied between some mat tests, sufficient data were collected to make comparisons for each mat type. To minimize data processing, pressure values were recorded at certain intervals at a sampling rate of 250 Hz. Typically, pressure was recorded during the first 16 passes (one pattern) after each pass level, where traffic was paused for collecting deformation and mat breakage data. For example, if traffic was paused at pass 112, EPC data were recorded during passes 113 through 128. A summary of the data collection activities in each test section is shown in Table 9.

Table 9. Data collection activities in each test section.

Mat Test Section	Visual Inspection	Survey of Cross Sections	Elastic Deflection Measurements	Loaded Deflection Procedure	EPC
AM2	X	X	X	N/A	X
M19	X	X	X	N/A	X
Carbon Fiber Composite	X	X	X	X	X
Aluminum Honeycomb Composite	X	X	X	X	X
MLC-70 Trackway	X	X	X	X	X
Aluminum Truss	X	X	N/A	X	N/A

4.3 Failure criteria

The failure criteria established for simulated F-15E traffic were either (1) 10 percent mat breakage or (2) the development of 1.25-in. surface deformation. These failure criteria were developed based on previous testing of airfield matting and U.S. Air Force requirements. Failure criteria values were recorded and monitored for compliance.

4.3.1 Mat breakage

Mat breakage percentages were calculated by dividing the area of a failed panel (or half-panel) by the total area influenced by the simulated traffic application in the assembled test section. A panel was considered failed if the observed damage posed a significant tire hazard or caused instability of the load cart. A tire hazard was defined as any damage that could not be reasonably maintained by simple field maintenance procedures (e.g., skin delamination).

4.3.2 Deformation

The permanent deformation limit of 1.25 in. was based on roughness limitations for the F-15E aircraft. The limit is required because many connecting taxiways and aprons intersect at a 90-deg angle, and crossing perpendicular to a preformed rut that exceeds the aircraft limit may damage the aircraft or risk the safety of personnel operating the aircraft. Both δ_s and δ_m were used for comparison to the deformation failure criterion, with specific details provided elsewhere in this report.

5 Test Results

5.1 Overview of test results

Results of full-scale testing are summarized in this chapter. Trafficking was typically continued after failure (mat breakage or deformation) to capture additional information. With the exception of MLC-70 Trackway mat system, mat panel failures occurred at different levels. In some cases, panels had to be replaced to be able to continue trafficking.

Section 5.2 focuses on mat behavior and reports the data collected for determining deformation, including plots of the surveyed cross sections and the elastic deflection measurements. Damage and failure mechanisms described by Rushing and Tingle (2007) for the AM2 and M19 mat systems, Rushing et al. (2011) for the Carbon Fiber Composite and Aluminum Honeycomb Composite mat systems, and Rushing et al. (2012) for the MLC-70 Trackway and Aluminum Truss systems are summarized. Plots of cross sections show the average of the data collected along each cross section in a test section. To show only the changes that occurred because of trafficking, the pre-traffic data collected along the cross sections were subtracted from all subsequent data collected after trafficking began. The discussions and results that follow are based on the normalized data. To avoid crowding cross-section plots, only data for certain scheduled data collection pass levels are shown. The average elastic deflection at different pass levels for each mat is also reported. The data were plotted on a logarithmic scale to increase the resolution of values at lower pass numbers.

For determining δ_m and δ_s, survey data were re-evaluated using methods different from those applied for the originally funded work. For example, $\delta_{s\text{-}1}$ was not determined by Rushing and Tingle (2007), Rushing et al. (2011), and Rushing et al. (2012) but is used for assessing mat system performance in this report. Therefore, some differences relative to the original research final results are presented in this document.

The value of δ_m was determined from the survey data collected along the cross sections and is reported as the difference in elevation from the average height of the upheaval on each side of the trough to the deepest point in the bottom of the trough. $\delta_{s\text{-}2}$ was determined in the same manner using cross-section measurements from the loaded deflection procedure. For

determining δ_{s-1}, the sum of the average elastic deflection and δ_m value for the same pass level was used. An example showing how δ_m and δ_{s-1} were calculated is presented in Section 5.2.1. An example showing how δ_{s-2} was determined is provided in Section 5.2.3. The final data set presenting the development of δ_m, δ_{s-1}, and δ_{s-2} throughout each test (determined using the information shown in this chapter) are reported in Chapter 6 for analysis.

Table 10 shows a results summary that is discussed in more detail in the following sections. Section 5.3 summarizes EPC data acquisition for each of the instrumented subgrades. Plots of the average maximum normalized pressure measured at different depths are shown for pass intervals where data collection was conducted.

Table 10. Summary of test section results.

Mat	MB [a] > 10%	$\delta_m \geq$ 1.25 in.	$\delta_{s-1} \geq$ 1.25 in.	$\delta_{s-2} \geq$ 1.25 in.	Pass Level at End of Test
	Pass Level When Criterion Was Met or Exceeded				
AM2	1,536	N/A [b]	384	--- [c]	1,792
M19	2,085	N/A [b]	192	--- [c]	2,085
Carbon Fiber Composite	3,404	N/A [b]	496	3,404	3,404
Aluminum Honeycomb Composite	662	N/A [b]	240	N/A [b]	720
MLC-70 Trackway	N/A [b]	124	16	48	350
Aluminum Truss	752	N/A [b]	--- [c]	752	752

[a] MB = Mat breakage.

[b] Criterion not exceeded.

[c] Not measured.

5.2 Mat behavior and permanent deformation

5.2.1 AM2 results

The AM2 test section was divided into two test areas, or test items, that were subjected to different traffic conditions. One test item was subjected to simulated F-15E traffic (i.e., F-15E test item), and the other was subjected to simulated C-17 traffic (i.e., C-17 test item). The summary that follows pertains to the behavior of the F-15E test item.

Mat breakage began after about 400 passes of the F-15E load cart. Several panels were replaced after 1,200 passes due to imminent tire hazards. The

fourth AM2 panel failure occurred at 1,536 passes, which increased the mat breakage to approximately 11 percent of the test item. Therefore, the mat breakage criterion was exceeded after 1,536 passes. Trafficking was continued to 1,792 passes, and an additional set of panels failed, increasing the level of mat breakage at the end of the test. Most mat breakage was associated with failure at the end connectors where rails would separate from the panel and cause panel joints to separate. Tearing at the top skin along the top flange of the female hinge was also common and created severe tire hazards (Figure 40). A plot of average cross-section development throughout the test is shown in Figure 41, and the average elastic deflection results are shown in Figure 42. After 384 passes, δ_m was 0.28 in. and δ_{s-1} was 1.32 in. In the following text is an example of how these values were determined.

Figure 40. Top skin tear on AM2 panel.

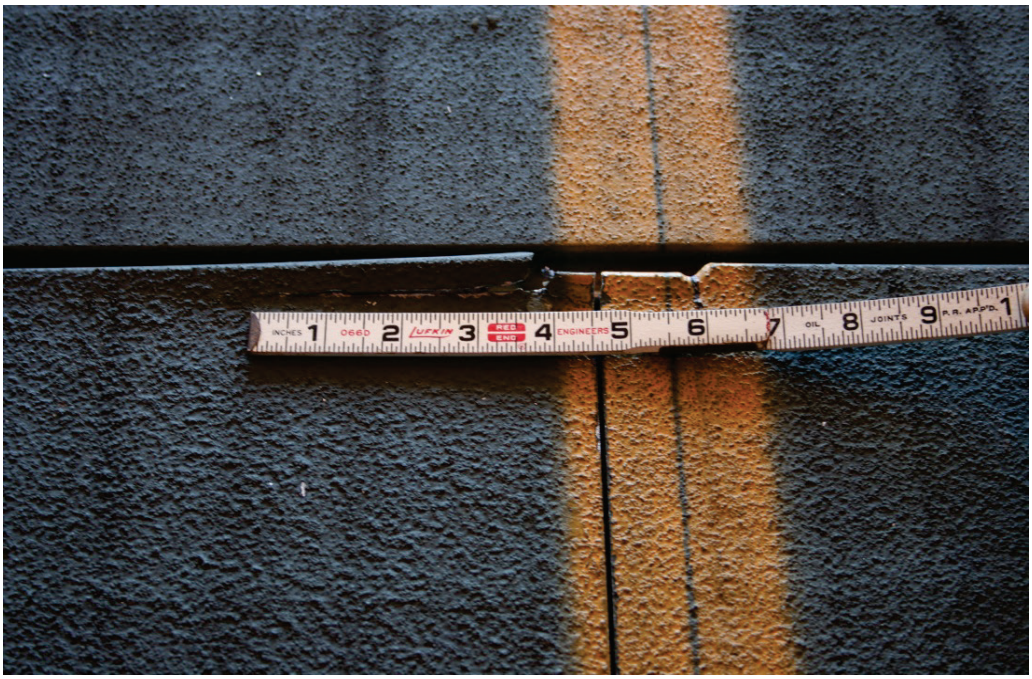

According to Figure 41, the average of the elevation of the maximum points of the upheaval on each side of the trough (i.e., the elevation at positions -7 and +7) at pass level 384 was 0 in. The elevation of the trough value (i.e., at position 0 in Figure 41) at the same pass level was –0.28 in. The difference of the trough value from the average elevation of the upheaval represents the value of δ_m at 384 passes, where δ_m = 0 in. - (-0.28 in.) = 0.28 in. The average elastic deflection at 384 passes was 1.04 in., according to Figure 42. Therefore, δ_{s-1} = δ_m + elastic deflection = 0.28 in. + 1.04 in. = 1.32 in. at 384 passes.

Figure 41. AM2 cross-section development corresponding to δ_m and δ_{s-1}.

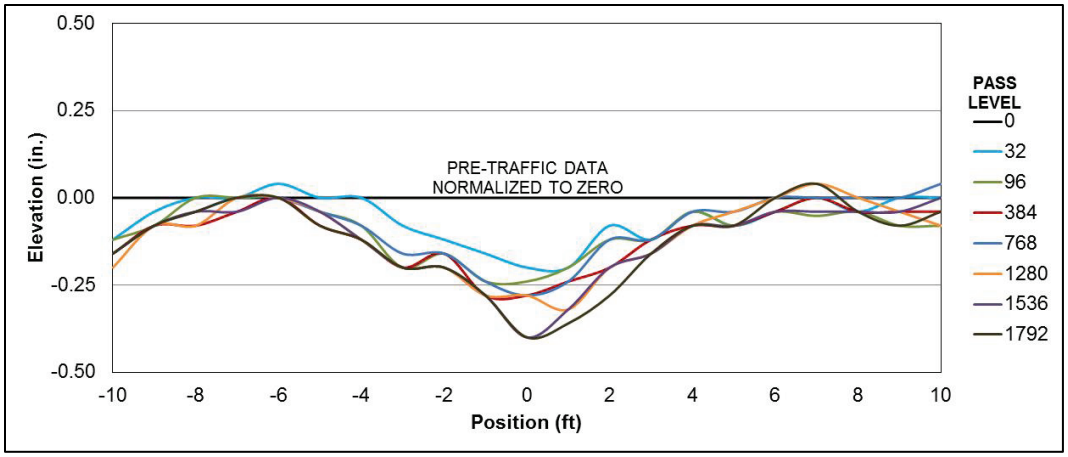

Figure 42. AM2 average elastic deflection corresponding to δ_{s-1}.

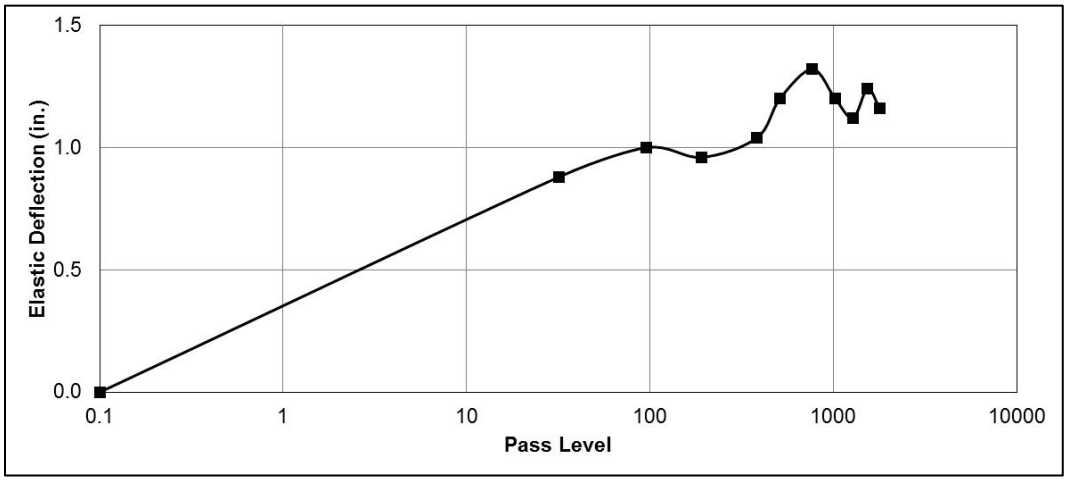

5.2.2 M19 results

The first M19 panel failure occurred after 530 passes were applied to the mat surface. The panel was replaced since severe damage to the core (Figure 43) and top skin posed a tire risk. Most subsequent panels failed by the same mechanism and several needed to be replaced throughout the test to prevent tire damage. End connector failures similar to those of the AM2 mat system were also common. After 2,085 passes, more than six panels were considered failed; therefore, the mat breakage criterion was exceeded at 2,085 passes. Traffic application was concluded at this pass level. A plot of average cross-section development throughout the test is shown in Figure 44, and the average elastic deflection results are shown in Figure 45. δ_{s-1} exceeded 1.25 in. after 192 passes were applied.

Figure 43. Core crushing in M19 panel.

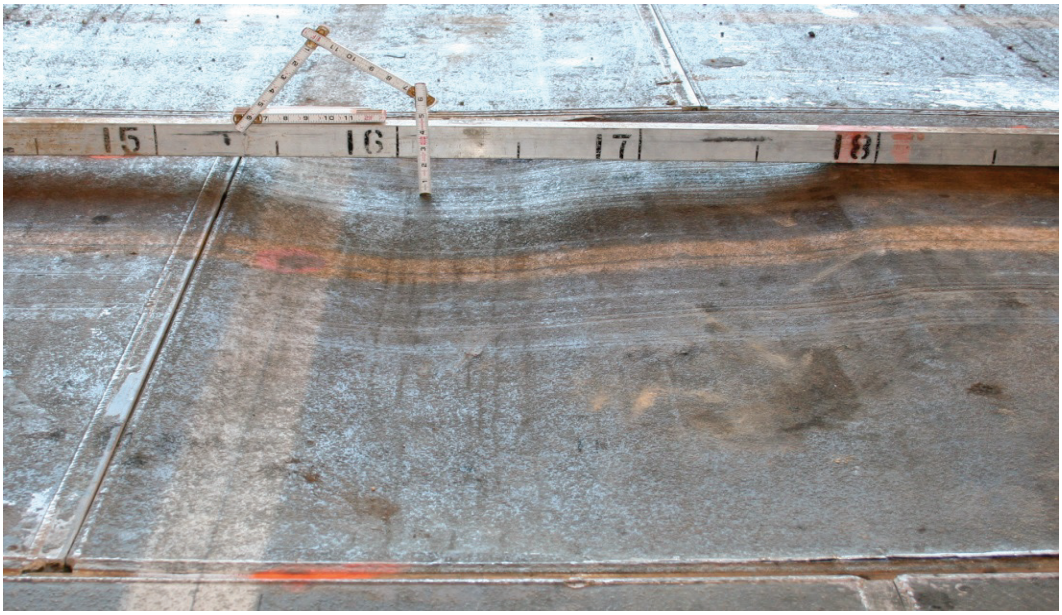

Figure 44. M19 cross-section development corresponding to δ_m and δ_{s-1}.

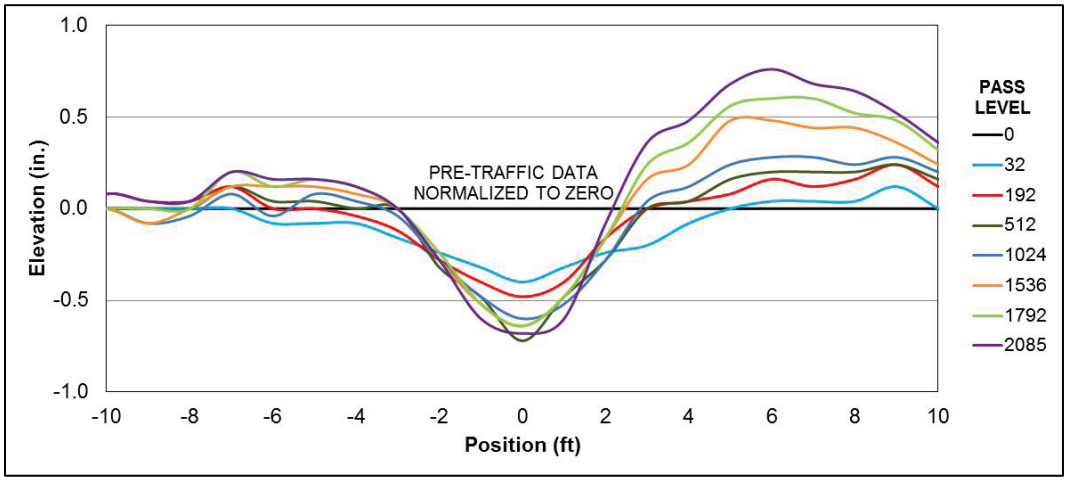

Figure 45. M19 average elastic deflection corresponding to δ_{s-1}.

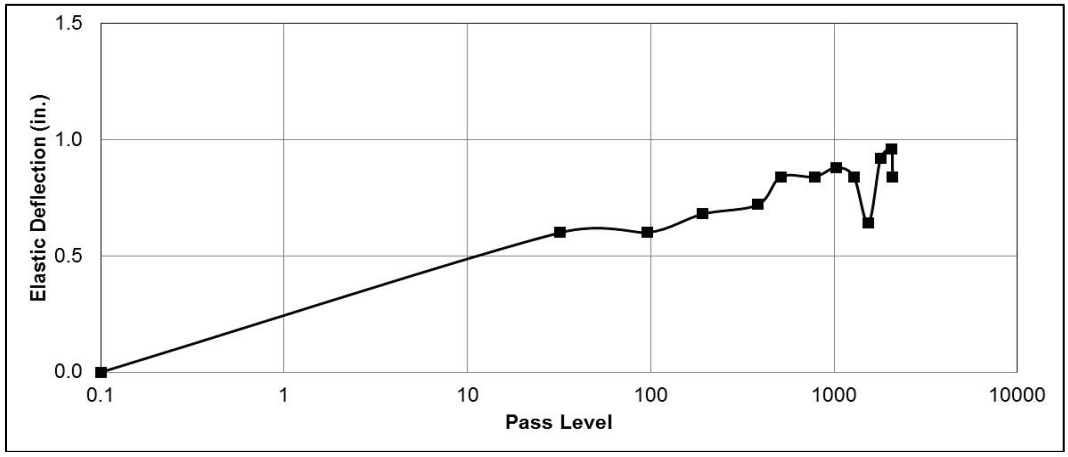

5.2.3 Carbon Fiber Composite results

The first mat panel to fail in the Carbon Fiber Composite mat test section was documented after nearly 1,700 passes of the F-15E load cart. Since the system was composed of stiff, brittle materials, all mat breakage occurred quickly, with little advanced warning, and created tire hazards that required panel replacement immediately. Failures at the centers of panels as a result of core crushing was the most common failure mechanism. After 3,404 passes were applied, the mat breakage criterion was exceeded. Plots of average cross-section development throughout the test are shown in Figures 46 and 47. Figure 48 shows the average elastic deflection results.

Figure 46. Carbon Fiber Composite cross section development corresponding to δ_m and δ_{s-1}.

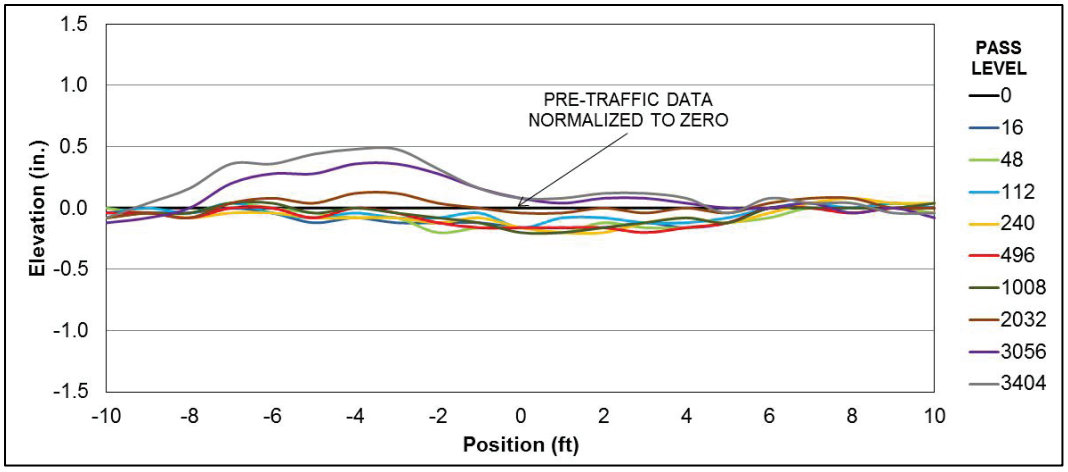

Figure 47. Carbon Fiber Composite cross-section development using loaded deflection procedure corresponding to δ_{s-2}.

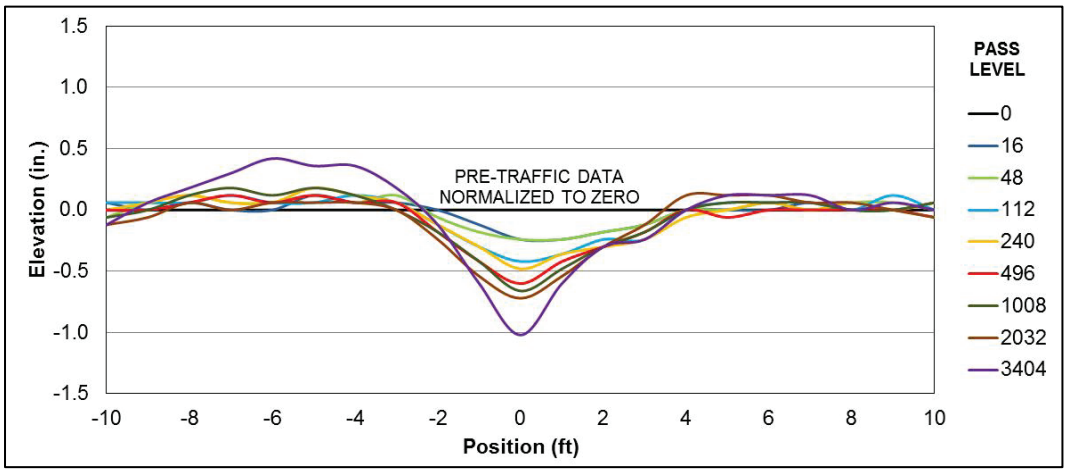

Figure 48. Carbon Fiber Composite average elastic deflection corresponding to δ_{s-1}.

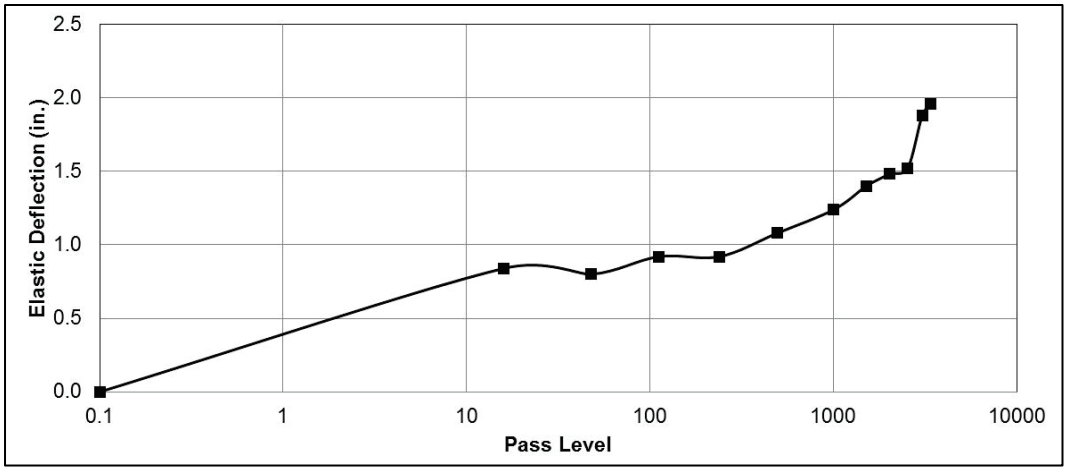

δ_{s-1} and δ_{s-2} exceeded 1.25 in. after 496 and 3,404 passes, respectively. As an example, below are the series of calculations conducted to determine δ_{s-2} at pass level 496.

According to Figure 47, the elevation of the maximum point of the upheaval on the left side of the trough (i.e., position -7) was 0.12 in. at 496 passes. The maximum elevation on the right side of the trough (i.e., position +7) was 0 in. The average of these two values is 0.06 in. The elevation of the trough value (i.e., at position 0 in Figure 47) at the same pass level was –0.60 in. The difference of the trough value from the average elevation of the upheaval represents the value of δ_{s-2} at 496 passes, where δ_{s-2} = 0.06 in. – (–0.60 in.) = 0.66 in. δ_m at the same pass level was 0.17 in., according to Figure 46. The elastic deflection was 1.08 in., according to Figure 48. Therefore, δ_{s-1} = 0.17 in. + 1.08 in. = 1.25 in. at 496 passes.

5.2.4 Aluminum Honeycomb Composite results

Initial mat breakage in the Aluminum Honeycomb Composite mat section was noted at approximately 400 passes. Panels had to be replaced since tire hazards were present in the traffic area. The maximum mat breakage criterion was exceeded after 662 passes were applied to the mat surface, but trafficking was continued until 720 passes were completed. Mat panel damage was most common around the edges, where skin delamination (Figure 49) and crushing of the honeycomb core occurred. Plots of average cross-section development throughout the test are shown in Figures 50 and 51. Figure 52 shows the average elastic deflection results. δ_{s-2} did not exceed the maximum deformation criterion of 1.25 in. δ_{s-1} exceeded 1.25 in. after 240 passes.

Figure 49. Skin delamination in Aluminum Honeycomb Composite panel.

Figure 50. Aluminum Honeycomb Composite cross-section development corresponding to δ_m and δ_{s-1}.

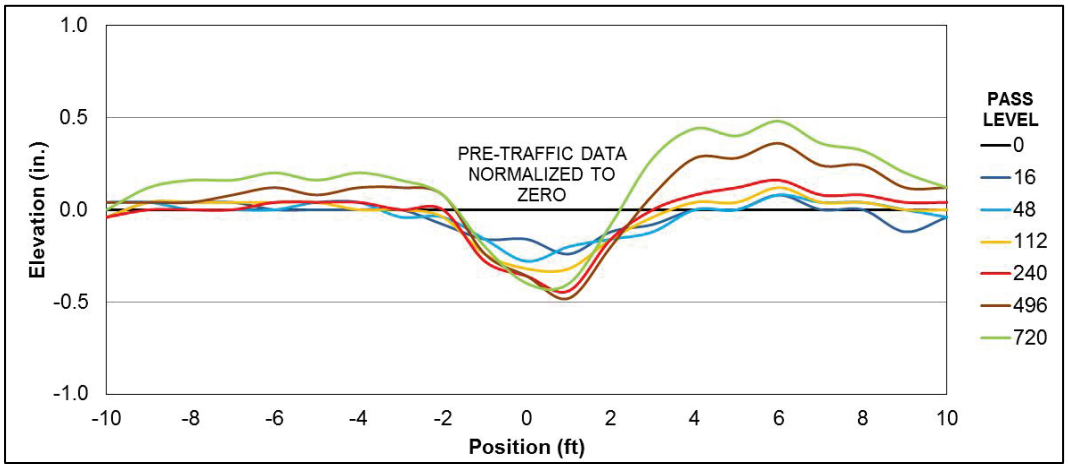

Figure 51. Aluminum Honeycomb Composite cross-section development using loaded deflection procedure corresponding to δ_{s-2}.

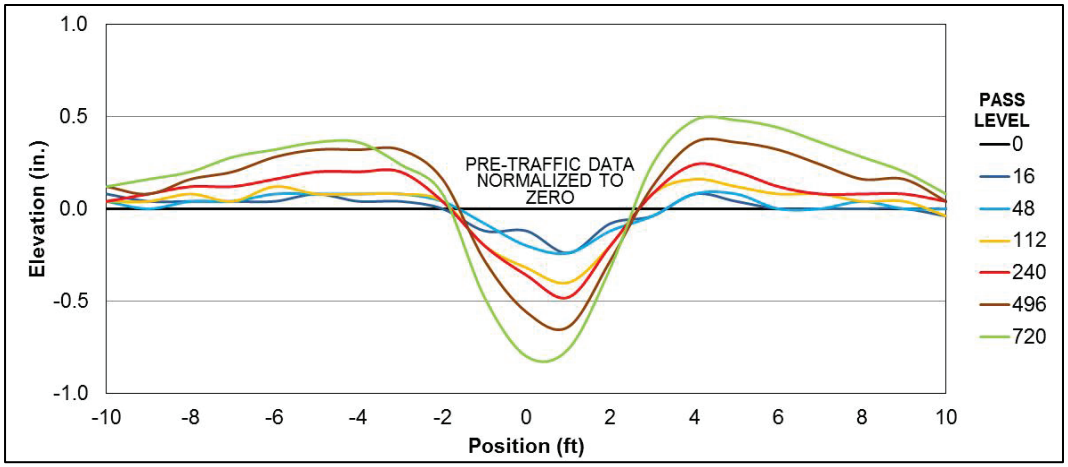

Figure 52. Aluminum Honeycomb Composite average elastic deflection corresponding to δ_{s-1}.

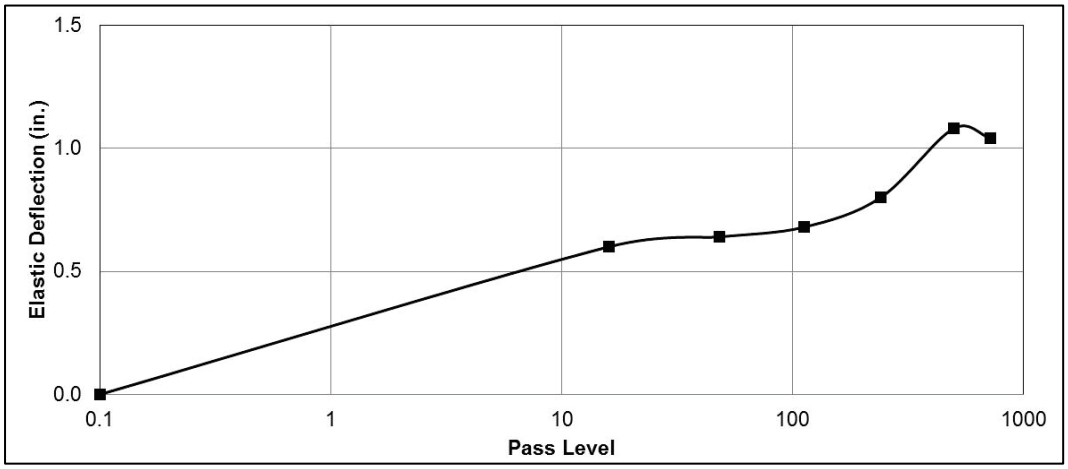

5.2.5 MLC-70 Trackway results

The MLC-70 Trackway mat system did not experience mat breakage under the simulated F-15E traffic. A total of 350 passes were applied to the mat surface. Panels lacked the stiffness properties to prevent subgrade deformation from occurring at a slow rate, but were flexible enough to yield and plastically deform without causing tire hazards or preventing further operations from occurring. A photograph of a portion of the deformed section is shown in Figure 53. Plots of average cross-section development throughout the test are shown in Figures 54 and 55. The average elastic deflection results are shown in Figure 56. δ_{s-1} and δ_{s-2} exceeded 1.25 in. after 16 and 48 passes, respectively.

Figure 53. MLC-70 Trackway deformation on mat surface.

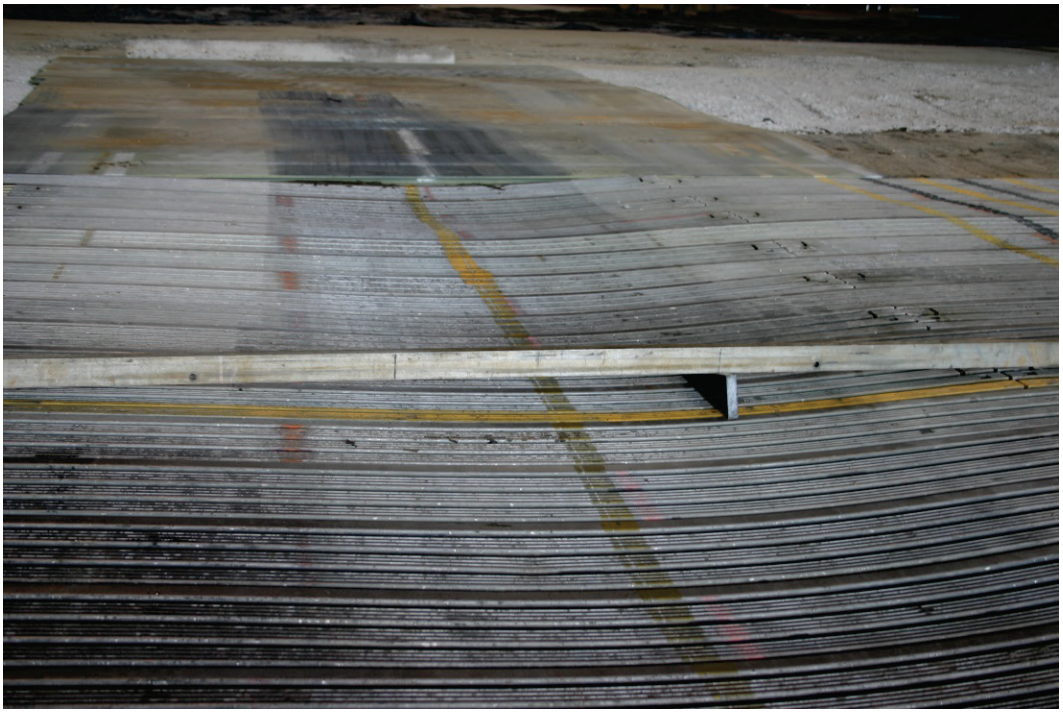

Figure 54. MLC-70 Trackway cross-section development corresponding to δ_m and δ_{s-1}.

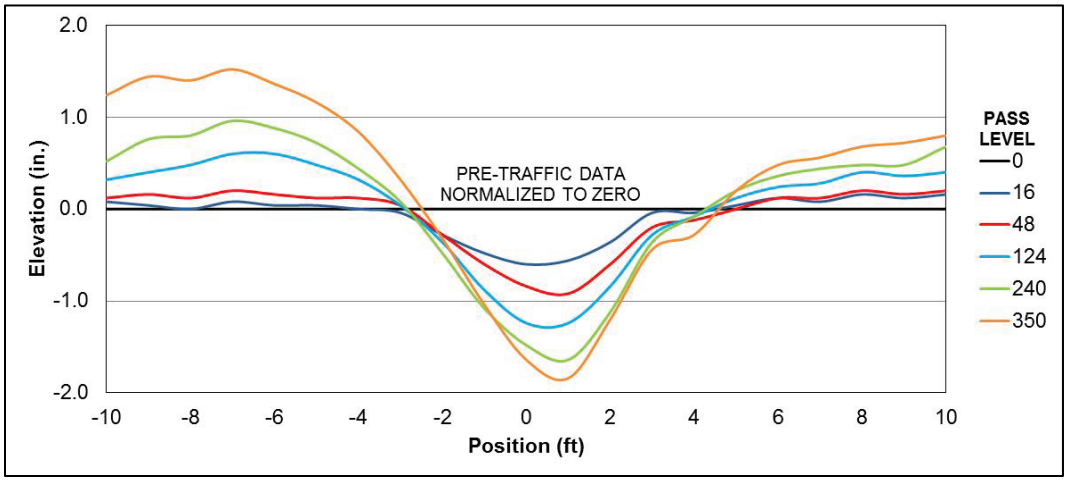

Figure 55. MLC-70 Trackway cross-section development using loaded deflection procedure corresponding to δ_{s-2}.

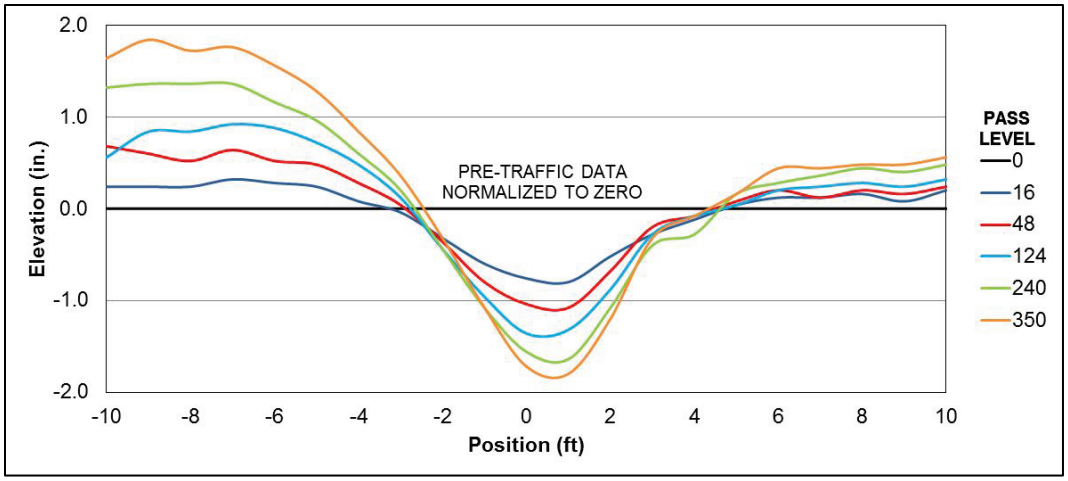

Figure 56. MLC-70 Trackway average elastic deflection corresponding to δ_{s-1}.

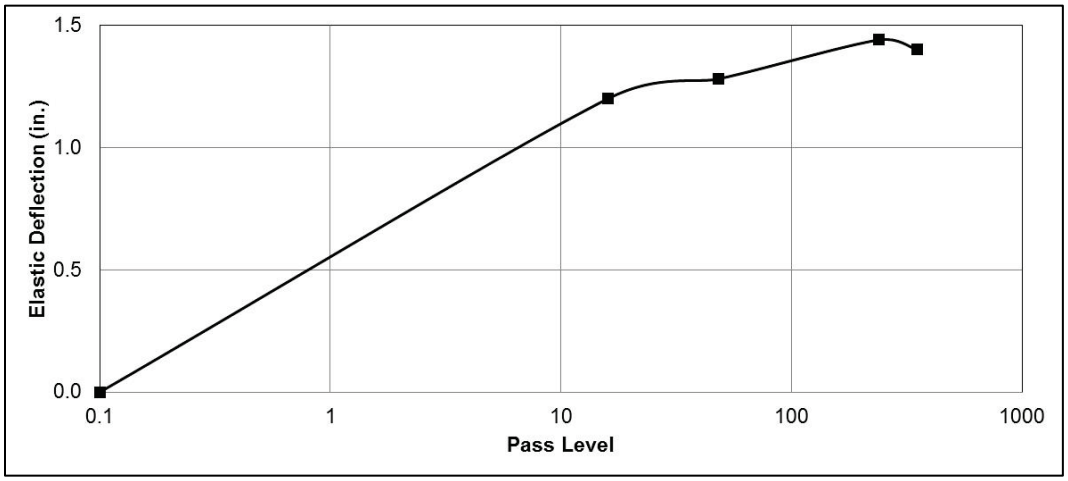

5.2.6 Aluminum Truss results

The first mat panel failure to occur in the Aluminum Truss mat test section was after 496 passes were applied. The mat breakage criterion was exceeded at 752 passes, but no panel replacements were required during the test. Most damage occurred at the male hinge connector and at the weld of the end connectors (Figure 57). Top skin tearing in these areas became severe tire hazards. Corrugation of the top skin between the internal supports also occurred. Traffic was discontinued on the brickwork pattern item at 752 passes. Plots of average cross-section development throughout the test are shown in Figures 58 and 59.

Figure 57. Damage on surface of Aluminum Truss panel.

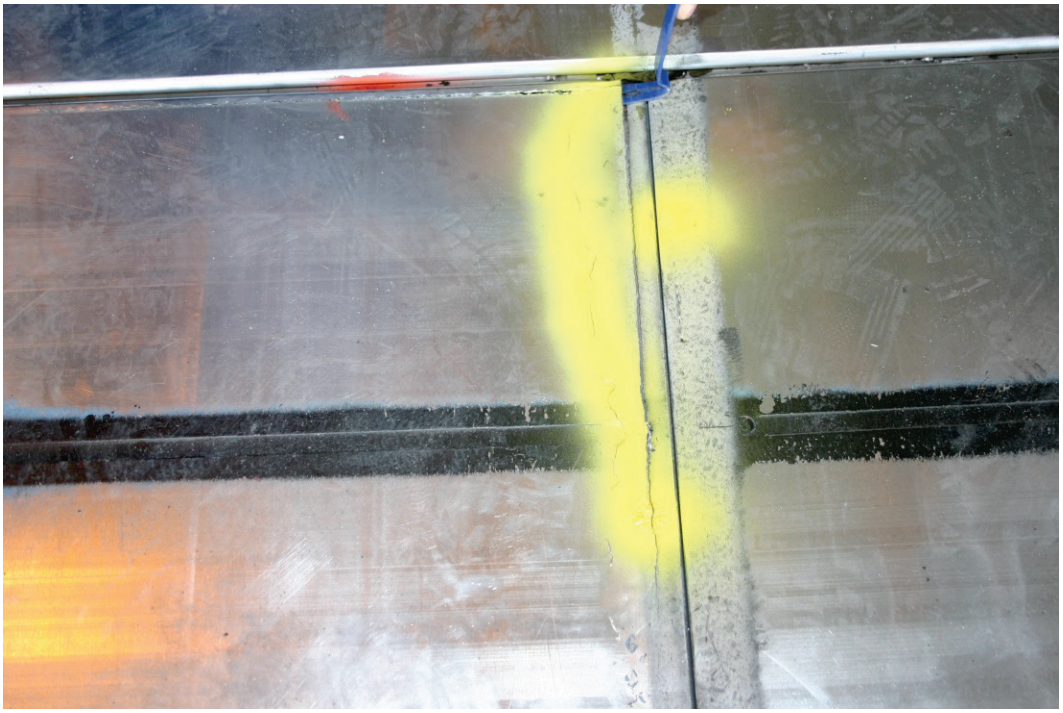

Figure 58. Aluminum Truss cross-section development corresponding to δ_m and δ_{s-1}.

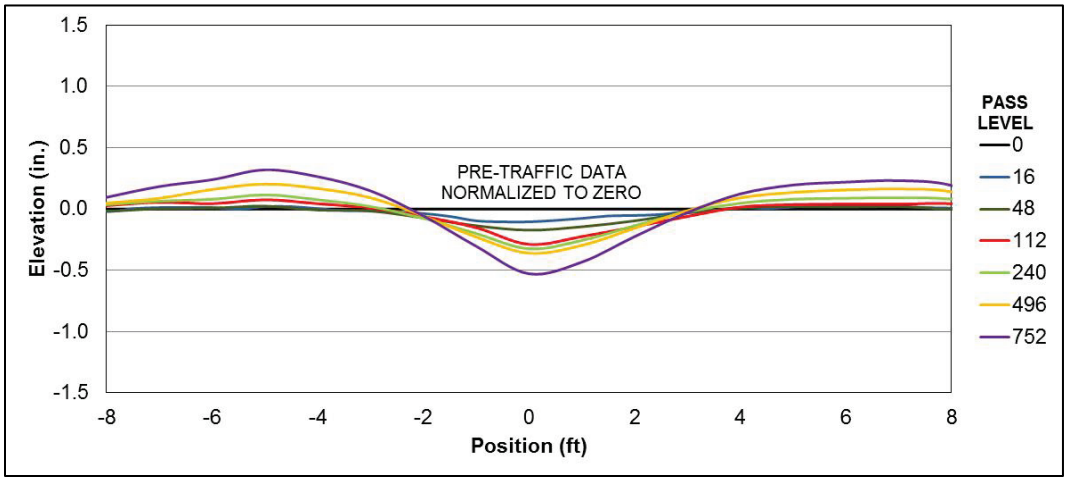

Figure 59. Aluminum Truss cross-section development using loaded deflection procedure corresponding to $\delta_{s\text{-}2}$.

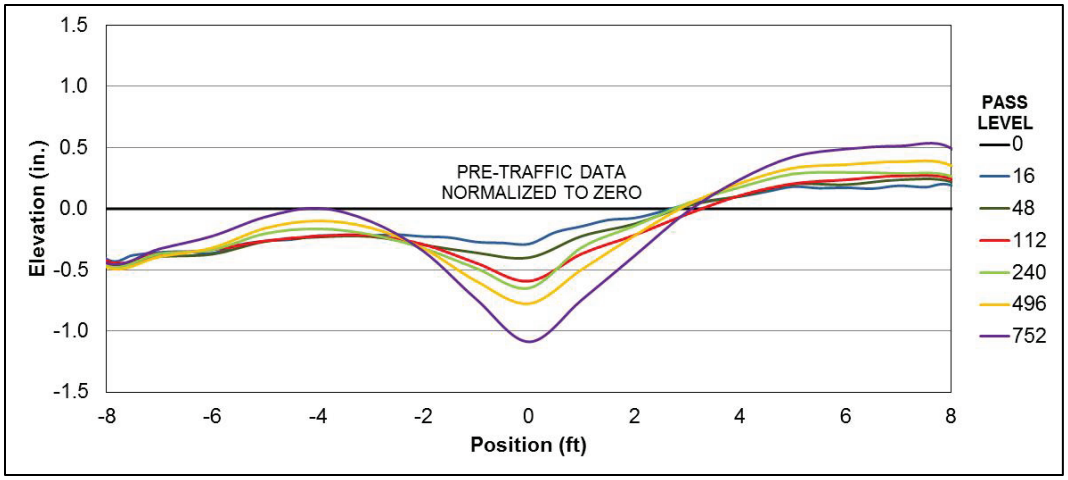

5.3 Earth pressure measurements

An example of the pressures recorded by an EPC placed under the centerline of the Aluminum Honeycomb Composite mat system test section is shown in Figure 60. The data shown were collected from an EPC located 6 in. below the subgrade surface during one traffic pattern (i.e., 16 passes). Each of the peaks shown represents one forward/backward pass by the load cart. The wander pattern used during trafficking (Figure 36) is evident from the peaks' increasing as the load cart moved toward the gauge location at the centerline and then decrease as the load cart moved laterally away from the gauge. Load cart operations were operator dependent and precise positions could not be documented, other than the assumption that the load cart was traveling along the appropriate lane. Therefore, each pair of peaks corresponding to two passes by the load cart along the same lane did not yield exactly the same value. In Figure 60, each pair of peaks is labeled with the average pressure measured for the two passes along the same lane and the lateral distance of the lane relative to the location of the EPC. Maximum pressure was measured when the test tire was located on the centerline.

Figure 60. Pressure response under Aluminum Honeycomb Composite during one pattern (16 passes).

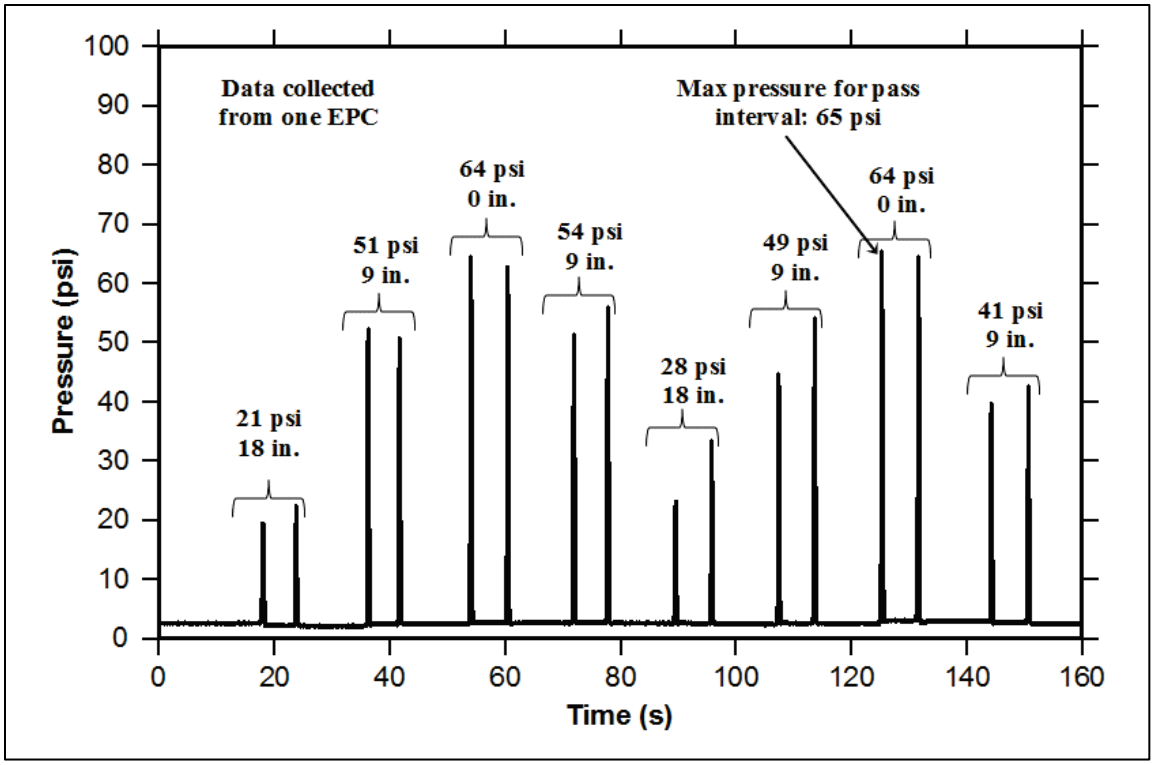

Data were processed by selecting the maximum pressure value recorded by each pressure cell during each pass interval where data collection was activated. For example, in Figure 60, this value would be 65 psi. Each of the maximum pressure values was then normalized to only show the influence of the load cart on the subgrade by removing the effects of soil overburden pressure. The normalized pressure values for EPCs at the same depth and offset distance were averaged to report one value for each depth and offset distance. Figures 61 through 65 are graphical summaries of the average maximum normalized vertical pressure values for data collection intervals in each test section. EPC locations in these figures are described by the legend. The first number is the depth from the subgrade surface, and the second is the lateral distance of the EPC from the center-line of traffic.

Figure 61. Average maximum normalized pressure under AM2.

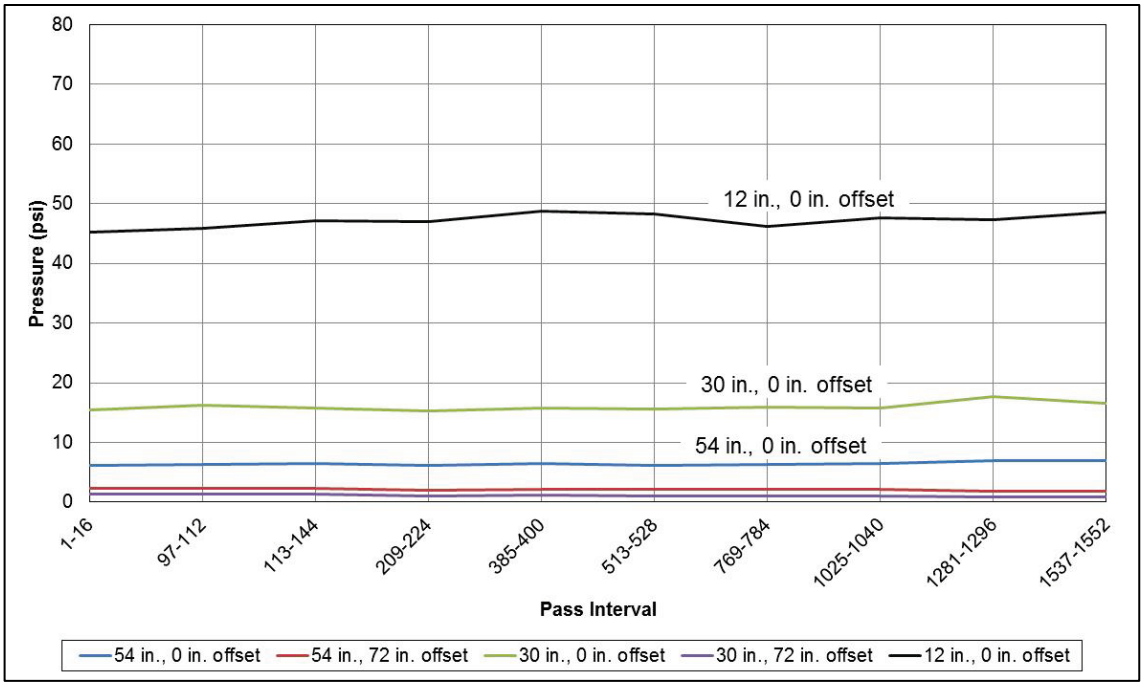

Figure 62. Average maximum normalized pressure under M19.

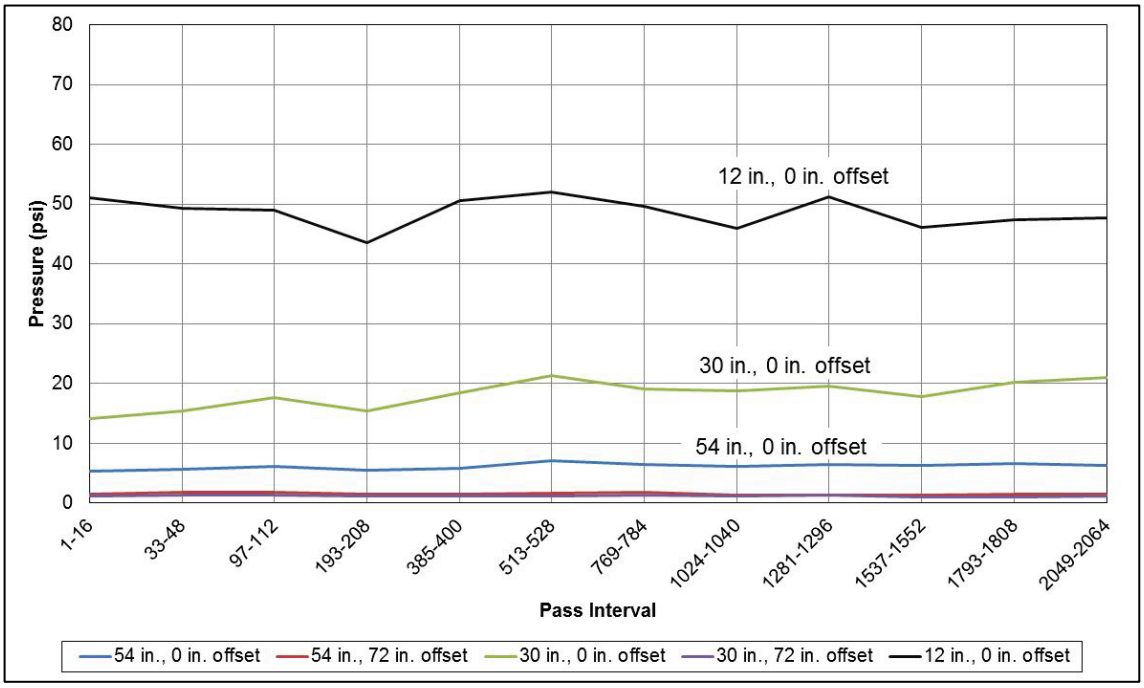

Figure 63. Average maximum normalized pressure under Carbon Fiber Composite.

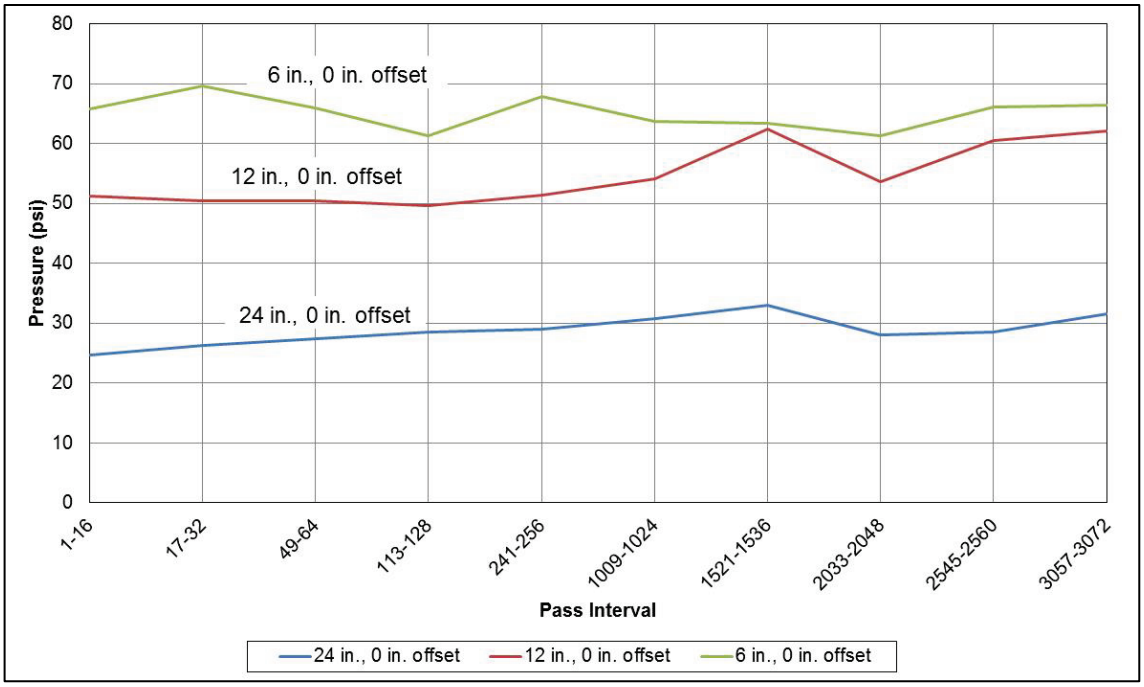

Figure 64. Average maximum normalized pressure under Aluminum Honeycomb Composite.

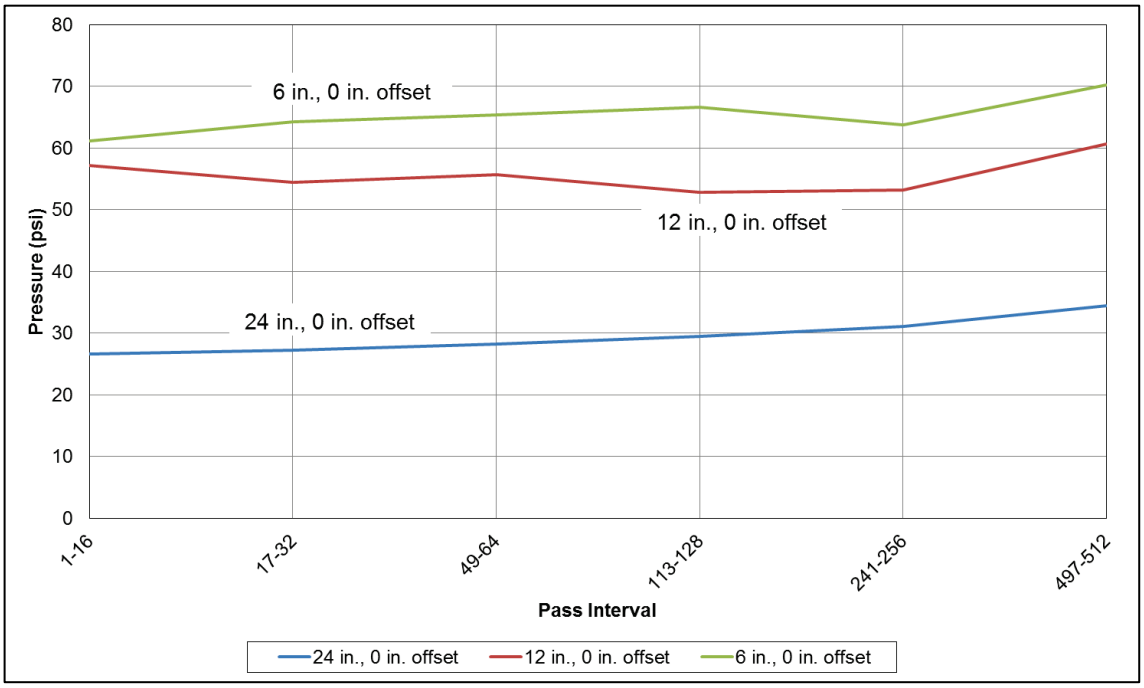

Figure 65. Average maximum normalized pressure under MLC-70 Trackway.

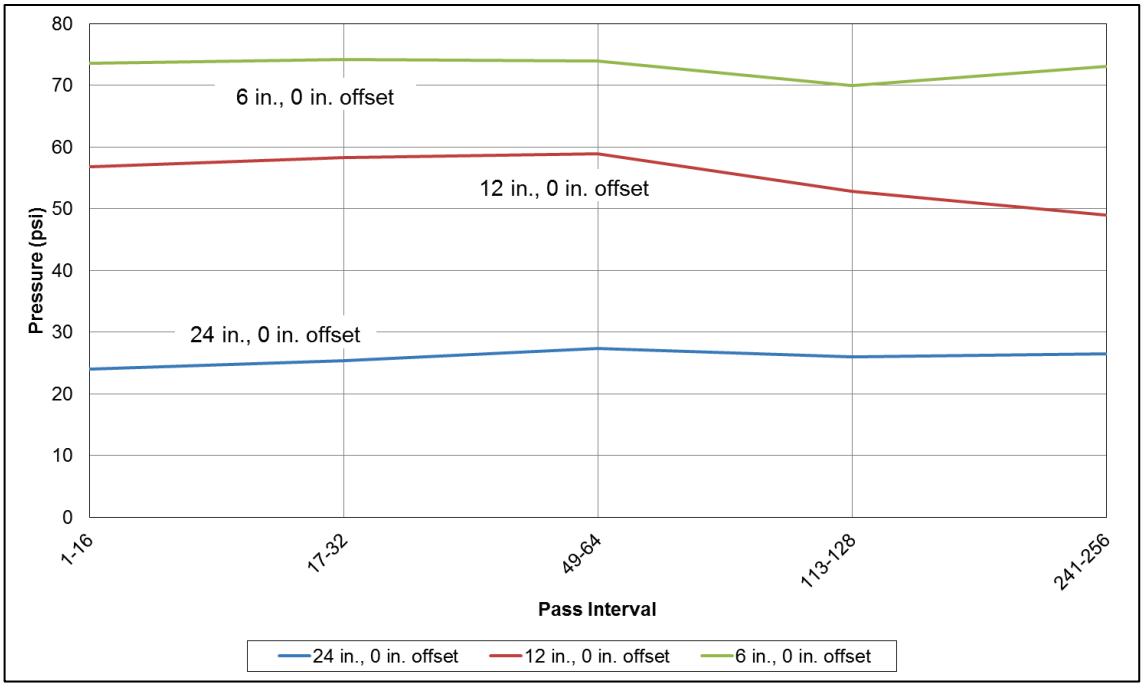

6 Analysis

This chapter provides analyses of the test results presented in Chapter 5 and discusses methods to predict mat subgrade deformation characteristics. The analysis aims at relating mat properties to measured deformation and earth pressure and providing a usable tool to make informed decisions when selecting an airfield matting system for a given application.

6.1 Permanent deformation

The progression of δ_m and δ_s (δ_{s-1} and δ_{s-2}) as a function of F-15E aircraft passes for each of the mat systems are shown in Figures 66, 67, and 68, respectively. The data were plotted on a logarithmic scale to increase the deformation resolution at lower pass numbers, especially for mats that were trafficked to less than 1,000 passes.

Figure 66. Rate of δ_m for each mat system.

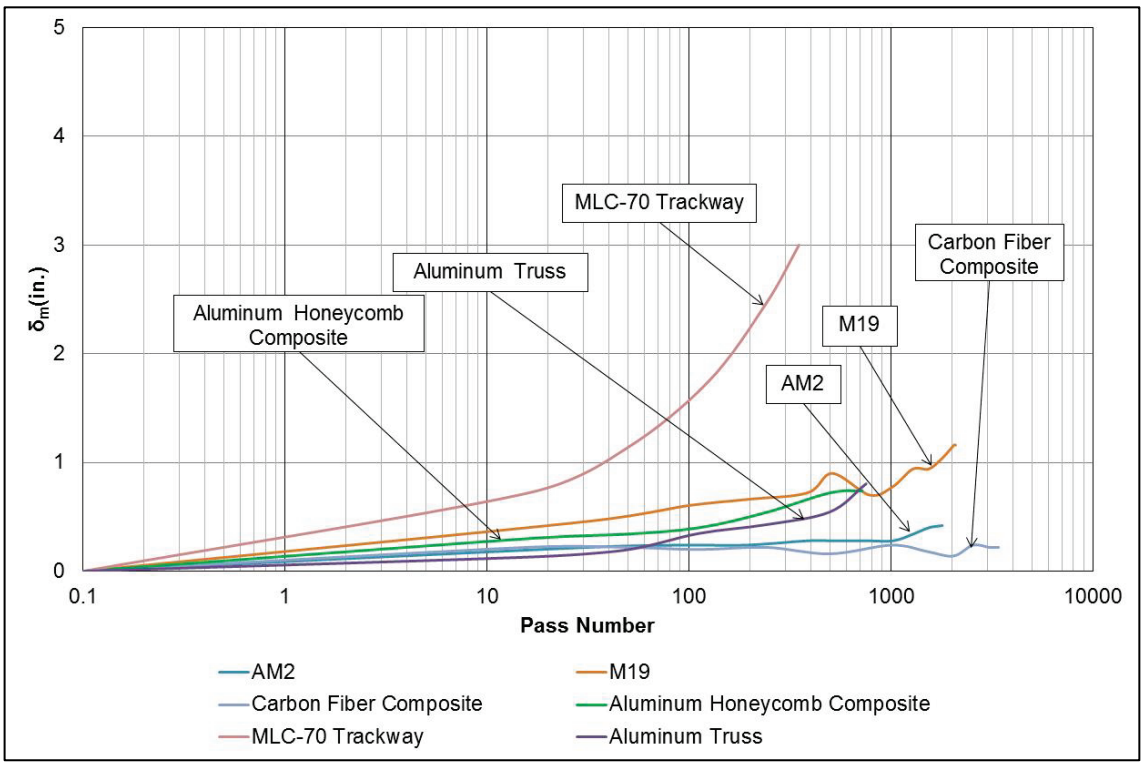

Figure 67. Rate of δ_{s-1} for each mat system where δ_{s-1} was measured.

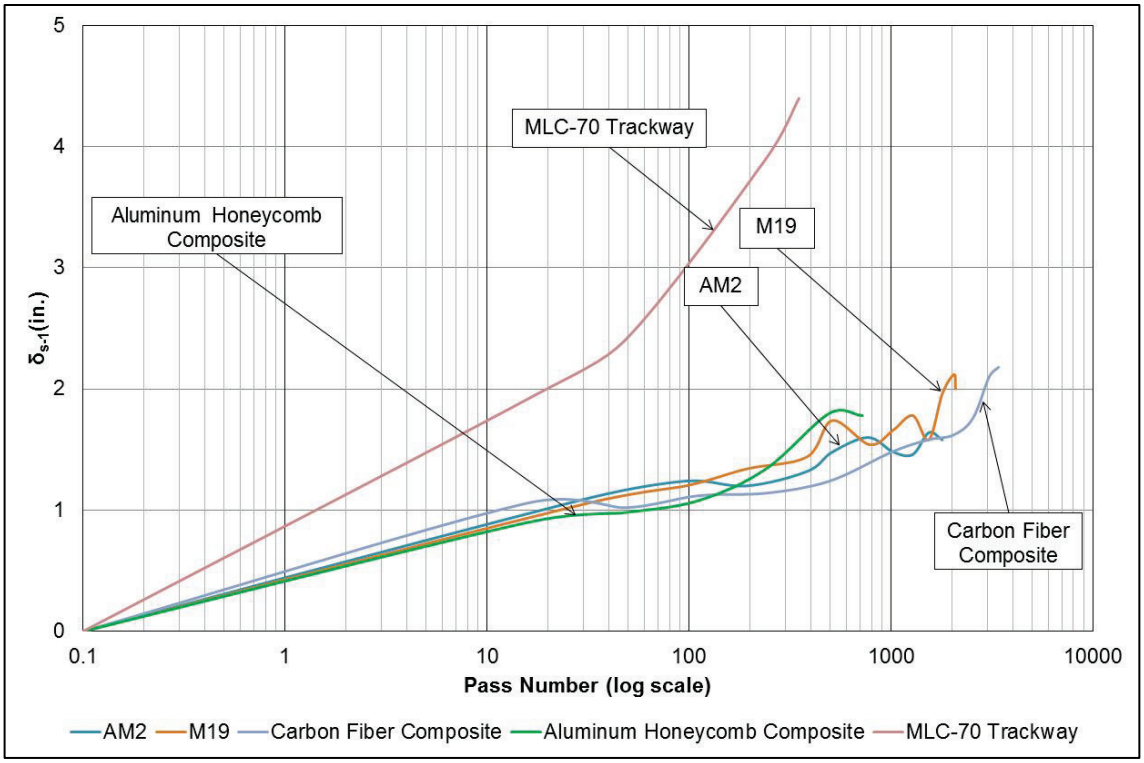

Figure 68. Rate of δ_{s-2} for each mat system where δ_{s-2} was measured.

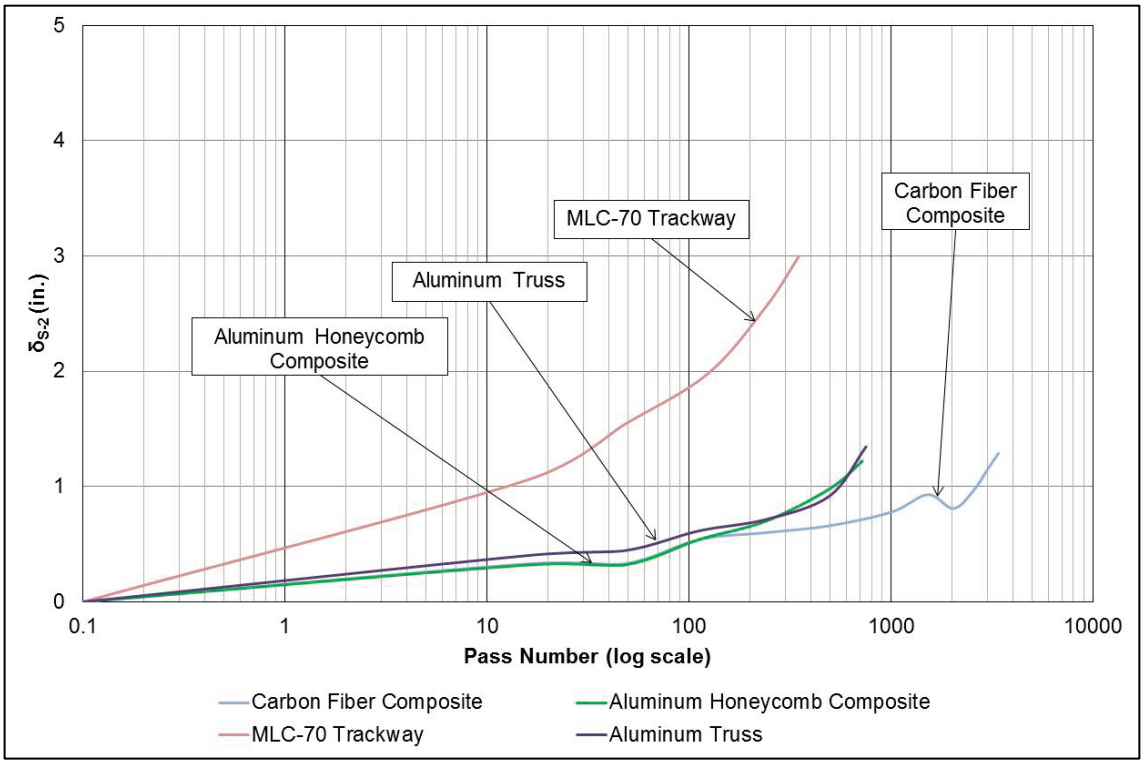

With the exception of the MLC-70 Trackway mat system, the rate of δ_s was generally higher than δ_m. δ_{s-1} increased more quickly than δ_{s-2}, which was expected since δ_{s-1} is based on load-cart induced elastic deflection, a difference of nearly 30 kips more than the weight applied by the forklift (6 kips) during the loaded deflection procedure. The rate of δ_m for the Carbon Fiber Composite mat was lower than the other mat systems. However, the rate of δ_{s-1} was nearly the same as AM2, M19, and the Aluminum Honeycomb Composite mat, and the rate of δ_{s-2} was also similar to the Aluminum Truss and Aluminum Honeycomb Composite mats. The opposite is true for the MLC-70 Trackway mat. This can be explained due to the very stiff properties of carbon fiber as compared to the lower modulus and dimensional characteristics of the MLC-70 Trackway mat. The MLC-70 Trackway panels are merely 9in. wide, preventing the assembled system from providing adequate bridging over any deformation on the subgrade compared to the other systems with much larger horizontal dimensions. This explains the similarity between the rate of δ_m and δ_{s-2} for the MLC-70 Trackway mat.

It appears that the most relevant performance property is δ_s (as opposed to δ_m), since the rate of δ_s increase is higher than that of δ_m. From Figure 68, the initial slope for the δ_{s-2} curves of the Carbon Fiber Composite, Aluminum Honeycomb Composite, and the Aluminum Truss mats are closely related. The lower rate of increase in δ_{s-2} for the Carbon Fiber Composite and Aluminum Honeycomb Composite mats may be largely attributed to the carbon fiber material in the composite cross section of both mats. For the Aluminum Truss system, the internal support provided by the "truss-like" members appears to be a key contributor to preventing excessive subgrade deformation.

The rate of δ_{s-1} increase was similar for AM2, M19, Carbon Fiber Composite, and the Aluminum Honeycomb Composite mats. The relationship between these curves may be a combination of the optimal dimensional properties of the Carbon Fiber Composite and the Aluminum Honeycomb Composite mats (i.e., larger width than AM2) and the increased stiffness of AM2. Although the stiffness of M19 mat as measured is the lowest of the systems tested ($E_c^{NJ(2)}$ = 500 ksi), its performance was close to that of the stiffer AM2, which had an $E_c^{NJ(2)}$ = 3,970 ksi. Gonzalez and Rushing (2010) explained in their analysis that M19 mat $E_c^{NJ(2)}$ determination was likely affected by the narrow and square geometry of the panel. The authors concluded that the rigid plate analysis used for back calculating $E_c^{NJ(2)}$ was

probably not suitable for representing the systems stiffness, thus bringing its use into question for purposes of this report.

6.2 Prediction of subgrade deformation

To remove any bias associated with structural failures of the mat panels for each system, the data shown in Figures 67 and 68 were revised so that δ_s was plotted until that point in which structural mat failures (or panel replacements) were judged to have affected the measurements. The revised data are shown in Figures 69 and 70 for δ_{s-1} and δ_{s-2} measurements, respectively. The data were plotted in terms of the logarithm of pass number. For example, $\log_{10}$ of 16 is 1.20; therefore, the data for pass 16 were plotted 1.20 units from the origin of the x-axis.

With the revised data, linear trend lines were fitted to each set of data plotted on a logarithmic scale and forced through the origin to determine whether the data were suitable for predicting δ_{s-1} and δ_{s-2}. The results showed that the R^2 value was 0.84 or greater for all mats tested, indicating reasonable predictions. Since the rate of deformation was largely exponential, a logarithmic function fit the data better.

Figure 69. δ_{s-1} predictions using revised data.

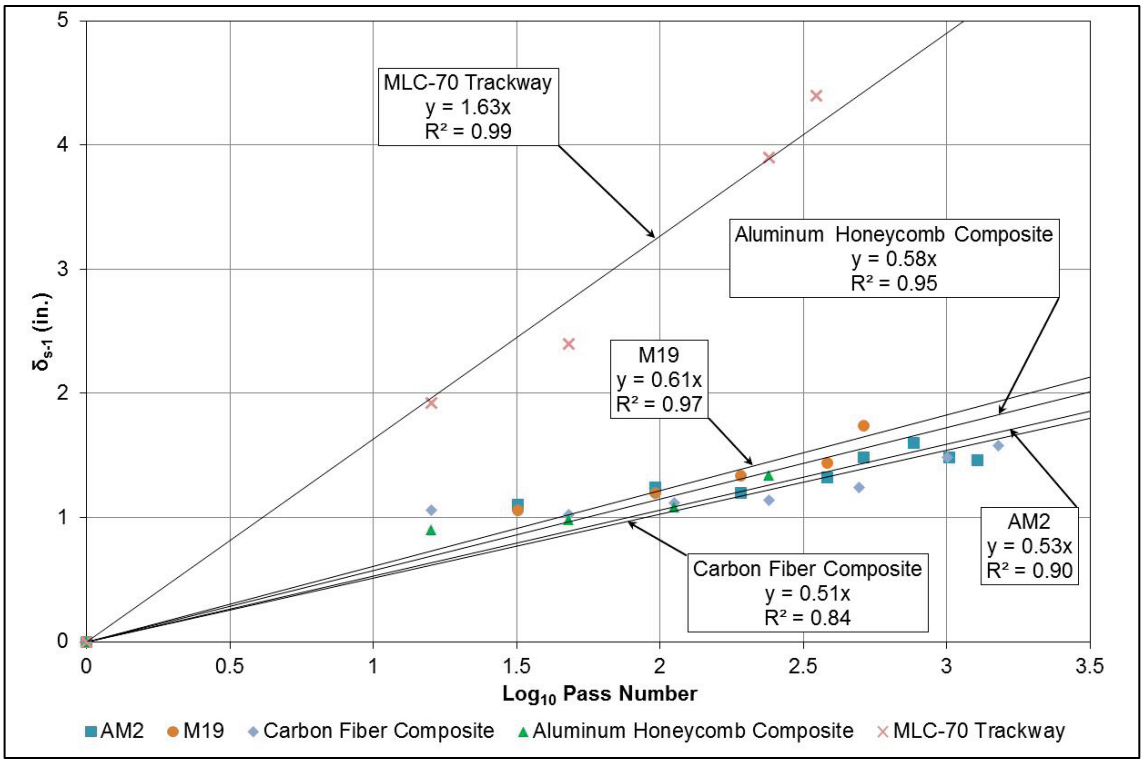

Figure 70. δ_{s-2} predictions using revised data.

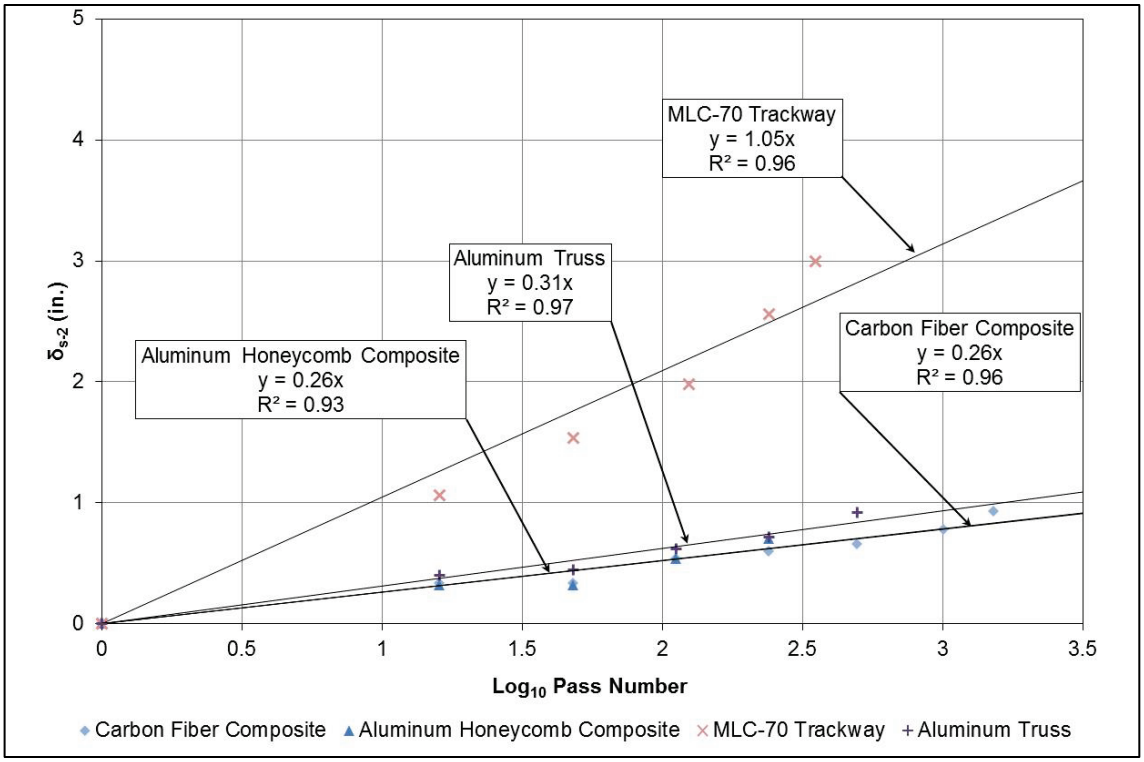

Note that Figure 69 and 70 trendlines were determined with Regression Through Origin (RTO) techniques, so the R^2 values reported should be interpreted accordingly. A summary of the regression coefficients and R^2 values in Figures 69 and 70 are provided in Table 11. The regression data provided are to be used in Equation 4, where δ_{s-n} = the subgrade deformation, in., P = the number of passes, C_n = the regression coefficient, and n corresponds to δ_{s-1} or δ_{s-2}.

$$\delta_{s-n} = C_n[log_{10}(P)] \quad (4)$$

Table 11. Summary of regression coefficients for Equation 4.

	n=1 (δ_{s-1})		n=2 (δ_{s-2})	
Mat	C_1	R^2	C_2	R^2
AM2	0.53	0.90	---	---
M19	0.61	0.97	---	---
Carbon Fiber Composite	0.51	0.84	0.26	0.96
Aluminum Honeycomb Composite	0.58	0.95	0.26	0.93
MLC-70 Trackway	1.63	0.99	1.05	0.96
Aluminum Truss	---	---	0.31	0.97

As noted by the regression coefficients (C_1 and C_2) for the Carbon Fiber Composite and the Aluminum Honeycomb Composite, the rate of increase of δ_{s-1} was about twice the rate of δ_{s-2}. Discrepancies in these measurements can be accounted for by the much heavier load applied during the elastic deflection measurements (load cart) than during the loaded deflection procedure (forklift). Although both measurements are useful for providing predictions of airfield matting behavior, δ_{s-1} seems to provide a more conservative approach. Using regression coefficients to calculate δ_{s-2} for the Carbon Fiber Composite, Aluminum Honeycomb Composite, and the Aluminum Truss systems actually yields pass levels when the deformation criterion is exceeded that are outside of the test limits. Since these mat systems are typically used for aircraft operations, overpredicting their capabilities is problematic and unsafe for aircraft and personnel. Therefore, curves developed using δ_{s-1} measurements were used for relating subgrade deformation to a given mat composite modulus ($E_c^{NJ(2)}$) and number of passes. In addition, to maintain consistency with information already available in literature and to provide viable comparisons to AM2, use of δ_{s-1} curves seems more practical. Since δ_{s-1} was not determined for the Aluminum Truss system, it was not included in the following discussion.

To relate mat composite modulus, deformation, and number of passes, δ_{s-1} was calculated for the AM2, M19, Carbon Fiber Composite, Aluminum Honeycomb Composite, and MLC-70 Trackway mat systems using the regression coefficients in Figure 69 at 10 passes (i.e., $\log_{10}(10) = 1$). The values determined were plotted against $E_c^{NJ(2)}$. Different trends were fitted to the data, and a power function proved to be the most suitable. The simplified expression (Equation 5) was developed, where $\delta_{s-1-pred-1}$ = the predicted subgrade deformation according to Equation 5, in., P = the number of passes, and $E_c^{NJ(2)}$ = the composite modulus, ksi. However, the relationship had an R^2 value of 0.43.

$$\delta_{s-1-pred-1} = log_{10}(P) * 7.89 * \left[E_c^{NJ(2)}\right]^{-0.33}, R^2 = 0.43 \quad (5)$$

The values used to develop Equation 5 were revisited, and it became clear that data relative to the M19 mat were affecting the regressions. As explained previously, the back calculated $E_c^{NJ(2)}$ for the M19 mat was not representative of the mat's actual performance and was considered an outlier in the analysis presented by Gonzalez and Rushing (2010). Therefore, data relative to the M19 mat system were removed from the

analysis. A power function was fitted to the revised data (Equation 6), which showed a stronger relationship (R^2=0.93). $\delta_{s\text{-}1\text{-}pred}$ is the predicted subgrade deformation, in., according to Equation 6. It should be noted that the R^2 values for Equations 5 and 6 do not take into account the variability (i.e., $R^2 < 1$) around the regressions developed in Figure 69, and are therefore expected to be less (i.e., less than 0.43 and 0.93, respectively).

$$\delta_{s-1-pred} = log_{10}(P) * 80.60 * \left[E_c^{NJ(2)}\right]^{-0.63}, R^2 = 0.93 \quad (6)$$

To provide a better understanding of the relationship between Equation 6 and the actual measured data, an equality plot was created and is shown in Figure 71. The measured data set used to create Figure 71 is the same set used to create the regressions in Figure 69. $\delta_{s\text{-}1\text{-}pred}$ was calculated for the same pass levels and associated $E_c^{NJ(2)}$ values of the mats. Note that data relative to M19 were not used for this analysis. The R^2 value associated with the data shown in Figure 71 is 0.91, which is likely more representative of the error associated with Equation 6 than the R^2 value of 0.93 discussed earlier.

Figure 71. Equality plot of predicted vs. measured $\delta_{s\text{-}1}$.

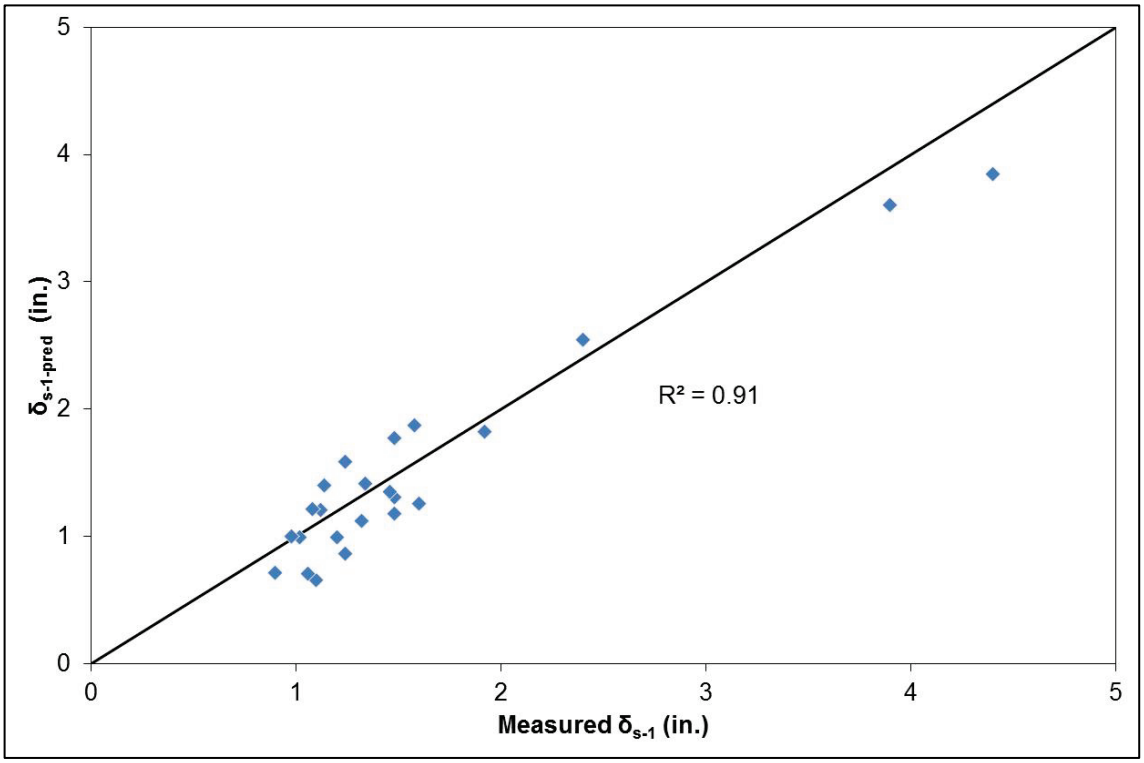

To illustrate curves developed based on Equation 6, Figure 72 was created for arbitrarily selected passes. Figure 72 indicates that an increase in mat stiffness for weaker mats causes large decreases in δ_{s-1}. If there is an increase in stiffness at the stronger end of the spectrum, only minimal decreases in δ_{s-1} are observed.

Equation 6 and Figure 72 can be used to approximate the subgrade deformation for a given number of F-15E aircraft passes and $E_c^{NJ(2)}$ for a mat system that will be placed on a CBR of 6. To use these curves, $E_c^{NJ(2)}$ should be determined using the test method described by Berney et al. (2006) and back calculated according to the approach used by Gonzalez and Rushing (2010). Any other method for determining mat stiffness (e.g., laboratory four-point bending test) is not necessarily applicable to the approach previously presented , absent further investigation. The curves are also limited to mat systems with panels that have rectangular geometries. Potential users of Equation 6 are advised to look at the relationship as predicting a range of allowable passes to failure (e.g., Table 12), since small changes in δ_{s-1} can result in large changes in pass levels.

Figure 72. δ_{s-1} predictions for a given $E_c^{NJ(2)}$ and pass number.

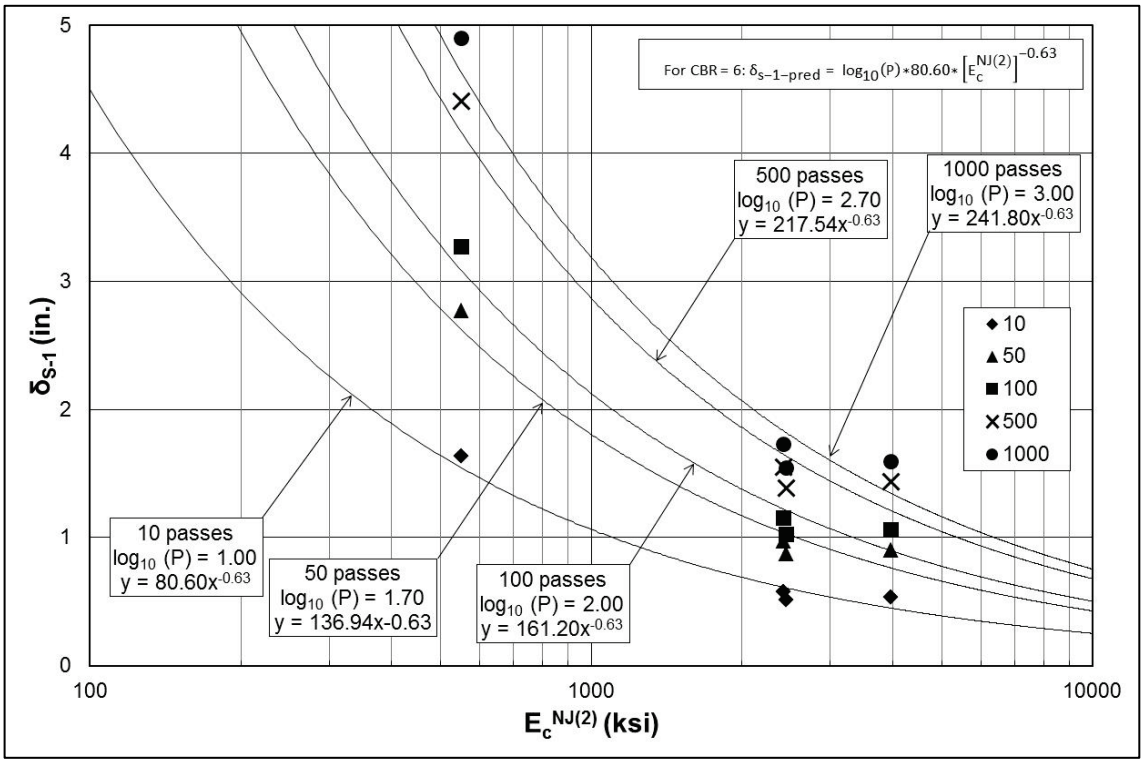

To demonstrate the ability of Equation 6 to determine $\delta_{s\text{-}1}$, data from the AM2, Carbon Fiber Composite, Aluminum Honeycomb Composite, and MLC-70 Trackway mat systems' full-scale tests were investigated in terms of $\delta_{s\text{-}1}$ failures (i.e., $\delta_{s\text{-}1} \geq 1.25$ in.). The test results and solutions for *P* (pass level) using Equation 6 are shown in Table 12 for comparison. The predicted values are conservative for weaker mat systems, but Equation 6 tends to overpredict the performance of AM2. To gain some insight of the sensitivity of the relationship when solving for *P*, Equation 6 was solved for three levels of deformation, i.e., 1.15 in., 1.25 in., and 1.35 in. The results showed a wide scatter in the predicted *P*. It seems that small changes in $\delta_{s\text{-}1\text{-}pred}$ yield large changes in the predicted *P* when using the inverse relationship. However, the overall tendency of Equation 6 is to yield more conservative results for weaker mat systems.

Table 12. Comparison of measured and predicted results.

Mat	$E_c^{NJ(2)}$ (ksi)	Test Results		Pass Level Prediction at:			
		Pass Level When $\delta_{s\text{-}1} \geq 1.25$ in.	$\delta_{s\text{-}1}$ (in.)	$\delta_{s\text{-}1}$ = Value From Test Results	$\delta_{s\text{-}1}$ = 1.15 in.	$\delta_{s\text{-}1}$ = 1.25 in.	$\delta_{s\text{-}1}$ = 1.35 in.
AM2	3,970	384	1.32	1072	436	741	1256
Carbon Fiber Composite	2,455	496	1.25	132	89	132	195
Aluminum Honeycomb Composite	2,420	240	1.34	179	86	126	186
MLC-70 Trackway	550	16	1.92	19	6	7	8

As discussed in Chapter 2, Rushing and Howard (2015) published design curves and an expression (Equation 3) to determine δ_s as a function of F-15E passes and subgrade CBR, specifically for AM2. The expression was a power function that used CBR to characterize varying conditions, as opposed to mat properties ($E_c^{NJ(2)}$) as shown in this analysis. The design curves showed that small CBR increases on the weak end of the spectrum cause large decreases in δ_s. As the CBR increases, the same increase in subgrade strength only provides minimal decreases in δ_s, similar to what is shown here for increasing mat stiffness. To make a direct comparison between the relationships, *P* (Rushing and Howard 2015) was calculated for AM2 on a CBR of 6 at δ_s failure. The result is 188 passes. This is a difference of 196 passes from the actual value (384 passes), whereas Equation 6 yielded a difference of 357 passes from the actual value. The

correlation developed by Rushing and Howard (2015) is more conservative and closer to the measured data, indicating that it should be more reliable for stiffer mat systems like AM2.

It should be noted that the performance curves and relationship developed are based on deformation rate analyses. Structural mat failures were not taken into account, and failure by exceeding the mat breakage criterion cannot be determined from the analyses presented thus far. It is possible for a mat system to fail by mat breakage prior to $\delta_{s\text{-}1}$ failure. Therefore, further investigation into the available data would be needed to connect the two failure mechanisms into one function (or series of functions) that can predict which failure component may occur first.

6.3 Earth pressure measurements

Airfield mats primarily act to distribute aircraft tire loads to the subgrade in a way to minimize stress concentrations. If the aircraft load is spread over a large area, as is typical of cargo aircraft, less rigid mats are required, all other factors being equal, than when a load is concentrated over a small area, like in the case of the F-15E aircraft. The magnitude of vertical subgrade stress reduction underneath a mat system from the stress that would exist if a mat were not used to surface the subgrade is dependent on mat properties, mostly on its stiffness (panel and joint stiffness) and its ability to maintain stiffness with repeated loads. Stiffer mat systems distribute applied loads over a larger area, thus reducing the amount of stress beneath the surface. Therefore, it is reasonable to expect that systems with higher surface deformation rates are less effective at distributing the applied load and will have higher pressures measured under the surface for a given confinement, soil type, and CBR. Thus, it is expected that the stress is highest under the MLC-70 mat system and lowest for the AM2 mat system.

From Figures 22 through 26, it is evident that each of the matting systems worked well at distributing the applied load and stress (35 kips, 325 psi) so that a fraction of that was experienced by the subgrade. Pressure distribution was relatively stable and did not change much throughout each test for the mats with instrumented subgrades. To make a valid comparison of the pressure distribution, the average maximum normalized pressures determined for the first traffic pattern at different depths (i.e., interval of passes 1 to 16) were plotted in Figure 73 relative to the measured $E_c^{NJ(2)}$ of the mats. As expected, mat systems with higher stiffness values were gen-

erally able to diminish pressure in the subgrade more than those with less stiffness. Although the M19 mat system $E_c^{NJ(2)}$ is the lowest, discrepancies in the determination of mat properties due to its square geometry make it difficult to relate its stiffness to measured pressure. Based on a comparison of deformation rates, pressure distribution under the M19 mat system should be comparable to that under the AM2 or Aluminum Honeycomb Composite mats. The data shown in Figure 73 support this statement. The most notable differences in pressure are noted at the 6-in. and 12-in. depths, indicating that the mat systems' stiffness properties have more effect on the near surface pressure distribution, an expected behavior.

Figure 73. Average maximum normalized pressure during the first pass interval (passes 1-16).

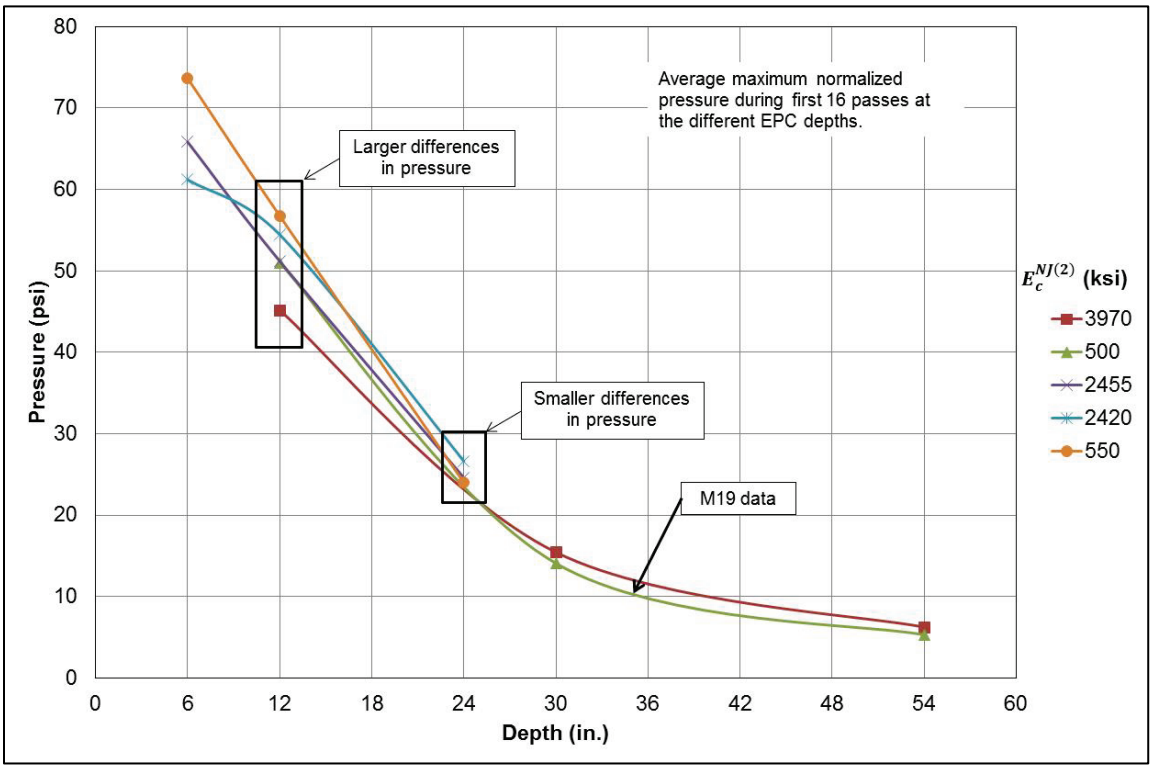

A comparison of pressure to deformation was established with pressure values reported at the 12-in. depth, since all instrumented subgrades had EPCs installed at this depth. Absent M19 pressure data, the average maximum pressure values shown in Figure 73 at the 12-in. depth were plotted against the predicted $\delta_{s\text{-}1}$ at 10 passes using Equation 6, as shown in Figure 74. This was conducted to provide an approximate measure of $\delta_{s\text{-}1}$ during the first pass interval for relating stiffness, deformation, and pressure. A linear trend line was fitted to the data. Although the R^2 value was 0.56, the lack of correlation does not dismiss the idea that pressure

beneath a stiffer system should be less than a weaker system. The four data points (AM2, Carbon Fiber Composite, Aluminum Honeycomb Composite, and MLC-70 Trackway) generally follow the trend of increasing pressure and deformation with decreasing mat stiffness. With this information, Equation 6 is further validated and indicates that a reasonable value can be determined for deformation based on a known $E_c^{NJ(2)}$ and required number of passes.

Figure 74. Average maximum normalized pressure during the first pass interval related to predicted deformation.

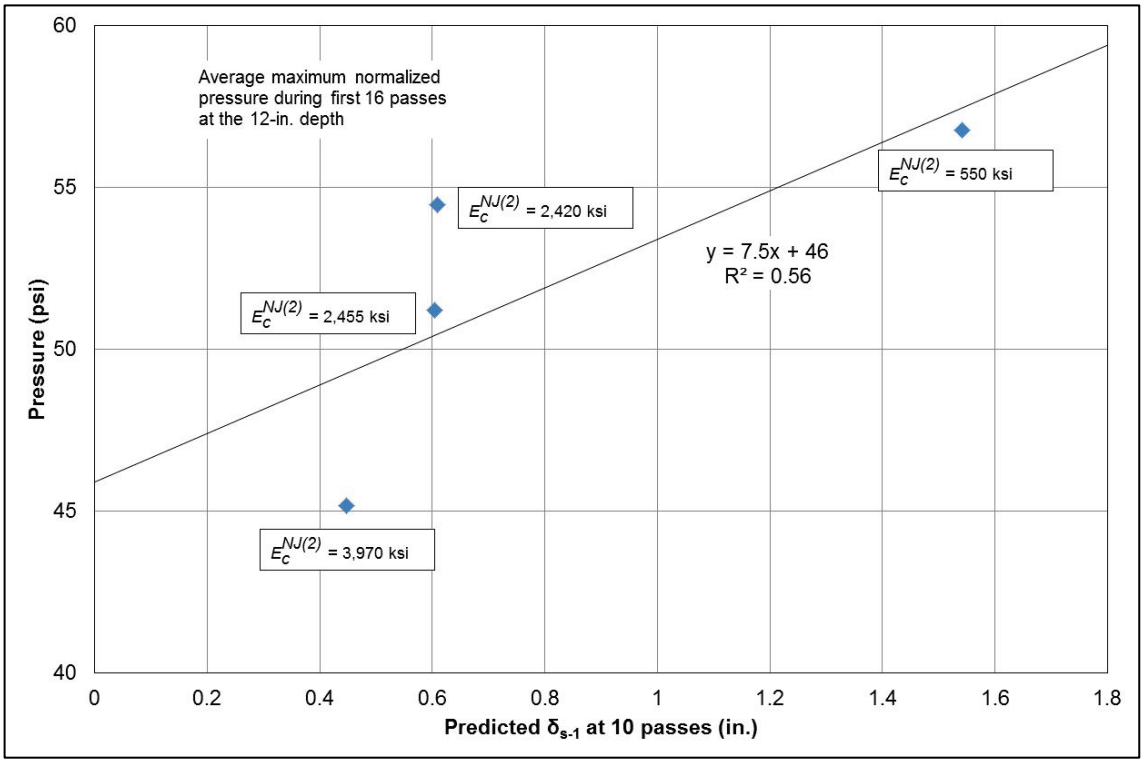

7 Conclusions and Recommendations

7.1 Summary and conclusions

The experimental program presented compiled data from six full-scale test sections of airfield matting systems of varying materials and designs. Each matting system was placed on a CBR of 6 and subjected to simulated modern fighter aircraft traffic. Mat breakage, deformation, and earth pressure were monitored throughout the tests.

The focus of the investigation was to compare the matting systems in terms of accumulated subgrade deformation and to develop relationships that could help make informed decisions when selecting an airfield mat system. A simplified expression was developed to estimate subgrade deformation, based on mat properties, for a given number of passes and a CBR of 6. The following are generalized conclusions from the research conducted.

1. The resistance to subgrade deformation is exponentially related to mat properties and follows the general trend of decreasing deformation with increasing mat stiffness.
2. An appreciable decrease in the rate of subgrade deformation can be achieved when the composite modulus of the mat system (as determined according the methods discussed herein) is increased from approximately 500 ksi to 2,400 ksi. However, minor decreases are offered when the modulus is increased from 2,400 ksi to 4,000 ksi (a comparable increase relative to 500 ksi to 2,400 ksi).
3. Since most of the data were revised and limited to the first 1,500 passes (or less) for use in the analysis (to avoid the influence of mat breakage on deformation), the developed predictive relationship should be used for estimating subgrade deformation up to 1,500 F-15E passes. Results determined for greater than 1,500 F-15E passes may be misleading.
4. The correlation developed is comparable conceptually to that available in literature for the AM2 mat system. Trade-off analyses can be conducted in the future to determine the subgrade CBR required for a weaker mat to work as well as a stiffer mat on a lower CBR.
5. Measured subgrade earth pressures in instrumented test sections showed that a more significant reduction in pressure can be achieved near the surface as a function of increasing mat stiffness. With increasing subgrade

depth, mat stiffness does not have much influence in the distributed pressure.

7.2 Recommendations for future work

The work presented is a partial experimental study (albeit at full scale), which limits detailed relationship development between the different mat systems. The following is recommended to improve understanding of airfield matting for considerations in future work.

1. Prior to conducting additional full-scale evaluations on airfield matting systems, mat system properties should be determined according to the methods described in this report. That way, additional mat systems can be added to the data set to further improve the performance curves and relationship developed.
2. Laboratory 3-point bending tests should be conducted on mat samples to compare the effectiveness of laboratory determined composite modulus to that determined using the test described by Berney et al. (2006). Performance curves could be established using mat properties determined by laboratory 3-point bending tests so that users can have two options available for estimating mat resistance to subgrade deformation. Development of additional laboratory protocols suitable for characterizing matting system properties are also needed.
3. The research conducted should be expanded to encompass other aircraft, such as the C-17. It should also be extended to provide a model that can predict subgrade deformation for any mat system over a given subgrade strength (other than just a CBR of 6).
4. The data available from the full-scale tests discussed herein should be revisited to determine if a function or series of functions can be developed to determine which failure component (i.e., mat breakage or deformation) is exceeded first. Laboratory testing should be conducted on mat samples of the systems presented to aide in these efforts.

References

Anderton, G., and C. Gartrell. 2005. *Rapid maximum-on-ground (MOG) enhancement technologies*. Technical Report ERDC/GSL TR-05-2. Vicksburg, MS: U.S. Army Engineer Research and Development Center.

ASTM International. 2007. *Standard test method for California Bearing Ratio (CBR) of laboratory-compacted soils*. Standard D1883. West Conshohocken, PA: ASTM International.

ASTM International. 2007. *Standard test method for particle-size analysis of soils*. Standard D422. West Conshohocken, PA: ASTM International.

ASTM International. 2010. *Standard test method for in-place density and water content of soil and soil aggregate by nuclear methods (shallow depth)*. Standard D6938. West Conshohocken, PA: ASTM International.

ASTM International. 2010. *Standard test method for laboratory determination of water (moisture) content of soil and rock by mass*. Standard D2216. West Conshohocken, PA: ASTM International.

ASTM International. 2011. *Standard practice for classification of soils for engineering purposes (Unified Soil Classification System)*. Standard D2487. West Conshohocken, PA: ASTM International.

ASTM International. 2012. *Standard test methods for laboratory compaction characteristics of soil using modified effort (56,000 ft-lbf/ft3 (2,700 kN-m/m3))*. Standard D1557. West Conshohocken, PA: ASTM International.

ASTM International. 2014. *Standard test methods for liquid limit, plastic limit, and plasticity index of soils*. Standard D4318. West Conshohocken, PA: ASTM International.

Bell, H.P., and Q. Mason. 2012. *Brick paving systems in expeditionary environments: Field testing*. Technical Report ERDC/GSL TR-12-24. Vicksburg, MS: U.S. Army Engineer Research and Development Center.

Berney, E.S., W. D. Hodo, and J. A Vera. 2006. *Determination of unit section modulus for finite element modeling of matting systems*. Technical Report ERDC/GSL TR-06-10. Vicksburg, MS: U.S. Army Engineer Research and Development Center.

Burgmann, R. A., and C. O. Ingebretson. 1969. *Military potential test of Class 60 Assault Trackway*. USATECOM Project No. 7-6-0642-01. Fort Knox, KY: U.S. Army Armor & Engineer Board.

Burns, C.D., and W. R. Barker. 1967. *Comparative performance tests of AM2 mat from various extruders and fabricators*. Miscellaneous Paper 4-954, Vicksburg, MS: U.S. Army Engineer Waterways Experiment Station.

Burns, C. D., and D. P. Wolf. 1969. *Evaluation of Washington Aluminum Company, Inc. production AM2 landing mat*. Miscellaneous Paper S-69-3. Vicksburg, MS: U.S. Army Engineer Waterways Experiment Station.

Carr, G.L., and D. A. Ellison. 1973. *Evaluation of Kaiser MX19-B and MX19-C aluminum honeycomb landing mat*. Miscellaneous Paper S-73-11. Vicksburg, MS: U.S. Army Engineer Waterways Experiment Station.

Doyle, J.D., I. L. Howard, C. A. Gartrell, G. L. Anderton, J. K. Newman, and E. S. Berney IV. 2014. Full-scale instrumented testing and three-dimensional modeling of airfield matting systems. *International Journal of Geomechanics* 14(2):161–170.

Dura-Base Technical Information. 2014. http://www.newpark.com/capabilities/mats-and-integrated-services/dura-base-mats-1/technical-information.

Event Deck. 2010. Event Deck: Manufacturers of tent flooring, stadium & arena flooring, temporary roadways, and access mats [pamphlet]. http://www.eventdeck.com/brochure/3-10/EventDeck%20Brochure%20LO%20RES%20Jan10.pdf.

Foster, D., and M. Anderson. 2003. Rapid forward deployment made easier with composite airfield matting. *AMPTIAC Quarterly 7*(1):17-22.

Garcia, L., T. W. Rushing, and Q. S. Mason. 2014a. *AM2 25 CBR subgrade sensitivity test*. Technical Report ERDC/GSL TR-14-7. Vicksburg, MS: U.S. Army Engineer Research and Development Center.

Garcia. L., T. W. Rushing, B.A. Williams, and C. A. Rutland. 2014b. *AM2 100 CBR subgrade sensitivity test*. Technical Report ERDC/GSL TR-14-37. Vicksburg, MS: U.S. Army Engineer Research and Development Center.

Garrett, J. L., and J. J. Horslev. 1957. *Engineering tests of experimental T7 magnesium and modified standard steel airplane landing mats*. Technical Report 3-461. Vicksburg, MS: U.S. Army Engineer Waterways Experiment Station.

Gartrell, C. A. 2007. Full-scale instrumented testing and analysis of matting systems for airfield parking ramps and taxiways. MS thesis, Mississippi State University Libraries. (etd-10052007-145227).

Gartrell, C. A., J. K. Newman, and G. L. Anderton. 2009. Performance measurements of pavement matting systems by full-scale testing over differing soil strengths. *Journal of Materials in Civil Engineering* 21(10):561–568.

Gonzalez, C. R., and T. W. Rushing. 2010. Development of a new design methodology for structural airfield mats. *International Journal of Pavement Research and Technology* 3(3):102-109.

Greulich, G. G. 1943. Pierced steel landing mats for airplane runways. *The Military Engineer: Journal of the Society of American Military Engineer, XXXV* (215):445-452.

Handbook for Concrete and Cement. 1995. *Standard test method for determining the California Bearing Ratio of Soils. CRD-C 654-95*. Vicksburg, MS: U.S. Army Corps of Engineers.

Industrial Matting-Composite Mats. 2014. http://industrialmatting.com/composite-mats/.

Macroplastics. 2014a. I-trac [Specifications Sheet]. http://www.macroplastics.com/images/docs/i-trac-salessheet.pdf.

Macroplastics. 2014b. Supa-trac [Specifications Sheet]. http://www.macroplastics.com/images/docs/Supa-Trac-Sales-Sheet.pdf.

Mindlin, R. D. 1951. Influence of rotatory inertia and shear on flexural motions of isotropic elastic plates. *Journal of Applied Mechanics* 18:31-38.

Portafloor. 2014a. Portafloor MAX [Brochure]. http://cdn.sqhk.co/portafloor/ifvUjjg/PortaFloorMAXProductInformation.pdf.

Portafloor. 2014b. Portafloor Pro [Brochure]. http://s3.amazonaws.com/leulymedia/portafloor/635320481506313677/PortaFloor%20PRO%20Product%20Information.pdf.

Robinson. M. C. 1992. Landing mat development at WES. In *Builders and fighters: U.S. Army Engineers in World War II*, ed. B. W. Fowle, 195-206. Fort Belvoir, VA: Office of History United States Army Corps of Engineers.

Rollings, R. S. 1975. *Comparison of the British Class 60 Trackway and AM-2 mat for bomb damage repair applications*. Report No. AFWL-TR-75-149. Kirtland Air Force Base, NM: Air Force Weapons Laboratory.

Rushing, T. W., and J. S. Tingle. 2007. *AM2 and M19 airfield mat evaluation for the rapid parking ramp expansion program*. Technical Report ERDC/GSL TR-07-5. Vicksburg, MS: U.S. Army Engineer Research and Development Center.

Rushing, T. W., and Q. S. Mason. 2008. *AM2 15 CBR subgrade sensitivity test for the rapid parking ramp expansion program*. Technical Report ERDC/GSL TR-08-25. Vicksburg, MS: U.S. Army Engineer Research and Development Center.

Rushing, T. W., Torres, N., and Mason, Q. 2008. *AM2 10 CBR subgrade sensitivity test for the rapid parking ramp expansion program*. Technical Report ERDC/GSL TR-08-13. Vicksburg, MS: U.S. Army Engineer Research and Development Center.

Rushing, T.W. 2010. Full-scale evaluation of matting systems for temporary roads. MS thesis. Retrieved from Mississippi State University Libraries. (etd-11032010-171135).

Rushing, T. W., and L. Garcia. 2013. *Full-scale evaluation of DuraDeck® and MegaDeck™ matting systems*. Technical Report ERDC/GSL TR-13-27. Vicksburg, MS: U.S. Army Engineer Research and Development Center.

Rushing, T. W., and I. L. Howard. 2011. Matting solutions for low-volume roads. *Transportation Research Record: Journal of the Transportation Research Board 2204*(1), 92-101.

Rushing, T. W., L. Garcia, and Q. S. Mason. 2011. *Large-scale 6-CBR prototype mat system evaluation for the AMX program*. Technical Report ERDC/GSL TR-11-37. Vicksburg, MS: U.S. Army Engineer Research and Development Center.

Rushing, T. W., L. Garcia, and Q. S. Mason. 2012. *Evaluation of faun aluminum mat systems*. Technical Report ERDC/GSL TR-12-32. Vicksburg, MS: U.S. Army Engineer Research and Development Center.

Rushing, T. W., L. Garcia, and Q. S. Mason. 2014. *Evaluation of Faun MLC-70 Trackway Mat System under Simulated F-15 Traffic*." Technical Report ERDC/GSL TR-14-13, U.S. Army Engineer Research and Development Center, Vicksburg, MS.

Rushing, T. W., and I. L. Howard. 2015. Prediction of Soil Deformation Rate beneath Temporary Airfield Matting Systems Based on Full-Scale Testing. *Journal of Terramechanics 58*, 1-9.

Signature Systems Group, LLC. 2012. MegaDeck Product Specifications [pamphlet]. http://www.megadeckrigmats.com/pdf/MegaDeck%20Brochure%20Mar2014%20low%20res.pdf.

SVE Portable Roadway Systems. 2014. http://sveproducts.com/mud-traks.html.

TerraPro. 2014. Retrieved from http://www.terraprogroup.com/access-mats.

Tolbert, R. L. 1945. Development of airplane landing mats. *Road and Bridges* 83(11):62-64, 108, 110.

Turner, R. 1961. *Engineering tests of T12 plastic airplane landing mat*. Technical Report 3-563. Vicksburg, MS: U.S. Army Engineer Waterways Experiment Station.

U.S. Army Engineer Waterways Experiment Station (WES). 1951. *Airplane landing mat investigation, engineering tests on steel, pierced type, M8, and aluminum, pierced type, M9*. Technical Memorandum 3-324. Vicksburg, MS: U.S. Army Engineer Waterways Experiment Station.

REPORT DOCUMENTATION PAGE

Form Approved
OMB No. 0704-0188

1. REPORT DATE *(DD-MM-YYYY)*	2. REPORT TYPE	3. DATES COVERED *(From - To)*
June 2016	Final report	

4. TITLE AND SUBTITLE
Full-Scale Instrumented Evaluations of Multiple Airfield Matting Systems on Soft Soil to Characterize Permanent Deformation

5a. CONTRACT NUMBER

5b. GRANT NUMBER

5c. PROGRAM ELEMENT NUMBER

6. AUTHOR(S)
Lyan Garcia

5d. PROJECT NUMBER
P2457442

5e. TASK NUMBER

5f. WORK UNIT NUMBER
FWIC91796K

7. PERFORMING ORGANIZATION NAME(S) AND ADDRESS(ES)

U.S. Army Engineer Research and Development Center
Geotechnical and Structures Laboratory
3909 Halls Ferry Road
Vicksburg, MS 39180-6199

8. PERFORMING ORGANIZATION REPORT NUMBER

ERDC/GSL TR-16-15

9. SPONSORING / MONITORING AGENCY NAME(S) AND ADDRESS(ES)
Headquarters, Air Force Civil Engineer Center
Tyndall Air Force Base, FL 32403-5319

10. SPONSOR/MONITOR'S ACRONYM(S)

11. SPONSOR/MONITOR'S REPORT NUMBER(S)

12. DISTRIBUTION / AVAILABILITY STATEMENT
Approved for public release; distribution is unlimited.

13. SUPPLEMENTARY NOTES

14. ABSTRACT

Airfield matting systems are used for the expedient construction of temporary airfields and rapid expansion of existing airfields to provide maneuvering support for military aircraft. They protect the subgrade by distributing the load exerted by aircraft over a larger area. Six airfield matting systems of varying materials and designs were evaluated through the construction of full-scale test sections to determine their effectiveness at reducing the accumulation of subgrade deformation and decreasing the pressure experienced by the subgrade. The matting systems were tested on a California Bearing Ratio (CBR) of 6 and subjected to simulated F-15E aircraft traffic while monitoring mat breakage, deformation, and subgrade earth pressure. The systems were compared in terms of the rate of subgrade permanent deformation. Based on test results, a simplified expression was developed to predict subgrade deformation on a CBR of 6 as a function of F-15E aircraft passes and airfield mat properties.

15. SUBJECT TERMS
Landing mats - Evaluation
Trafficability
Soil mechanics
Deformations (Mechanics)
Mathematical models

16. SECURITY CLASSIFICATION OF:			17. LIMITATION OF ABSTRACT	18. NUMBER OF PAGES	19a. NAME OF RESPONSIBLE PERSON
a. REPORT	b. ABSTRACT	c. THIS PAGE			19b. TELEPHONE NUMBER *(include area code)*
UNCLASSIFIED	UNCLASSIFIED	UNCLASSIFIED		95	